NONINVASIVE TECHNIQUES IN ASSESSING CORONARY ARTERY DISEASE

Miia Holmström

Helsinki University Central hospital

Helsinki Medical Imaging Center

Helsinki, Finland

Academic Dissertation

To be publicly discussed, with the permission of the Medical Faculty

of the University of Helsinki, in Auditorium Arppeanum

on May 12th, 2006, at 12 noon.

Supervisor:
Docent Kirsi Lauerma
Helsinki Medical Imaging Center
Hospital for Children and Adolescents
Helsinki University Central Hospital
Helsinki, Finland

Reviewers:
Docent Pekka Niemi
Diagnostic Radiology
Turku University Central Hospital
Turku, Finland

Docent Esko Vanninen
Department of Clinical Physiology and Nuclear Medicine
University Hospital of Kuopio
Kuopio, Finland

Opponent:
Docent Jaakko Hartiala
Department of Clinical Physiology and Nuclear Medicine
Turku University Central Hospital
Turku, Finland

ISBN 952-92-0167-2 (paperback)
ISBN 952-10-3073-9 (PDF)
Helsinki 2006, Yliopistopaino

to Peter, Amanda, and Emil

TABLE OF CONTENTS

LIST OF ORIGINAL PUBLICATIONS

This thesis is based on the following original publications, which are referred to in the text by their Roman numerals:

I Holmström M, Hänninen H, Simpanen J, Virtanen KS, Werkkala K, Aronen HJ, Lauerma K: Wall motion and perfusion analysis of transmyocardial laser revascularization. Scandinavian Cardiovascular Journal 2003; 37: 91-97.

II Hänninen H, Holmström M, Vesterinen P, Karvonen M, Väänänen H, Oikarinen L, Korhonen P, Mäkijärvi M, Nenonen J, Lauerma K, Katila T, Toivonen L: Magnetocardiographic assessment of healed myocardial infarction. Annals of Noninvasive Electrocardiology. In press.

III Holmström M, Vesterinen P, Hänninen H, Sillanpää MA, Kivistö S, Lauerma K: Noninvasive analysis of coronary artery disease with combination of MDCT and Functional MRI.

Academic Radiology 2006 Feb;13(2):177-85.

IV Holmström M, Kupari M, Sillanpää MA, Kivistö S, Lauerma K: Eight-row multidetector computed tomography coronary angiography evaluation of significant coronary artery disease in patients with severe aortic valve stenosis. International Journal of Cardiovascular Imaging. Submitted.

LIST OF ABBREVIATIONS

AP	Angina pectoris
AVD	Aortic valve disease
CCA	Conventional coronary angiography
CABG	Coronary artery bypass grafting
CAD	Coronary artery disease
CMR	Cine magnetic resonance
CVS	Calcium volumetric score
DE-MRI	Delayed-enhancement magnetic resonance imaging
DSMR	Dobutamine stress magnetic resonance
DTPA	Diethylenetriaminepentacetic acid
ECG	Electrocardiogram
EDV	End-diastolic volume
EF	Ejection fraction
EPI	Echo planar imaging
ESV	End-systolic volume
FFE	Fast field echo
FISP	Fast imaging with steady-state free precession
FIESTA	Fast imaging employing steady-state acquisition
FLASH	Fast low angle shot
Gd	Gadolinium
GRE	Gradient echo
CT	Computed tomography
IR	Inversion recovery
LAD	Left anterior descending artery
LCM	Left circumflex marginal artery
LM	Left main artery
LV	Left ventricular /ventricle
MCG	Magnetocardiography
MDCT	Multidetector computed tomography
MDCT-CA	Multidetector computed tomography coronary angiography
MI	Myocardial infarction
MRFP	Magnetic resonance first-pass
MRI	Magnetic resonance imaging
NYHA	New York Heart Association
P	Pitch

PET	Positron emission tomography
PTCA	Percutaneous transluminar coronary angioplasty
RI	Reconstruction increment
SC	Section collimation
SD	Standard deviation
SE	Spin echo
SI	Signal intensity
SPECT	Single photon emission computed tomography
SR	Saturation recovery
SSFP	Steady-state free precession pulse
SW	Section width
T1	Longitudinal relaxation time (s)
T2	Transverse relaxation time (s)
T2*	Transverse relaxation time (s) of dephasing due to magnetic field inhomogenities
TCS	Total calcium score
TE	Time to echo (s)
TF	Table feed
TI	Time of inversion
TMLR	Transmyocardial laser revascularization
TR	Time (s) of repetition

1. ABSTRACT

The aim of the present series of studies was to evaluate changes in the myocardium assessed with single photon emission tomography (SPECT) and magnetic resonance imaging (MRI) caused by coronary artery disease, examine the capability of multidetector computed tomography coronary angiography (MDCT-CA) to detect significant stenoses in the coronary arteries, and magnetocardiography (MCG) to assess remote myocardial infarctions.

Study objectives

Study I: The purpose was to evaluate the effect of transmyocardial laser revascularization (TMLR) on myocardial function and perfusion with a combination of cine MRI and thallium myocardial perfusion SPECT.

Study II: We evaluated the capability of multichannel MCG to detect remote myocardial infarction.

Study III: We evaluated the diagnostic accuracy of 8-row MDCT-CA in detecting high-grade (>50%) stenoses in the tree main coronary arteries in patients with coronary artery disease. We correlated MRI findings of the myocardium with MDCT-CA of the coronary arteries.

Study IV: The aim of this study was to evaluate whether MDCT-CA could replace invasive CCA in patients with acquired severe aortic valve stenosis.

Methods

Study I: Eight patients with severe triple vessel CAD were studied with MRI and myocardial perfusion SPECT before and six months after laser treatment.

Study II: We evaluated the capability of multichannel MCG to detect remote myocardial infarction. Multichannel MCG over the frontal chest was recorded at rest in 21 patients with remote myocardial infarction , detected by MRI, and in 26 healthy controls.

Study III: Fourteen CAD patients underwent CCA, MDCT-CA, and MRI. We determined the calcium scores and stenoses of the coronary arteries from MDCT-CA. The left ventricular MR cine

imaging was assessed at rest and perfusion defects were observed during pharmacological stress after contrast administration. Delayed contrast-enhanced MRI was performed to picture infarctions.

Study IV: Twenty-three patients with acquired severe aortic stenosis underwent both CCA and MDCT-CA. The total and volumetric calcium scores were calculated. Image quality of each coronary segment was evaluated as assessable or nonassessable for stenosis. The images of the arteries were evaluated for presence of artifacts and presence of high-grade stenoses (≥ 50%) by visual estimation and compared with that of CCA.

Results

Study I: TMLR did not improve global left ventricular (LV) function or myocardial perfusion. However, systolic wall thickening decreased in segments with fixed perfusion defects at six months and laser treatment prevented this decrease (p=0.03). In addition, SPECT imaging indicated that TMLR prevented conversion of reversible defects into fixed defects.

Study II: MCG repolarization indexes, such as ST-segment and STT-wave integrals, separated the MI group from the controls. The abnormalities were more distinct in the Q-wave-MI than in the non-Q-wave MI subgroup. When comparing the MI group with controls, the orientation of the magnetic field maps differed in the STT-wave maps.

Study III: MDCT-CA had a sensitivity of 82%, a specificity of 94%, a positive predictive value of 79%, and a negative predictive value of 95% for stenoses over 50% in the main coronary arteries as compared with CCA. LV wall dysfunction, perfusion defects, and infarctions were detected in 50-78% of sectors assigned to calcifications or stenoses, but also in sectors supplied by normally perfused coronary arteries.

Study IV: A total of 224 out of 322 segments were assessable for stenosis. MDCT-CA had a sensitivity of 63%, a specificity of 96%, a positive predictive value of 52%, and a negative predictive value of 98% for ≥50% stenoses in the main coronary arteries as compared with CCA.

2. INTRODUCTION

Conventional invasive coronary angiography (CCA) is the clinical gold standard for detecting of coronary artery stenoses. However, the small risk of serious events, the discomfort for the patient, and the hospitalization required have led to a search for noninvasive methods. The ability to differentiate between viable and nonviable myocardium plays a critical role in the prognosis of patients with coronary artery disease (CAD) (42, 106, 143, 149). Until recently, single photon emission tomography (SPECT) and positron emission tomography (PET) were the primary tools for this evaluation (162).

Magnetic resonance imaging (MRI) and computed tomography (CT) imaging are emerging as promising complementary imaging modalities in the primary diagnosis of CAD and in the detection of subclinical atherosclerotic disease. For the detection or exclusion of significant CAD, both cardiac CT (including coronary calcium screening and noninvasive coronary angiography), and cardiac MRI (using stress function and perfusion imaging) are becoming widely available for routine clinical evaluation. The high negative predictive value, especially when combining two or more of these modalities, allows the exclusion of significant CAD with high certainty, provided that patients are selected appropriately. The advantage of multidetector computed tomography (MDCT) are the potentially complete assessment of the entire coronary artery tree within a very short scan time, and with combined MRI the excellent soft tissue contrast. For the diagnosis of obstructive coronary atherosclerosis and for screening, CT has shown potential in directly imaging the atherosclerotic lesion, measuring the atherosclerotic burden, and characterizing the plaque components (89, 90, 108, 169). The information obtained may be used to assess progression and regression of coronary atherosclerosis and may open new areas for diagnosis, prevention, and treatment of the disease. Further clinical investigation is needed to define the technical requirements for optimal imaging, to develop accurate quantitative image analysis techniques, to outline criteria for image interpretation, and to define the clinical indications for both MR and CT imaging.

Magnetocardiography (MCG) provides noninvasively information about myocardial excitation propagation and repolarization without the use of electrodes. This evolving technique may be considered the magnetic equivalent to electrocardiography. MCG has been used to stratify with respect to sudden death in patients with CAD (112) or dilated cardiomyopathy or long QT syndrome (165), to localize tachyarrhythmic foci in patients with CAD (65) or dilated cardiomyopathy, to map accessory pathways in patients with pre-excitation syndrome (113), to reveal fetal arrhytmias (186), and to detect myocardial ischemia (59, 71, 72).

3. REVIEW OF THE LITERATURE

3.1. Coronary artery disease (CAD)

3.1.1 Pathophysiology of acute ischemia

The coronary artery is vulnerable to atherosclerosis, which is the main cause of ischemic heart disease. Angina is caused by coronary artery atherosclerosis leading to luminal stenosis. In the early and clinically unapparent stage of atherosclerosis, smooth muscle cells are invading the intima and, by the apoptosis of macrophages, lipid is depositing in the intima layer of the coronary artery and is commonly associated with endothelia dysfunction.

The biomechanical stability of atherosclerotic lesions in coronary arteries is determined by their composition. The typical advanced atherosclerotic lesion is characterized by a core of extracellular lipid with an overlying fibrous collagen-rich cap (139). Lipid pools in human atherosclerotic lesions dramatically increase intimal wall shear stress compared with fibrous tissue and calcifications (69), rendering lipid-rich atherosclerotic plaques by far more unstable and vulnerable to sudden rupture than other types of lesions (14). Disruption of the fibrous cap of the atheroma in coronary arteries with consecutive thrombosis, and vessel occlusion is a common cause of myocardial infarction (MI) (139).

Advanced disease consists of multiple stenotic lesions varying degrees of severity, leading to a chronic or acute reduction of coronary perfusion. It is now recognized that accumulation of atherosclerotic plaque in the coronary arteries begins much earlier than the development of luminal narrowing, with acute coronary syndromes often precipitated by the sudden rupture of a previously nonsignificant stenosed plaque (184).

Although coronary artery calcification is associated with worse cardiovascular prognosis, the influence of calcification on biomechanical plaque stresses is unclear (164). However, it is possible that

the stiff calcification is a marker for the extent of disease or for another process such as inflammation or infection (69).

Trombotic occlusion of an epicardial coronary artery is usually the cause of acute MI. Within 10 seconds after occlusion of a coronary artery, the myocardium initiates anaerobic glycolysis with accumulation of lactate and other metabolites (19, 153). If the duration of coronary occlusion is extended beyond 20 min, a wavefront of necrosis marches from subendocardium over mid-myocardium to subepicardium over time (86). Mechanisms of muscle necrosis in irreversible ischemic myocyte injury are loss of cell membrane integrity and of intracellular-extracellular ion homeostasis, resulting in swelling of the infarcted cells. Microvascular endothelial damage leads to increased leakage of macromolecules into the interstitium of the injured territory. This combined with the liberation of intracellular proteins increases the osmolarity in the interstitium and leads to interstitial edema (46). "No-reflow" is possible if capillaries have been occluded by extravascular compression, endothelial swelling, and intravascular elements such as platelet aggregates (150). The course of myocardial necrosis will be completed in 6 h (150, 153).

3.1.2 Hibernation, stunning, and scar formation

During ischemia, a large portion of the area at risk undergoes biochemical and pathological changes associated with anoxia, but remains potentially viable. At reperfusion, the potentially viable cells may reverse the changes occurring during ischemia and recover normal function or progress to necrosis (110).

The infarct-associated region often shows impaired contractile function. Three mechanisms may be responsible for this: chronic scar formation, stunning, and hibernation (19, 86, 87).

The recovery of contractile function following an acute ischemic event may be delayed for some time despite the restoration of adequate blood flow (perfusion-contraction mismatch). This condition is called stunning (19). A stunned myocardium usually recovers spontaneously after reperfu-

sion, but myocardial dysfunction may be present for several days although coronary blood flow is normal (17). The mechanism of stunning involves generation of oxygen radicals, alteration in calcium homeostasis, and a contracted protein structure (86, 87).

Hibernation describes a condition of persistently impaired myocardial function at rest caused by chronic hypoperfusion (20). After revascularization, which re-establishes adequate perfusion and oxygen supply, the hibernating myocardium is capable of regaining normal contractile function. Whereas a stunned myocardium shows minimal microscopic change, a hibernating myocardium has a pattern reminiscent of degenerating cardiomyocytes, with large perinuclear pools of glycogen and mitochondria and the presence of myofilaments limited to the cell periphery. This loss of myofilaments probably contributes to the hibernating phenomenon (86, 87, 162).

Contractile failure of hibernation is described as being chronic stunning caused by multiple episodes of severe ischemia. This leads to an increase in oxygen demand, such as exercise, or a reduction of flow, as in coronary spasm, each followed by the equivalent of reperfusion. The result is a persistent stunned, acontractile state arising from downregulation of metabolism or chronic stunning. In these cases, arterial flow must be improved with a revascularization procedure (87).

The time course of stunning is acute or subacute, in the order of hours to weeks, depending on the degree and duration of the ischemic insult. Once the duration of ischemia is extended beyond 20 minutes and cell death begins to occur in the subendocardium, recovery of function may require days or perhaps even longer. In contrast, hibernating myocardium results from months or years of ischemia and ventricular dysfunction. Thus, hibernation represents a chronic phenomenon (86, 87).

3.1.3 Imaging of CAD

3.1.3.1 Detection of lumen narrowing

Angina is caused by coronary artery atherosclerosis leading to luminal stenosis. Invasive conventional coronary angiography (CCA) is accepted reference standard for the assessment of coronary

artery stenoses because of its unprecedented temporal and spatial resolution and the ability to perform therapeutic interventions in the same session. Angiography depicts intricate coronary cross-sectional anatomy from a planar two-dimensional silhouette of the contrast-filled vessel lumen. However, both necropsy studies and intravascular ultrasonography demonstrate that coronary lesions are often complex, with markedly distorted or eccentric luminal shapes. The traditional method for characterizing angiographic lesion severity relies on measurement of the percent stenosis. This process requires comparison of dimensions within both the lesion and an adjacent, uninvolved "normal" reference segment. In the presence of diffuse disease, calculation of the angiographic percent stenosis will be predictably underestimate disease severity (184).

Current multidetector computed tomography (MDCT) scanners provide promising results in the assessment of CAD, but some segments are not evaluative because of motion artifacts or severe wall calcification. CT reliably detects arterial calcification and allows quantification. Importantly, the presence of calcium within the coronary arteries almost always signifies atherosclerosis. A negative CT indicates that the presence of atherosclerotic plaque, including unstable plaque, is unlikely (13, 14, 21, 51, 66). CT provides a high diagnostic accuracy in assessing coronary artery stenosis (3, 88-90, 98, 109, 130). Coronary intravascular ultrasound provides valuable insights into the mechanisms underlying the dissociation between angiographic and clinical outcomes (184). However, intravascular ultrasound is an invasive and expensive way to characterize plaque. MDCT-CA has the advantage of demonstrating the vessel wall atherosclerotic plaque (91, 108).

3.1.3.2 Stress testing

Patients with CAD usually have sufficient blood flow at rest, however, during stress, which induces a fourfold to fivefold increase in blood flow in healthy persons, the myocardium supplied by the stenotic coronary artery does not receive enough blood because blood flow is impeded through the narrowed coronary artery lumen. Thus, except in very severe cases, in which the patients have ischemia at rest, stress testing is required to induce ischemia.

The ergometric stress measure is the most physiologic stress test, but images with any modality may be hard to acquire because of motion. Pharmacologic stress measurement is preferred by many clinicians because the results are highly reproducible and diagnostic in most patients (127).

Dobutamine has positive inotropic and chronotropic effects, both of which increase myocardial oxygen requirements. During low-dose infusion (5-10 μg/min) increased myocardial contractility is the major effect. At higher dosages, the increased consumption of oxygen causes contraction abnormalities in myocardial segments supplied by stenotic coronary arteries (127). Dobutamine enhances regional contractility, increases heart rate, and decreases the systolic vascular resistance leading to ischemia in areas supplied by stenotic coronary arteries. The majority of experience using the dobutamine stress test has accumulated in conjunction with echocardiography (172). Stress is induced by increasing doses of dobutamine, started at 10 ug/kg of body weight per minute for 3 min and increased in increments of 10 ug/kg of body weight per minute every 3 min until a maximal dose of 40 ug/kg of body weight per minute is reached (100). Dobutamine is particularly useful for inducing wall motion abnormalities (127).

Dipyridamole, its metabolic product, and the active component adenosine are vasodilators. Incremental doses of dipyridamole causes increasing vasodilatation and relative hypoperfusion in areas supplied by significantly diseased vessels (83). Vasodilators are the preferred stressors for perfusion and flow measurements. Dipyridamole (0.56 mg/kg) is infused over a period of 4 minutes during continuous monitoring of one ECG lead and blood pressure (107). The effect of adenosine is almost instaneous, where as the reaction for dipyridamole takes minutes to reach its peak. A typical dose of short-acting adenosine is 140 μg/minute for maximum of 6 min (127).

3.1.3.3 Left ventricular (LV) function

LV functional status is well recognized as a predictor of future cardiac events after myocardial infarction. Blood flow during systole is a measure of global myocardial contractility, but it is influenced by afterload. Afterload is the resistance against which a ventricle contracts. Contractility de-

scribes the force of myocardial fiber contraction. Cardiac function is proportional to the product of contractility and preload and inversely proportional to the afterload (53).

Ejection fraction (EF) is a global assessment of LV performance (33). EF as well as LV volumes are important clinical variables with respect to diagnosis, management, and prognosis of patients with cardiac diseases. The stroke volume, the difference between end-diastolic and end-systolic volumes, increases with increasing end-diastolic volume if the afterload remains constant. The EF correlates contractility with volume measurements and is calculated by the formula EF= (EDV-ESV)/EDV, where EDV is the end-diastolic volume and ESV the end-systolic volume. The normal EF for the LV is greater than or equal to 0.55. The gold standard for measurement of ventricular volumes has been to apply Simpson´s rule to short axis cine MR images and summarized by the equation: V=£ΣA (S+G), where V is the chamber volume, A the area of the lumen of the slice, S the slice section thickness, G the gap thickness, and n the number of slices to encompass the ventricle (53).

Several techniques have been used for determination of LV volumes and EF; among these echocardiography, cineventriculography, radionuclide-ventriculography, and MRI (64).

As an imaging modality, echocardiography has the advantage of being widely available for assessment of LV. It provides an efficient semiquantitative assessment of global cardiac function (8). Nuclear cardiology is said to provide an accurate assessment of LV function with good reproducibility using gated myocardial perfusion SPECT (175). This technique is frequently utilized when a SPECT perfusion scan is performed and adds prognostic value (160). However, the exposure to ionizing radiation is unsuitable when repeated measurements are required. Cardiac MRI has been shown to be an accurate and reproducible tool for the estimation of LV volumes and function (8).

Of particular interest in patients with ischemic heart disease is the assessment of regional LV function. This can be easily estimated by visualization of short-axis cine sequences of the LV. LV short-

axis sections are divided into six sectors from the interventricular groove in a clockwise fashion according to the standards suggested by the American Society of Echocardiography and the AHA. A proposal for a unitary method of division into 17 segments has been made that requires the analysis of three equidistant transverse short-axis planes and longitudinal plane of the LV (23). Each segment is assigned to a specific coronary artery; however, depending on the coronary artery anatomy or degree of collateralization, some segments may be supplied by different arteries (127) (Figure 1).

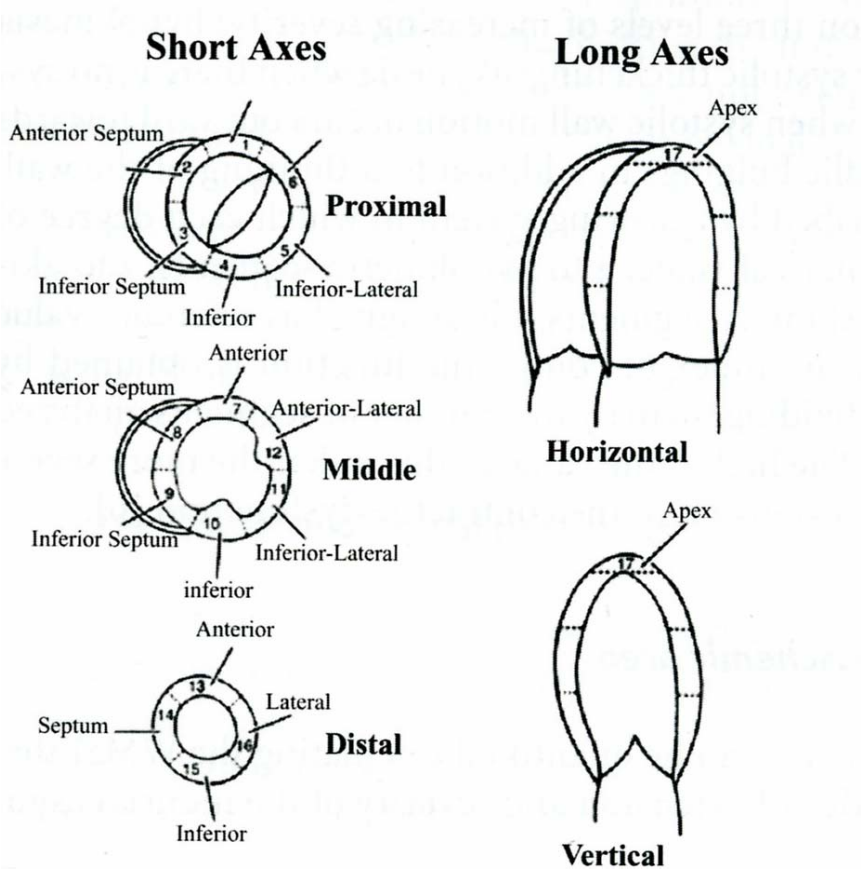

Figure 1.

Left ventricular (LV) short axis segments suggested by American Heart Association.

3.1.3.4 Detection of perfusion defects

Impaired blood flow through a stenosed coronary artery results in reduced perfusion and correspondingly diminished myocardial oxygen delivery. Initially, hypoperfusion is seen in the subendocardial portion of the cardiac muscle. As blood flow is further reduced, the perfusion deficit becomes transmural, so that first diastolic and then systolic myocardial function become impaired (174).

To detect significant stenoses of the epicardial coronary arteries, it is helpful to stress the patient so that a measure of the coronary flow reserve or similar measures (127). Under pharmacological stress, the stenotic vessel is unable to respond like a healthy vessel because of its higher vascular resistance, which results in a vascular steal phenomenon with increased blood flow to the territories supplied by the nonstenotic vessels. Thus, a perfusion defect appears in the perfused myocardial territory served by the stenotic vessel. Other possible causes of microvascular obstruction include myocardial edema and endothelial cell damage from free radical formation and endothelial dysfunction (15, 150, 196).

Stress myocardial perfusion SPECT has been widely used for demonstrating altered regional myocardial perfusion in patients with CAD. Perfusion-metabolism mismatch- that is, preserved metabolism in an area of decreased perfusion- is considered as the gold standard for myocardial viability assessment (142). However, the method suffers from attenuation artifacts and exposes patients to radiation. PET imaging corrects for attenuation and allows for the quantification of perfusion, but it is not widely available (60, 99).

Dynamic MRI with a bolus injection of contrast material enables assessment of first-pass myocardial enhancement during pharmacologic stress, which can provide information regarding the presence and extent of CAD. Myocardial territory affected by a coronary lesion may or may not exhibit a perfusion deficit during first-pass imaging under resting conditions. Hypoenhancement during first-pass is caused by reduced blood flow (194). This can be due to a severely stenosed, already at

rest hypoperfused coronary artery, or to impaired microvascular blood flow in infarcted regions (162). Hypo-enhancement at rest during first-pass is a sign of nonviability (163). Underperfused regions of the myocardium in resting studies correlate with increased amounts of nonviable tissue. Lesser stenoses can prove undetectable at rest (35).

In recent studies stress perfusion MRI showed a sensitivity of 87-90% and specificity of approximately 85% when coronary angiography was used as a gold standard (73, 171). In addition, the enhancement at dynamic MRI during stress correlated more closely with CCA results than stress SPECT findings in patients without myocardial infarction (73).

3.1.4 Interventional treatment strategies

The basic technique of percutaneous transluminar angioplasty (PTA) involves passing of guide-wire and catheter across stenosis or through an occlusion in a blood vessel. A balloon catheter is then positioned across the diseased segment and dilated up to the same size as the adjacent lumen, in order to increase the blood flow through the artery or vein (181).

Mechanical rotation devices are used to recanalize complete occlusions, where conventional catheter and guide-wire combinations have failed (198). Atheroma-removing devices are also used to recanalize complete occlusion (184).

Intravascular stents are used to maintain the lumen of a vessel by a mechanical supporting effect of its wall. The indications for their use are to prevent an acute occlusion developing after an intimal flap has been produced by angioplasty, to abolish the pressure gradient across a significant residual stenosis after angioplasty, and to treat recurrent stenoses and following recanalization of an artery (181).

Fibrinolytic therapy has been used in the treatment of various thrombotic diseases, such as acute myocardial infarction. A tip of the catheter is placed in the acute occlusion to deliver intra-arterial infusion of a low dose streptokinase into the thrombus (181).

Transmyocardial laser revascularization (TMLR) is a technique in which laser ablation creates transmural channels in the ischemic myocardium. This procedure is used as the sole therapy for patients with severe angina refractory to medical therapy or not amenable to new conventional by-pass procedures (134).

Three different types of lasers are used. The high power carbon dioxide (CO_2) laser is creating the laser channel by a single shot and Holmium: Yttrium-Aluminium-Garnet (YAG) and Excimer lasers are creating the channels with multiple impulses of lower power guided in a fibreoptic into the myocardium (34).

The procedure is based on the premise that laser-created transmural channels allow blood to flow directly from the left ventricle to myocardial vascular plexus, thus allevating ischemia in potentially viable myocardium (4).

3.2 Multidetector computed tomography (MDCT)

MDCT represents the next breakthrough in computed tomography (CT) technology.

Multislice CT systems are equipped with four or more parallel detector arrays and always utilize a third-generation technology with synchronously rotating tube and detector array. Scanning is done by proper collimation and summing the signals of neighboring detector rows. As in spiral CT scanning, section collimation (SC), table feed per rotation (TF), and pitch (P) are the most important acquisition parameters in multislice CT. In addition to the reconstruction increment (RI), an effective section thickness or section width (SW) of reconstructed images contributes to the most important reconstruction parameters. All other parameters are varied only in exceptional cases (148).

Advantages of MDCT compared with single detector-row CT are shorter scan duration, longer scan ranges, and thinner sections. The downside of multislice CT is that image noise grows as the section collimation (SC) is reduced. To limit the noise, either the radiation dose needs to be raised or

thicker sections must be reconstructed. Radiation dose is substantially increased in MDCT if the same mAs settings as in single-slice scanning are used, but conscientious choice of scanning parameters will avoid this problem (148).

3.2.1 Assessment of coronary arteries with MDCT

A new generation with subsecond rotation MDCT scanners that allow complete coronary coverage, has become widely available.

Cardiac MDCT imaging can be done using two basic modes of operation for image acquisition: prospective triggering and retrospective gating (135). For sequential imaging, a prospective trigger is derived from the ECG trace to initiate the CT scan with user selected delay after the R-wave. For spiral imaging, the ECG trace and the CT data are recorded simultaneously. Retrospective gating can be then used to select the spiral data for image reconstruction relative to a selected heart phase (85). When images are obtained in the diastolic cardiac phase motion artifacts are minimized, even in patients with faster heart rates (135).

3.2.1.2 Coronary calcium assessment

Calcified deposits within the coronary arteries have been shown to be an independent predictor of CAD. At present, coronary calcium scoring is in widespread use for risk stratification. Ultrafast CT has previously been demonstrated to be a sensitive detector of coronary artery calcium (30).

A method for semiquantative assessment of the amount of coronary calcium based on electron-beam CT findings has been introduced by Agatston et al. (5). The calcium score derived with this method appears to correlate closely with the overall atherosclerotic coronary plaque burden (192). With this algorithm, two or more contiguous pixels with attenuation of 130 HU or greater in the suspected location of an epicardial artery are considered indicative of a calcified lesion. Lesions with peak attenuation of 130-200 HU are assigned a value of 1, 201-300 HU a value of 2, those with 301-400 HU a value of 3, those with value greater than 400 HU a value of 4. The integer value

of the area of each lesion is multiplied by a lesion-specific calcium score (5). However, some analyses have revealed that this traditional scoring method is not suited for accurate and reproducible determination of the amount of coronary calcium for clinical purposes (189). This method is based on the multiplication of the area of calcified plaque by an arbitrary coefficient that is derived from peak plaque attenuation. For this reason, a volumetric method, based on the principle of isotropic interpolation, that allows more precise and reproducible measurements of calcified plaque volume was developed by Callister et al. In this method, all voxels with a value greater than 130 are used in the final three-dimensional reconstruction of the calcified plaque (21, 66).

CT is probably the most sensitive and reproducible imaging method to quantify coronary calcifications. Even the tiniest calcification will be visible by reconstruction with a soft tissue kernel. In general, a coronary calcium scan is acquired in a single breath hold with 3-mm ECG-triggered slices of the heart. Retrospective ECG gating is superior for capturing the entire volume and reconstruct the images with overlapping increment (135). After the acquisition, the data are post processed by a dedicated workstation.

3.2.1.3 Plaque imaging

In the process of atherogenesis, lipid accumulation, cell proliferation, and extracellular matrix synthesis are expected to be linear over time. However, angiographic studies show that the progression of CAD in humans is neither linear nor predictable. Indeed, recently, it has become apparent that angiographically mild coronary lesions may undergo significant progression to severe stenosis or total occlusion within a few months. This unpredictable and episodic progression is likely caused by plaque disruption with subsequent thrombus formation that changes the plaque geometry, leading to plaque growth and acute occlusive coronary syndromes (192).

It is widely accepted that only one-third of myocardial infarctions directly arise from significant coronary stenosis. Nonstenotic (<75%) plaques cause about 80% of fatal myocardial infarctions (90).

The differentiation of coronary plaque morphology has gained interest with respect to risk stratification of patients with known or suspected CAD (39). The current gold standard for in vivo coronary tissue analysis is intracoronary ultrasound, which is an invasive procedure (91, 108).

Preliminary data indicate that MDCT angiography allows detection and assessment of noncalcified lipid-rich plaques (89, 90, 108, 169). Low density plaques (40 HU) may consist of a larger fraction of lipid than high-density plaques (90 HU), which predominantly contain fibrous tissue (14).

3.2.1.4 Detection of stenoses

Invasive CCA constitutes the clinical gold standard for detection of coronary artery stenoses.

MDCT in combination with retrospective ECG gating has recently been shown to permit visualization of the coronary artery lumen and detection of coronary artery stenoses. In other studies, sensitivity of 37-93%, specificity of 89-99%, positive predictive value of 66-84%, and negative predictive value of 89-98 % have been reported performed with 4- or 16-slice techniques (49, 89, 90, 92, 93, 98, 104, 130, 131, 156, 185). Initial results of two groups suggest that 64-slice CT allows a nonivasive assessment of haemodynamically significant CAD with even higher diagnostic accuracy. The overall sensitivity was 94% and 99%, the specificity was 97% and 95%, the positive predictive value was 87% and 76% and the negative predictive value was in both studies 99% (109, 122).

There are several limitations of MDCT-CA. The presence of extensive calcifications can complicate correct assessment of the lumen of the coronary arteries. High-contrast calcium depositions cannot be sufficiently isolated from the contrast-enhanced vessel lumen, leading to nonassessable segments or misinterpretations (49, 89, 90, 92, 93, 98, 130). A heart rate of over 65 beats per minute has yielded unsatisfactory results in a few studies (90, 98, 170).

Although manual repositioning of the R-wave indicators during retrograde gating improves the synchronization of acquisition intervals between consecutive heart beats, cardiac motion artifacts cannot be entirely prevented. Movement of the patient, such as breathing, also causes motion artifacts,

which can be reduced by appropriate instruction before scanning (130). Blending with overlying vessels can lead to false-positive interpretations (116, 131). In addition, small vessel size renders evaluation of stenoses more difficult (195).

3.3 Magnetic resonance imaging (MRI)

The use of MRI for cardiac diagnosis is expanding, aided by the administration of paramagnetic contrast agents for a growing number of clinical applications.

MR imaging is an excellent means to depict cardiac anatomy. In general, contrast agents are not required for morphologic evaluation. In evaluation of LV function cine images show the motion of the heart and blood over multiple phases of the cardiac cycle (35). Myocardial regional blood flow can be assessed using dynamic MRI during the first-pass of a contrast agent. The ability to differentiate between viable and nonviable myocardium plays a critical role in the prognosis of patients with coronary artery disease. Delayed enhancement MRI technique can be used to identify irreversible myocardial damage in both the acute and chronic settings (33). One of the advantages of MRI in cardiovascular diagnosis is its ability to measure flow velocity and flow volume (103). MRI of the coronary arteries is potentially useful in a variety of clinical situations such as congenital coronary artery anomalies, determination of the patency of bypass grafts, and follow-up of known proximal coronary lesions (35).

The challenge in cardiac MRI is to cope with the motion of the heart due to ventricular contraction and the superimposed respiratory movement during the time needed for imaging. Breath-hold imaging is the approach used most widely to avoid respiratory-related displacement of the heart. MRI systems also incorporate respiratory-sensing devices to reduce the number of artifacts resulting from chest wall motion (138). Electrocardiography (ECG)-gating synchronizes cardiac imaging at pre-selected intervals during the cardiac cycle. Data are collected in gates or time windows at inter-

vals synchronized with the ECG to produce gated images throughout the phases of the cardiac cycle (53).

In retrospective ECG gating, image data are acquired irrespective of the ECG, and the ECG is recorded in parallel. Once the MRI acquisition is finished, the computer retrospectively calculates the appropriate cardiac phases based on the stored ECG and k-space data. The entire cardiac cycle can be imaged efficiently (40). Retrospective gating was developed for synchronization of rapid repetitive cine acquisition to the cardiac cycle (103).

In prospective triggering, the image acquisition starts immediately after the R-peak of the ECG complex which is the initiation of systole. The duration of image acquisition must be less than or equal to the duration of the shortest R-R interval. In practice, this usually means that the last data from 10-20 % of diastole is not acquired (103).

3.3.1 MRI sequences

3.3.1.1 Spin echo (SE)

In cardiac MRI SE sequence is particularly useful for evaluating cardiac structure, paracardiac and intracardiac masses and thrombi, and acute and remote myocardial infarctions (146).

With the SE technique, an initial excitation pulse at resonance (90° radio frequency pulse) is applied to tilt the spins around the axis of the excitatory magnetic field. Longitudinal magnetization is reduced and transverse magnetization is generated, but starts to disappear rapidly because of spin dephasing. After a time period of half of echo time (TE), a refocusing pulse (180° RF pulse) is applied, and after another one half of TE an echo is produced (146). The combination of selected time of repetition (TR) and TE determines whether images have T1- or T2-weighting. T1-weighted SE images are acquired with a combination of short TR and short TE (154). The images obtained with shorter echo times have a better signal-to-noise ratio and excellent contrast among epicardial fat, myocardium, and rapidly flowing blood. The absence of signal from flowing blood (flow void or

dark blood) is also a feature of the SE sequence (146). T2-weighted SE images are acquired with a combination of long TR and long TE (154).

Faster turbo spin echo (TSE) has replaced conventional SE imaging. TSE uses a long train of 180° refocusing pulses to generate multiple spin echoes after an initial 90° excitation. Each echo in the train is phase-encoded to generate a different line in k-space (146). The possible reduction in measurement time is directly proportional to the number of echoes used (154). Although the technique is much faster than conventional SE, disadvantage is the poorer soft tissue contrast (146).

3.3.1.2 Gradient echo (GRE) based sequences

The white-blood sequences are widely being used at present for assessment of the LV, including the measurement of dimensions and wall thickness, and the calculation of functional parameters (54).

The basic GRE technique uses a single radio frequency pulse to produce an echo signal. Following excitation by the RF pulse, a magnetic field gradients are used to focus the protons to produce a coherent MR signal. This signal is called a gradient echo, and the process that produces it can occur very quickly (1-10 ms). Typically gradient echoes are obtained at TE of 2-8 ms, and this can be repeated approximately every 10-20 ms (146). Blood appears bright compared with the to adjacent myocardium due to time-of-flight effects as well as the relatively long T2 (33).

A new approach to improve cine imaging involves a technique known as steady-state free precession pulse (SSFP) sequence e.g. trueFISP (= fast imaging with steady state precession), balanced FFE (=fast field echo), and FIESTA (=fast imaging employing steady-state acquisition) (33). In SSFP sequences, both the transverse and the longitudinal magnetizations attain steady-state while TR is kept shorter than T2. When TR is much less than T2, the transverse magnetization can be detected over many TR time-in-time intervals (199). TrueFISP is a steady-state technique that recycles coherent transverse magnetization, and the steady state signal is determined by the T2-to-T1-signal ratio (22). Because blood has significantly higher T2-to-T1 ratio than the myocardium and

because trueFISP uses the available blood signal very efficiently, trueFISP differentiates the blood, myocardium, and epicardial fat exceptionally well (199). On the other hand, trueFISP is quite sensitive to magnetic field nonuniformity caused by, for instance, metallic objects such as sternal wires. In addition, cancellation artifacts are frequently seen as dark etched outlines at the major interfaces between fat and water (144).

Recently, the saturation recovery (SR) true fast imaging with a SSFP sequence proved to give superior image quality, since it makes the most efficient use of the available magnetization (168). The SR prepared sequence comprises a magnetization preparation period consisting of a nonselective 90º pulse, followed by a gradient crusher gradient and a subsequent short TR/short TE (22). The saturation technique in cardiac MRI is used to maximize the T1 contrast between a normal and a hypoperfused myocardium during a dynamic contrast-enhanced first-pass acquisition of the myocardium. Because of good T1 contrast between a normal and a hypoperfused myocardium, this technique is well suited for first-pass imaging (179).

TR can be shortened to several milliseconds with GRE techniques such as fast-low angle shot (FLASH), which uses a very short flip angle and TR (56, 154). A turboFLASH sequence consists of a single 180º inversion recovery (IR) preparation followed by rapid gradient echo acquisition (110). This sequence produces strongly T1-weighted images owing to use of the inversion pulse before image acquisition (177). IR pulse sequence consists of a 180º inversion pulse followed by either a SE, GRE, or echo planar imaging (EPI) sequence. After the inversion pulse, the magnetization recovers exponentially from the maximal negative value to a maximal positive value through the T1 null point. Inversion pulse can also be applied to null fat. The time interval between the inversion pulse and the excitation pulse is known as time of inversion (TI) (174).

The TI is then defined as the time between this 180º pulse and the center of acquisition of the segmented k-space lines. The TI is chosen such that the magnetization of the normal myocardium is near its zero crossing to ensure that these regions appear as dark as possible (79).

The IR technique in cardiac MR is used for characterization of tissue after administration of contrast media. The signal of the normal-perfused myocardium is suppressed to better visualize hyperintense areas due to contrast uptake. One can distinguish perfused tissue in the endocardial and epicardial layers of the myocardium (179).

3.3.2 Contrast media

Two classes of MR contrast agents have been used for myocardial imaging. Paramagnetic agents are used in a dose range that causes shortening of T1 and hence higher signal intensity (SI) in the area to which they are distributed. The effect of these T1-enhancing agents can be observed in T1-weighted SE, GRE, and EPI. The second group, magnetic susceptibility agents, induce local variations in the tissue magnetic field, thereby causing a decrease in SI. This effect can be in T2-weighted SE, T2* sensitive GRE, and EPI (159)**.**

Based of their mechanisms of distribution contrast agents are classified as extracellular, intravascular, targeted, or intracellular agents. The molecular weight is a major factor in the distribution and elimination of MR contrast agents in the body (18)**.**

Widely used gadolinium (Gd) has the greatest influence on the relaxation times of proton nuclei. This is due to the presence of seven unpaired electrons with the long electron T1 times, which are important for proton relaxation. Extracellular agents are distributed rapidly into both the intravascular and extracellular spaces, typically with a plasma half-life on the order of 20 min. Most Gd-chelates, including gadopentetate dimeglumine, gadodiamide, gadoteridol, and gadoversetamide, belong to this category (35).

Extracellular Gd-chelates enhance the blood and normal myocardium in a homogenous fashion. Peak enhancement is achieved within 1 min of intravenous injection of these agents. Extracellular

agents diffuse out of capillaries into the interstitium but do not enter the intracellular space of viable tissue (159). Rupture of the cellular membrane, which signifies the death of a cell, allows Gd-chelate to enter the cell, and its tissue concentration at equilibrium is increased proportionally (191). Extracellular contrast agents are widely used outside of the heart, for a large number of clinical applications. In the heart, they are used mainly for the evaluation of myocardial viability and for characterization of masses (35).

3.3.3 MRI of the ischemic myocardium

3.3.3.1 Wall motion abnormalities

The ability of cine MR to visualize global and regional wall motion and systolic thickening of the LV with a high degree of spatial and temporal resolution makes it an excellent method to detect abnormalities in contractility. Except for high-grade coronary artery stenosis, abnormalities can typically only be identified under stress conditions. Stress can be induced with infusions of pharmacologic agents such as dobutamine/atropine, dipyridamole, or adenosine (127).

Echocardiographic detection of wall motion abnormalities during high-dose dobutamine or exercise stress has been shown to be an accurate diagnostic tool for screening patients with suspected CAD. However, dobutamine stress echocardiography has inherent disadvantages. Even with the most advanced machines, 10-15% of patients yield suboptimal or nondiagnostic images. Mainly basal and lateral and inferior segments show poor endocardial delineation. Accuracy largely depends on the experience of diagnostic centers and observers, and test reproducibility is low (63). Dobutamine cardiovascular MRI is used to identify wall motion abnormalities of the left ventricle, indicative of myocardial ischemia in patients with proven or suspected CAD (100, 101). Analysis of viability can be done qualitatively by visual analysis of wall motion at rest and during infusion of low-dose dobutamine or by measuring wall thickness and wall thickening (106, 107, 127, 155). Segmental wall motion is graded as normokinesia, hypokinesia, akinesia, or dyskinesia (127). A minimal end-

diastolic wall thickness of more than 5 mm with resting thickening or resting akinesis and an improvement in systolic wall thickening of 2 mm or more during dobutamine stimulation are clinically diagnostic criteria for myocardial viability (9, 10). Myocardial wall thickening is useful for measuring regional function, and it is more precise than subjective visualization of wall motion. Experimental and clinical studies have shown that myocardial dysfunction caused by hibernation or stunning, but not by scaring, can be transiently reversed by positive inotropic stimulation. During dobutamine infusion, systolic wall thickness increases in viable, but not scarred, myocardium, because only the viable cells are able to respond to inotropic stimulus (9, 162).

Echocardiography and cine MR have been compared with angiography for the detection of CAD (128). According to this study, with dobutamine stress MR, stress-induced wall motion abnormalities were detected with a significantly higher diagnostic accuracy than with dobutamine stress echocardiography in patients with suspected CAD, (sensitivity 86.2% vs. 74.3% and specificity 85.7% vs. 69%). Because high-dose dobutamine stress cine MRI is highly accurate and can be performed within less than 40 min, it has the potential to replace dobutamine stress echocardiography for the detection of CAD in patients with nondiagnostic or suboptimal echocardiographic image quality (128).

3.3.3.2 First-pass imaging

The development of high-speed MRI techniques has enabled assessment of relative perfusion of the myocardium by monitoring the first transit of a bolus of contrast agent. When a compact bolus of Gd contrast agent is administered intravenously, its first passage into the heart reflects delivery at the myocardial level. Under normal circumstances, a bright or enhanced image can be obtained in all regions of the myocardium. Perfusion deficits are recognized as areas of reduced SI due to either significant coronary artery stenosis or microvascular obstruction at the capillary level or delayed enhancement (194).

The results of Sakuma and colleagues showed that stress first-pass contrast-enhanced MRI provides the detection of significant stenosis in the coronary artery with a diagnostic accuracy comparable with that of stress ^{201}T1 SPECT without attenuation correction (161). In study by Keijer et al. during pharmacological stress, the MR perfusion parameters and slope of the SI-time curve showed moderate correlation with ^{201}T1 SPECT (77).

Changes in SI form the basis of both qualitative and quantitative methods of image analysis. Semi-quantitative and quantitative evaluations require the definition of myocardial regions-of-interest (ROIs), image registration, extraction of signal intensity time-curve data, and analysis or mathematical modelling of contrast agent kinetics to derive the chosen parameters (174).

The mean signal intensity for each determined ROI is measured on consecutive images. The data are presented as a series of signal intensity-time curves for myocardial regions and ventricular cavities. Peak enhancement and time-to-peak enhancement are the key criteria for the identification and characterization of perfusion defects. Any reduction or delay in regional peak signal intensity suggests hypoperfusion. This can be further categorized as reversible or fixed by a comparison of stress and rest studies (106).

The absolute quantification of myocardial blood flow requires a precise estimation of the volume of blood entering a unit weight of myocardium per unit time (174). Although this has been modelled, there are many assumptions, and in practice, a semiquantitative assessment is made that examines the change in signal intensity over time, the gradient of the unslope, peak signal intensity, and time to peak. The myocardial perfusion reserve index can be quantified by the difference between myocardial perfusion reserve (MPR) in stress and rest studies (28, 95, 96)**.**

Myocardial MR first-pass perfusion (MRFP) imaging can be applied for assessing the severity and extent of perfusion defects in CAD before and after interventions or for diagnostic purposes (194). Myocardial first-pass perfusion can predict whether myocardial function can recover after a myocardial infarction and revascularization (78, 155). Identifying inducible ischemia and the “area of

risk" during pharmacological stress is also possible. Another unique feature of MRFP is that subendocardial perfusion defects can be localised as an early sign of ischemia, particularly in a hibernating or stunned myocardium (194).

To detect significant stenoses of the epicardial coronary arteries, it is helpful to stress the patient so that a measure of the coronary flow reserve or similar measures, such as the MPR index, can be obtained (127).

The "no-reflow" phenomenon, which indicates lack of reperfusion from microvascular impairment at the core of a reperfused infarct, presents as a subendocardial region of persistent hypoenhancement (78, 196). Since flow at the core is very low but not zero, the hypoenhanced regions eventually become hyperenhanced (33). Lauerma et al. found a significantly higher first-pass enhancement slope in hypokinetic myocardial sectors that responded to dobutamine stressing as compared with ones that did not respond and with normal sectors (106). In a study of 34 patients with a stenosis of an epicardial coronary artery of at least 75%, a cut-off value of 1.5 for MRI perfusion reserve helped differentiate normal from ischemic myocardial segments (6).

3.3.3.3 Late enhancement imaging

Late enhancement MRI is performed following the intravenous administration of Gd-chelate. After an appropriate delay (typically 5-20 minutes), breath-hold IR-prepared, T1-weighted GRE images are acquired. The typical pulse sequence for myocardial late enhancement MRI is turboFLASH sequence. The correct choice of the appropriate inversion time (approximately 200 ms) to null the signal intensity of normal myocardium is important for accurate delineation of the infarcted region (35). The result is an image in which viable tissue is dark, and nonviable, fibrotic, or scarred tissue appears bright (33). Nonviable tissue has substantial amounts of interstitial space, while viable tissue has little interstitial space. The "wash-in/out" rates for Gd-chelate in nonviable tissue are reduced. As a result, Gd-chelate preferentially accumulates in irreversibly injured myocardium within minutes following contrast administration (78, 81, 151).

3.3.3.4 Assessment of chronic myocardial damage

Late enhancement MRI is usually performed under rest conditions and combined with cine MRI for wall motion information. Results are interpreted in one of three ways: 1. as viable normal tissue (dark on viability images, normal wall motion), 2. as nonviable or irreversible damaged tissue (bright on viability images, dysfunctional on cine images), or 3. as hibernating or down-regulated viable tissue (dark on viability images, dysfunctional on cine images) (33).

Several studies have shown that delayed contrast enhancement distinguishes between viable and nonviable regions within the myocardium at risk (42, 106, 143, 149). Regional elevations in concentrations of myocardial MRI contrast agents were exclusively associated with irreversible ischemic injury defined histologically and by regional electrolyte concentrations (151).

In an animal study, hyperenhancement occurred in infarcted regions but was not observed in regions subjected to reversible ischemic injury alone, despite the presence of myocardial stunning (42). Ramani et al. found delayed hyperenhancement of Gd-DTPA contrast-enhanced MRI occured frequently in dysfunctional areas of the LV in patients with stable CAD. Hyperenhancement was associated with nonviability by rest-redistribution T1 myocardial perfusion SPECT and dobutamine echocardiography, particularly regions exhibiting resting akinesis/dyskinesis. The absence of hyperenhancement correlated with radionuclide and echocardiographic determinations of viability, regardless of resting contractile function (149). This is in agreement with Sanstede et al., who reported that evidence of delayed hyperenhancement of dysfunctional myocardium may predict lack of mechanical improvement or nonviability, whereas the absence of hyperenhancement correlates with improvement of regional contractility or viability after revascularization (163).

3.3.3.5 Assessment of acute myocardial damage

While DE-MRI has rapidly gained acceptance in evaluating chronic ischemic disease, its role in the assessment of acute myocardial damage remains controversial. Different patterns of contrast en-

hancement in the setting of acute infarction have been reported by number of investigators both with and without reperfusion.

Large human infarcts, associated with prolonged obstruction of the infarct-related artery, are characterized by central dark zones surrounded by hyperenhanced regions in MRI. Conversely, reperfused infarcts with less regional dysfunction have uniform signal hyperenhancement (111). In an experimental study, a group with hypoenhanced regions within the infarct center, which were presumed to represent microvascular obstruction, had significantly more frequent cardiovascular complications associated with fibrous scar formation and left ventricular remodeling (196). These hypoenhanced areas were found to be experimentally produced "no-reflow" regions and to reflect myocardial microvascular obstruction (78).

Infarct size determined by MRI also relates directly to long-term prognosis in patients with acute myocardial infarction (196). A few studies have shown that the amount of delayed transmural enhancement predicts the degree of functional recovery after acute myocardial infarction (25, 81, 162). Extensive transmural myocardial late enhancement is highly predictive of a lack of functional improvement after revascularization (81). Choi et al. studied 24 patients with first acute myocardial infarction immediately following the acute event and then follow up. Regions of extensive enhancement were unlikely to recover function, while those with only mild damage recovered substantially (25).

It is widely accepted that delayed enhancement in certain locations, and in the appropriate clinical setting represents infarction, but some controversy remains (31). Contrary evidence has emerged that myocardial delayed enhancement in the acute postinfarct phase may cause an overestimation of the amount of irreversibly damaged tissue. Some investigators have suggested based on clinical and experimental research that the area of hyperenhancement on late enhancement images may be larger than the true necrosis and may include the adjacent area of risk (84, 137). One animal study has revealed that accurate determination of infarct size by delayed enhancement MRI requires imaging

at specific times after Gd-DTPA injection but provided a more accurate estimate with. The size of enhanced regions overestimated infarct size early after injection and receded over time (137). Nonetheless, the majority of published findings indicate that myocardial delayed enhancement accurately depicts the amount of nonviable myocardium.

3.4 Single photon emission computed tomography (SPECT)

SPECT is based on an ordinary gamma camera made to rotate around the patient. By recording the radioactivity at numerous angles, sectional images may be reconstructed. SPECT is a widely used technique, especially in cardiac and brain studies (178).

3.4.1 Technique

During myocardial perfusion SPECT studies, a perfusion tracer is injected. Thallium^{201}, ^{99m}Tc-sestamibi, and ^{99m}Tc-tetrofosmin are three routinely used myocardial perfusion imaging tracers with the last one being the preferred agent for SPECT studies (142). Standard myocardial perfusion SPECT can be gated at rest or after exercise-stress. Two types of pharmacological stress agents are used: coronary vasodilating agents, such as dipyridamole and adenosine, and cardiac positive inotropic agents, such as dobutamine and arbutamine (152). A same- day or separate day protocol can be used. With ^{99mTc} tracers, imaging is performed 30-60 min after the injection to allow clearance of the adjacent extracardiac activities (117).

During a SPECT acquisition, a gamma-camera records photons at multiple projection angles around the subject along a 180º or 360º arc. Acquisition starts with the R wave on the ECG, which corresponds to the end-diastole. One cardiac cycle, represented by the R-R interval, is divided into multiple frames of equal duration. Acquisition of 12 to 16 frames per cardiac cycle is considered satisfactory. To achieve adequate count density in each frame, non-gated data are acquired over many cardiac cycles (142).

3.4.2 Measurement and analysis

ECG gating of standard myocardial perfusion SPECT acquisition allows for the quantitative or semiquantitative assessment of the LV function simultaneously with the evaluation of LV perfusion.

LV volumes and LVEF can be obtained easily by applying commercially available software to the reconstructed gated dataset. LV regional function is more commonly evaluated visually on a cine-loop display. Regional endocardial wall motion can be quantitated by computing the distance of a given point on the endocardial surface between end-diastole and end-systole. Systolic wall thickness is assessed by evaluating the changes in brightness (count intensity) from the end-diastolic to the end-systolic frame (142).

The left ventricle is divided into a 20-segment model for scoring on the basis of short-axis slices. A severity scoring system of 0 to 4 was used for each segment: 0 = normal wall motion and thickening; 1 = mild hypokinesia/reduced thickening; 3 = severe hypokinesia /reduced thickening; and 4 = akinesia/absent thickening (36, 50).

The reconstructed images are oriented in the standard short axis, horizontal long axis, and vertical long axis for interpretation and quantification of radiotracer uptake (55). The rest and post-stress images are interpreted for the presence, extent, severity, and reversibility of perfusion. A 20-segment model of LV is used for scoring perfusion defects with a 5-point scoring system for defect severity (0 = normal perfusion; 1 = equivocal or mildly reduced; 2 = moderate reduction; 3 = severe reduction; 4 = absent perfusion (16, 36). This can be done using semiquantitative visual analysis or quantitatively calculated as the percentage of regional uptake of radiotracer (16, 50). A segment with a nonreversible defect in myocardial perfusion SPECT in an area >50% of the entire segment, and an end-diastolic wall thickness >6mm can be defined as nonviable (55).

3.4.3 Indications and clinical applications

SPECT is used for the assessment of the LV functional parameters and evaluation of risk and prognosis in CAD (36, 41), determination of the myocardial viability (50, 55, 161), and evaluation of the CAD and functional recovery after the revascularization procedure (73).

Myocardial perfusion has been evaluated most frequently with SPECT, and excellent sensitivity of stress myocardial perfusion SPECT has been reported in previous studies (41, 61, 133). One well-recognized application of SPECT is to classify a fixed perfusion defect as a soft-tissue attenuation (left breast, subcutaneous fat, left hemi-diaphragm) artifact or an infarct. Because an artifactual defect would show normal contraction on a gated image, artifacts can be differentiated from a true infarct (142).

Persistent LV dysfunction on poststress SPECT predicts a high-grade coronary stenosis (36). The magnitude of the poststress regional or global dysfunction correlates also with the severity of the ischemia. For detection of stunning in gated SPECT, LV regional dysfunction is probably more sensitive than global dysfunction (141). Stress induced reversible regional wall motion abnormalities on a single-day exercise Tc-99m-sestamibi-gated cardiac SPECT is highly specific for severe angiographic stenosis (36). MRI has become a genuine competitor of nuclear imaging in the evaluation of myocardial perfusion. The results of Sakuma and colleagues showed that stress first-pass contrast-enhanced MRI provides the detection of significant stenosis in the coronary artery with a diagnostic accuracy comparable with that of stress ^{201}T1 SPECT without attenuation correction (161). Recent studies have expanded the potential application of gated SPECT in the assessment of viability (50, 55). LV functional status can be compared before and after the revascularization procedure, the excellent reproducibility and repeatability of gated SPECT is a benefit of this method (142). Stress induced reversible regional wall motion abnormalities on a single-day exercise Tc-99m-sestamibi-gated cardiac SPECT is highly specific for severe angiographic stenosis (36).

3.5 Magnetocardiography (MCG)

Detection of new ischemic episodes in patients who have undergone a previous MI remains a diagnostic and monitoring challenge due to distortion of the baseline ECG.

MCG is a novel, noninvasive mapping technique to record cardiac magnetic field, generated by the same bioelectric currents as ECG. Interestingly, MCG is less affected by attenuation due to the intervening thoracic tissue than is the electric field (176). Recent developments in the MCG instrumentation have enabled MCG recordings to be made in the hospital environment (57, 129).

MCG has morphological features similar to the P-wave, QRS complex, and T- and U waves of ECG, and the temporal relationships between these parameters are generally the same. Almost all MCG studies are based on measurement of the magnetic field component perpendicular (radial z-component) to the anterior chest. MCG is thus most sensitive to currents tangential to the chest surface, whereas especially chest leads of ECG are more sensitive to radial currents. MCG may therefore show pathological deviation from the normal direction of depolarization and repolarization in a different manner than ECG. MCG is also less affected than ECG by conductivity variations caused by the lungs, pericardial effusion, muscles, and skin (176). In MCG, no problems with skin-electrode contact, common in ECG, exist (26).

3.5.1 Clinical applications

MCG is used in ischemia research, but also in some clinical indications. For detection of LV hypertrophy or dilatation from echocardiographic measurements, the sensitivity and specificity of MCG are similar or slightly better than standard ECG, or slightly better (45). The MCG technique is helpful in screening patients at risk of ventricular arrhythmias after myocardial infarction (94, 114). Noninvasive MCG mapping may significantly contribute to the invasive catheter mapping for opti-

mal preoperative localization or preexcitation site and atrioventricular accessory pathways in Wolff-Parkinson-White syndrome (113).

MCG permits localization of tachycardia points of origin with high spatial accuracy (124).

This technique has proven to be accurate in three-dimensional localization of magnetic pacing catheter in the heart (145). MCG offers a noninvasive method in the identification and classification of clinically relevant fetal arrhythmia and an aid in decisions concerning treatment (186).

3.5.2 MCG rest studies in MI patients

The largest differences between post-MI patients and controls have occurred in MCG during repolarization. The repolarization changes in MCG have been prominent in patients with inferior rather than than those with anterior Q-wave MI (105). In a study by Tsukada et al. the ratio of the maximum repolarization and depolarization values, found by compression between ST-T and QRS isointegral maxima, was reduced in patients with CAD as compared with values in healthy controls. The spatial evaluation of QT dispersion at rest has separated patients with CAD but without MI from healthy controls (187).

3.5.3 MCG stress studies in MI patients

MCG can be applied as an alternative to ECG during stress. In exercise stress studies ischemic ST depression appeared in MCG and the ST amplitude shift/R amplitude ratio was grater in MCG than in ECG (157). Cohen et al. found TQ baseline elevation and ST depression after a two-step exercise test in a patient with CAD (26). Heart-rate adjustment of the rotation of the magnetic field has improved ischemia detection during the recovery phase of a bicycle exercise test (182). Hailer et al. have studied CAD patients during pharmalogical stress (arbutamine) and at rest. The evaluation of spatial distribution of QT dispersion in MCG, reflecting regional heterogeneity of repolarization, enhanced the sensitivity of detection of CAD both at rest and during stress compared with QT dispersion assessed in 12-lead ECG (58). The presence and location of acute transient ischemia can be

detected in exercise magnetocardiography. The MCG method seems to be especially sensitive to inferior wall ischemia detected by T-wave changes in the postexercise period (72).

4. AIMS OF THE STUDY

The purpose of Studies I-IV was to examine noninvasive methods, single photon emission tomography (SPECT), magnetocardiography (MCG), magnetic resonance imaging (MRI), and multidetector computed tomography coronary angiography (MDCT-CA) to detect changes in the myocardium and coronary arteries in patients with coronary artery disease (CAD).

The purpose of Study I was to detect the effect of transmyocardial laser revascularization (TMLR) on left ventricular (LV) wall thickness and systolic wall thickening with cine MRI and myocardial perfusion with thallium SPECT.

In Study II, we evaluated the electrophysiological abnormalities produced by remote myocardial infarction (MI) in MCG mapping and applied cine-and contrast-enhanced MRI as a reference method.

The aim of Study III was to evaluate the diagnostic accuracy in detecting high-grade (>50%) stenoses in the main coronary arteries with MDCT-CA in patients with CAD recently diagnosed conventional coronary angiography (CCA). A further aim was to correlate the results of MRI techniques - resting cine, stress first-pass, and late enhancement imaging with results of MDCT-CA at regional level. We studied how calcifications and fibrous/fatty stenoses in the coronary artery lumen detected with MDCT-CA can predict regional LV dysfunction and perfusion changes in the myocardium evaluated with MRI.

The aim of Study IV was to evaluate whether MDCT-CA could be used to exclude clinically significant CAD in patients with severe aortic valve stenosis (AS).

5. MATERIALS AND METHODS

All study protocols were approved by the local ethics committee. All patients gave written informed consent after the procedure had been fully disclosed to them.

5.1 Subjects

This study consisted of 43 patients with coronary artery disease, 23 patients with aortic valve stenosis, and 26 healthy controls.

5.1.1 Wall motion and perfusion analysis of transmyocardial laser revascularization (TMLR) (Study I)

Eight patients with triple vessel CAD, documented in coronary angiography, were studied with MRI and myocardial perfusion SPECT before and six months after laser treatment.

The mean age of the patients was 64 (range 57-72) years. All patients belonged to group III or IV according to the New York Heart Association (NYHA) functional classification. Patients were symptomatic despite adequate medical management, and they were not candidates for new percutaneous transluminal coronary angioplasty or coronary artery bypass grafting. Patients in this study had severe and diffuse CAD but did not have a target vessel suitable for grafting. All patients had undergone multiple redo procedures with poor results.

All patients were treated with TMRL. This procedure is used as the sole therapy for patients with severe angina refractory to medical therapy or not amenable to new conventional bypass procedures.

5.1.2 Magnetocardiography (MCG) assessment of healed myocardial infarction (Study II)

The study population (n=47) consisted of two groups. The myocardial infarction group (n=21) included patients with a history of one or more remote MIs and angiographically verified triple-vessel CAD (MI group). None of the patients had unstable CAD, and they all were symptom-free at the time of the MCG recording.

The control subjects (n=26) were healthy middle-aged volunteers with no coronary risk factors and no history or signs of cardiovascular disease. They had normal symptom-limited bicycle exercise test results without angina or ST segment changes and a normal ECG.

5.1.3 Noninvasive analysis of coronary artery disease with combination of MDCT and functional MRI (Study III)

A total of 14 patients with coronary artery disease diagnosed with CCA underwent MDCT-CA and MRI between February 2003 and August 2003. CCA was performed 4-6 weeks prior to MDCT-CA and MRI. The time interval between CT and MRI study was 1-7 days.

Inclusion criteria were angiographically diagnosed CAD and no contraindications to CT or MRI examinations. Patients with previous coronary artery bypass surgery and unstable clinical condition were excluded from the study. Exclusion criteria for CT were renal insufficiency, heart failure, and arrhythmia. Contraindications to MRI were claustrophobia and metal implants (clips in the brain, a pacemaker, or other metal objects).

Three patients belonged to group I, nine to group II, and two to group III according to the NYHA functional classification. Nine patients had one affected vessel and five had two affected vessels. One patient underwent balloon angioplasty and stenting before MDCT-CA and MRI. The mean age was 59±8 (range 39-69) years, twelve men and two women.

5.1.4 Eight-row multidetector computed tomography coronary angiography evaluation of significant coronary artery disease in patients with severe aortic valve stenosis (Study IV)

Twenty-three patients undergoing cardiac catheterization because of severe aortic valve stenosis (AS) were studied. They constituted having severe AS with or without clinical suspicion of CAD. Thirteen patients suffered from dyspnea, 11 from angina, and 2 had a history of syncope. Exclusion criteria included renal insufficiency, heart failure, and unstable clinical condition.

The mean age was 71±10 years (range 46-85) years, thirteen men and ten women.

5.2 SPECT imaging protocol (Study I)

Multislice diagrams gated SPECT thallium^{201} myocardial perfusion studies were obtained from all patients before and 6 months after laser revascularization with Elscint Apex 425 ECT equipment. Imaging was acquired by 180° rotation, using SPECT single-head system and starting 5 min after injection of 74 MBq (2 mCi) thallium^{201} chloride at peak exercise. The redistribution images were obtained 3 h later. Thirty views were acquired by 180° rotation at 6° intervals for 20 minutes with a single-head low-energy all-purpose collimator (Elscint APC-3). Reinjection images were obtained 24 h later after a dose of 56 MBq (1.5 mCi) thallium. Routine uniformity and radius-of-rotation checks were performed. A 64 x 64 matrix with pixel size of 0.6 x 0.6 cm and slice thickness of 0.6 cm was used.

An exercise stress test was performed together with myocardial perfusion. The patients underwent symptom-limited bicycle stress testing in which the exercise load was increased every 4 min. Maximum exercise time, workload (Watts), stage duration, heart rate, and blood pressure, and reasons for stopping were recorded.

5.3 MCG (Study II)

A 67-channel magnetometer was used (Neuromag Ltd., Helsinki, Finland) for MCG recordings, which were performed in a magnetically shielded room (Euroshield Ltd., Eura, Finland) of the BioMag Laboratory in a hospital environment. The sensors, 7 co-axial and 60 planar dc-SQUID (Superconducting Quantum Interference Device) gradiometers, record the spatial change in the magnetic field component perpendicular to the measurement plane. The cardiometers are arranged on a slightly curved surface with a diameter of 30 cm and immersed in liquid helium inside a dewar. The dewar is supported by a gantry, allowing easy adjustment of the sensor array both in a horizontal and vertical direction and also tilting. During the measurement, the patient is lying on a magnetic bed. The center of the cardiomagnitometer sensor array is placed 15 cm down from the jugular notch and 5 cm to the left of midsternal line, as close to the chest as possible without touching the patient. All recordings were band-pass filtered to 0.03-300 Hz and digitized with a sampling frequency of 1000 Hz.

Multichannel MCG, covering a circular area of a diameter of 30 cm over the precordium, was recorded for 5 min. The signals were selectively averaged and processed to obtain MCG data of one cardiac cycle in 33 recording locations (Figure 2).

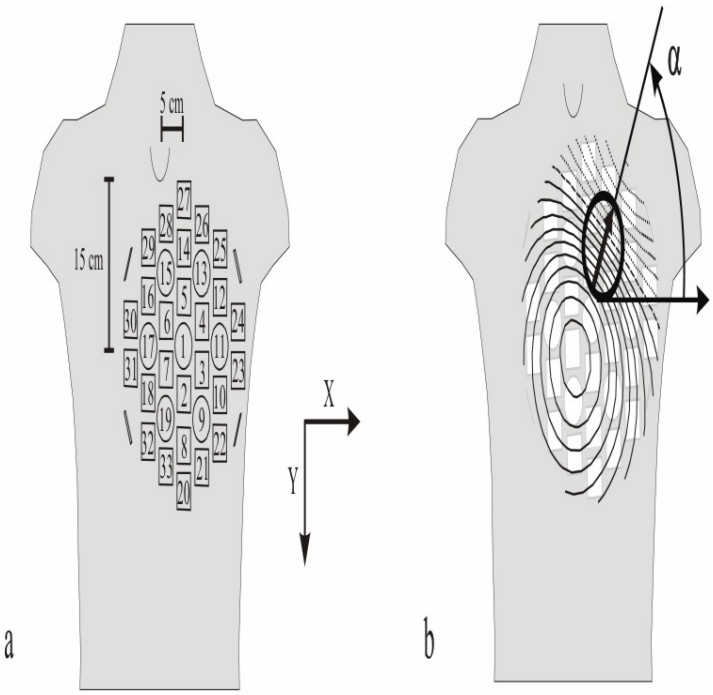

Figure 2.

MCG recording locations.

A) Sensor arrangement and positioning of the cardiomagnetometer with 33 recording locations in relation to the thorax. The device was placed anteriorly, with the center of the device 15 cm caudally from the jugular notch and 5 cm left of the midsternal line. B) In the magnetic field map (MFM), the location and orientation of the steepest spatial change in the signal, the peak gradient, is indicated by an arrow. Solid lines indicate positive values and magnetic flux toward the chest, and dotted lines indicate negative values and flux out of the chest. Orientation of the magnetic field was measured as the angle between the direction of the peak gradient and the horizontal x-axis.

5.4 MRI protocol (Studies I-III)

5.4.1 Cine imaging (Studies I-III)

Patients were positioned supine on the table of a 1.5-T imager (Magnetom Vision or Magnetom Sonata; Siemens, Erlangen, Germany), and imaging was performed with a body array coil as a receiver. Transverse, oblique sagittal, and double-oblique LV long-axis scout images were obtained to determine the final short-axis imaging plane. For LV wall motion assessment cine MR imaging was performed at rest with retrospectively ECG-gated segmented trueFISP pulse sequence.

In Studies I and III, four or five short-axis sections of 10 mm thickness 15 mm apart were registered with a electrocardiographically gated cine MRI, which produces a series of LV wall images within the cardiac cycle every 40 ms.

In Study I, the following imaging parameters were used: matrix 256 x 256, TR 80.0 ms, TE 6.1 ms and Flip angle (FA) 20º. In Study III, the imaging parameters were: matrix 256 X 256, field of view 240 X 340 mm, section thickness 6 mm, FA 52º, TR 3.0 ms, and TE 1.6 ms.

5.4.2 First-pass imaging (Study III)

An 18-gauge catheter was inserted into the antecubital vein for dipyridamole (Persantin; Boehringer Ingelheim, Helsinki, Finland) infusion and gadopentetate dimeglumine (Magnevist; Schering, Helsinki, Finland). Persantin was infused intravenously at a dose of 0.56 mg/kg over a 4-min period before contrast agent administration. Magnevist (0.05 mmol/kg) was injected intravenously at a rate of 5 ml/s. To view the perfusion defect, stress-induced first-pass images using a saturation prepared turboFLASH sequence were acquired in the four LV short-axis planes after dipyridamole infusion and during contrast agent injection. The following imaging parameters were used: matrix 256 X 256, field of view 240 X 340 mm, section thickness 6 mm, TR 183, and TE 0.99.

5.4.3 Late enhancement (Studies II and III)

For myocardial infarct imaging the late enhancement images were obtained 5-15 min after first-pass imaging using IR turboFLASH pulse sequence.

The following imaging parameters were used: matrix 256 X 256, field of view 240 X 340 mm, section thickness 6 mm, TR 750 ms, and TE 4.3 ms.

Time of inversion (TI) was determined from a single post-contrast slice, where the signal in normal perfused myocardium was optimally suppressed (dark) to visualize hyperintense areas due to contrast uptake. TI for late enhancement sequence was 250-300 ms.

5.5 MDCT imaging protocol (Studies III and IV)

MDCT was performed with an ECG-gated 8-slice scanner (GE Medical Systems LightSpeed Ultra, Milwaukee, WI, USA). Patients were examined in the supine position. A native, retrospectively ECG-gated scan was performed to determine the total calcium burden of the coronary tree. To image coronary arteries the scan delay was determined as the interval from the start of the test bolus (20ml) to the peak enhancement in the ascending aorta. A scan delay plus 8 seconds was kept between the initiation of the contrast agent injection and the start of the acquisition. A bolus of 120 ml nonionic contrast agent (Ultravist 370 mlI/ml; Schering, Helsinki, Finland) was injected through an 18-gauge catheter into the antecubital vein at a rate of 4 ml/sec.

The following scanning protocol was used for calcium scoring: 8 x 2.5 mm collimation, table feed 1.5 mm/rotation, effective tube current 300 mA at 120 kV, effective slice with 3.0 mm, reconstruction increment 1.5 mm. For coronary angiography parameters were 8 x 1.25 mm, table feed 1.5 mm/rotation, the tube current for coronary angiography was 270 mA at 140 kV, effective slice with 1.25 mm, reconstruction increment 0.6 mm. Patients with heart rate >65 beats per minute received

5 ml β-blocker intravenously (metoprolol 1 mg/ml; Leiras, Helsinki, Finland). The mean average radiation exposure per patient was 15.3 mSv.

All MDCT-CA datasets were reconstructed with retrospective gating at at 20%, 40%, 60%, 70%, and 80% relative to the cardiac cycle. The retrospective reconstructions and ECG tracing were transferred to a separate workstation (GE Advantage 4.0) for analysis with a software program (cardIQ).

5.6 SPECT image analysis

Images were reconstructed by a minicomputer (Apex F1, Elscint) from the early-systolic and late-diastolic phases of the gated frames. Three LV short-axis sections were selected to correlate the LV short-axis MR sections by determining their distance from the apex on LV long-axis MRIs and stacks of scintigraphy sections. Circumferential profiles of myocardial thallium uptake were generated by plotting transmural mean pixel intensity against the location of each 3° radius. The profiles were normalized to the maximum pixel intensity, and radial intensity of less than 75% of the maximum was classified as reduced perfusion. The sections were divided into septal, anterior, lateral, and inferior segments, as in MRI. The septal and inferior segments were not treated with TMLR; lateral and anterior segments were treated.

The segments were classified to normal tissue, reversible perfusion defect (ischemic myocardium) and fixed perfusion defect (scar) according to regional intensity as follows: normal; intensity >75% at stress and at reinjection; reversible; intensity ≤75% at stress and >75% at reinjection; fixed; intensity ≤75% at stress and at reinjection. Findings were interpreted by two observers in consensus, with both being blinded to MRI results.

5.7 MCG image analysis

The time instants of QRS onset, QRS offset, and T-wave offset in each location were determined automatically. Medians of all signals were calculated for QRS onset, QRS offset, and T-wave offset times and applied to define the time instants for measuring the amplitudes and the start and the end of the integrals in all channels. From the signal-averaged MCG data, the following indeces were calculated (Figure 3).

Integrals

QRS integral: In all channels, the QRS integral was calculated as the time integral from the QRS onset to QRS offset.

QRS sextiles: In all channels, the QRS integral was divided into 6 temporally equal time integral segments, referred as QRS sextiles.

QRS area: In all channels, the QRS area was calculated as the sum of the absolute values of Q-, R-, and S-wave areas.

ST-segment integral: In each channel, the ST-segment integral was obtained as the time integral from QRS offset to the midpoint between QRS offset and T-wave offset. The absolute value of the ST-segment integral was used to assess the QRS-ST discordance.

T-wave integral: In each channel, the T-wave integral was obtained as the time integral from the midpoint between QRS offset and T-wave offset to the T-wave offset. The absolute value of the T-wave integral was used to assess the QRS-T discordance.

STT-wave integral: In each channel, the STT-wave integral was obtained as the time integral from QRS offset to the T-wave offset. The absolute value of the STT-wave integral was used to assess the QRS-STT discordance.

QRS-STT discordance: To combine data of both ventricular de- and repolarization, the absolute value of the ST-segment integral (QRS-ST discordance), T-wave integral (QRS-T discordance), and

STT-wave integral (QRS-STT discordance) was subtracted from the QRS area. In channels where QRS integrals and ST, T-wave and STT-wave integrals were of opposite polarity, the latter were considered negative as used previously.

Amplitudes

ST-segment amplitude: In each channel, ST-segment amplitude was measured 60 ms after the J point.

T-wave amplitude: In each channel, T-wave amplitude was the amplitude with maximum absolute value from the QRS offset to the T-wave offset.

Optimal recording locations

To identify the recording locations with the best discriminative power for MI detection, we departure maps. In each channel and for each index, departure map values were calculated by subtracting mean value of the control group from the mean value of the MI group. The obtained difference was then divided by the SD of the control group. The larger the absolute departure map value, the better is the performance of that channel in separating the MI group from the controls.

Magnetic field map orientation

Mean magnetic field maps (MFMs) of the QRS complex and the STT wave were formed by calculating the mean of the MCG signal over the mapped area. The MFMs illustrate the spatial distribution of the MCG signal over the mapped area as isofield contours. Orientations of the MFMs were determined by use of the surface gradient method, described in detail earlier. First, the location of the steepest spatial change of the signal in the MFM was found. Then, the MFM orientation was defined as the direction of the steepest signal amplitude change at that location.

QRS angle and STT angle: The orientations were determined, in degrees, for the QRS complex (QRS angle) and for the STT wave (STT angle).

QRS-STT angle difference: The QRS-STT angle difference, in degrees, was calculated as the difference of the orientations of the MFMs of the QRS complex and the STT wave.

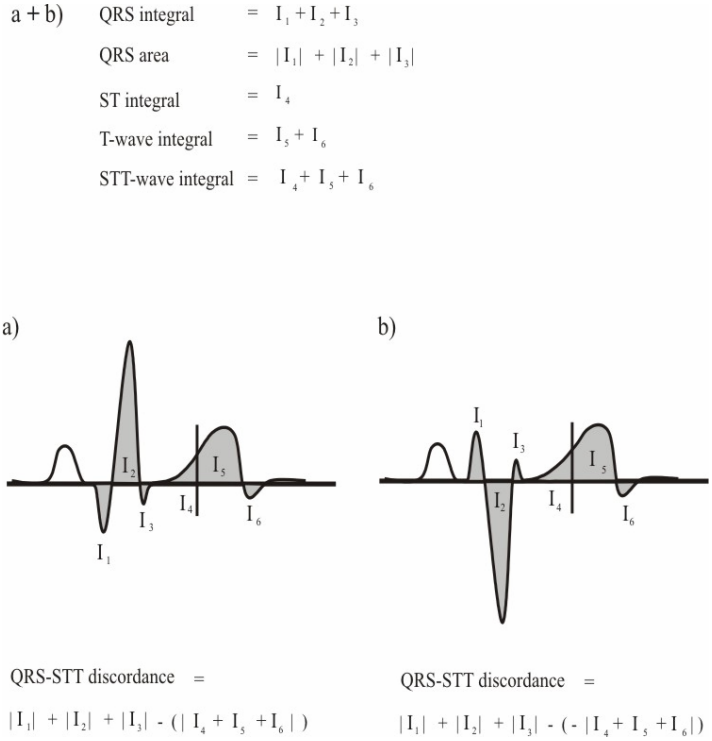

Figure 3.

Illustration of the calculation of QRS, ST-segment, T-wave, and STT-wave integrals and QRS-STT discordance in each MCG channel. The QRS integral was calculated as the time integral from QRS onset to QRS offset. TheQRS area was calculated as the sum of absolute values of Q-, R- and S-wave areas. The ST-segment, T-wave, and STT-wave integrals were obtained as the corresponding time integrals. a) If the main QRS deflection and the STT-wave were of same polarity, the STT-wave integral was subtracted from the QRS area when calculating the QRS-STT

discordance. The QRS-ST discordance and QRS-T discordance were calculated in an analogous manner. b) If the main QRS deflection and the STT-wave were of opposite polarity, the latter was multiplied by –1 when calculating the QRS-STT discordance. The QRS-ST discordance and QRS-T discordance were calculated in an analogous manner.

5.8 MRI analysis

5.8.1 Global and regional LV function

In Study I, LV diastolic and systolic volumes were assessed according to Simpson´s rule. LV volumes were measured at diastole and systole by multiplying the contour areas by the slice thickness. Slice volumes were summed to yield the total cavity volume at diastole and systole. The end-diastolic volume was obtained from the first image of the cine sequence. End-systolic volume was measured in the phase showing the smallest volume.

In Study I, quantitative end-diastolic wall thickness and systolic wall thickening were assessed from short-axis cine MR images before and after TMLR. Three short-axis sections at the mitral tendon, papillary muscle, and apex level were divided into four segments: septal, anterior, lateral, and inferior. Diastolic wall thickness for each segment was measured from the first image of the cine sequence; and systolic wall thickness from the image with the smallest LV chamber volume. Systolic wall thickening was calculated from these values. Interpretation was performed by two observers that were blinded from the myocardial perfusion SPECT results.

In Study II, when the diastolic wall thickness was less than 5.5 mm, there was less than 2 mm of systolic thickening, or there was significant late enhancement of more than two standard deviations of the normal myocardium, the myocardial segment was classified as infarcted (Study II).

In Study III, the four LV short-axis sections were divided into six 60° sectors from the interventricular groove in a clockwise fashion. These sectors were analyzed for regional LV wall motion at rest by visual estimation. Findings were interpreted by two observers in consensus, with both being blinded to CCA and MDCT findings. On cine images, segmental wall motion was graded as normokinesia or dyskinesia.

5.8.2 First-pass imaging

Findings of first-pass images were visually graded as normal or perfusion defect in the myocardium. Findings were interpreted by two observers in consensus, with both being blinded to CCA and MDCT findings. The myocardium perfused with gadopentate dimeglumine will show an increase in signal intensity because of predominant T1 shortening. Less enhanced regions of the myocardium were considered having a perfusion defect (Study III).

5.8.3 Late enhancement

On late enhancement images, the infarction scar with a larger interstitial space and a higher contrast agent concentration than healthy myocardium will have a higher signal intensity. The sectors were graded as normal or infarction by visual estimation. Findings were interpreted by two observers in consensus (Studies II and III).

5.9 MDCT Image analysis

5.9.1 Calcium scoring

The calcium score was determined on a workstation based on two different scoring systems. All areas of calcification within the borders of the coronary artery and with a minimum attenuation of 130 HU were analyzed. The total calcium score (TCS, Agatston) and the calcium volumetric score (CVS) were calculated for each individual plaque and for each patient by software program (Smartcore GE) (Studies III-IV).

5.9.2 Detection of stenoses

Depending on the individual coronary anatomy and image quality different visualization techniques such as multi-planar reconstruction, maximum intensity projections, and volume rendering techniques were used to analyse stenoses in the coronary arteries.

Fifteen datasets were produced during the different phases of the cardiac cycle (at 70% and at 20% to 80% in increments of 20%) for each patient. We chose the best-optimized time-window for each coronary artery which contained the fewest artifacts. The images of the arteries were evaluated for occurrence of artefacts and presence of high-grade stenoses by visual estimation. Findings were interpreted by two observers in consensus, with both being blinded to CCA findings. The main coronary arteries were divided into three segments; proximal (A), middle (B), and distal (C) according to the guidelines of the American Heart Association (Figure 4). In Study III side branches were excluded in the analysis.

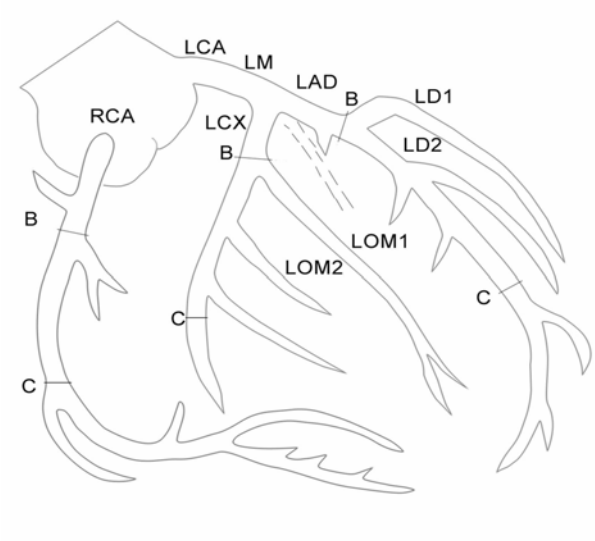

Figure 4.

American Heart Association coronary segments modified.

Left main (LM)/left anterior descending artery (LAD), left circumflex artery (LCX), and right coronary artery (RCA) were divided into three segments: proximal (A), middle (B), and distal (C).

LD 1-2 are left diagonal branches of LAD and LOM 1-2 left obtuse marginal branches of LCX.

Image quality of each coronary segment was evaluated as assessable or nonassessable for stenosis. Results were documented separately for the four major arteries: left main (LM), left anterior descending (LAD), left circumflex artery (LCX), and right coronary artery (RCA). Diagonal branches of LAD and the marginal branch of LCX were evaluated separately. Causes for invisibility were classified as follows: 1) motion artifact (caused by heart beating or breathing), 2) adjacent structure (vein, contrast filled ventricle/atrium or pace maker), 3) massive calcium (calcium score > 1000 for a single artery), and 4) small vascular diameter (vessel diameter <1.8 mm) (Study IV).

Coronary artery segments were classified as significantly stenosed (diameter reduction ≥50%) or normal by visual estimation. Each vessel was analysed on at least two plane. The datasets were analyzed in consensus by two different radiologists who were blinded to the results of CCA and MRI. MDCT results were compared with conventional coronary angiographic findings regarding location and degree of coronary artery stenoses (Studies III-IV).

In addition, in Study III, stenotic lesions were evaluated according to density. Density under 130 HU was categorized as soft plaque containing lipid or fibrotic material, and density over 130 HU as a calcified lesion.

5.10 Combined data analysis

Sectors 1 and 6 were assigned to LAD, sectors 2 and 3 to LCX, and sectors 4 and 5 to RCA (Figure 5).

We combined regional MDCT-CA findings with those of MRI. We compared calcified and fibrous or fatty calcified coronary artery stenoses detected with MDCT-CA to LV wall motion at rest, perfusion defects during stress, and myocardial infarctions seen with MRI. We analyzed how calcifications and stenoses in the main coronary arteries predicted regional LV dysfunction, affected perfu-

sion in the myocardium, and correlated with infarction scar in the territory of the calcified and/or stenosed vessel. Calcium depositions in each artery were estimated as significant or not significant. In addition, the total calcium burden of the coronary tree and stenoses was calculated as described earlier (Study III).

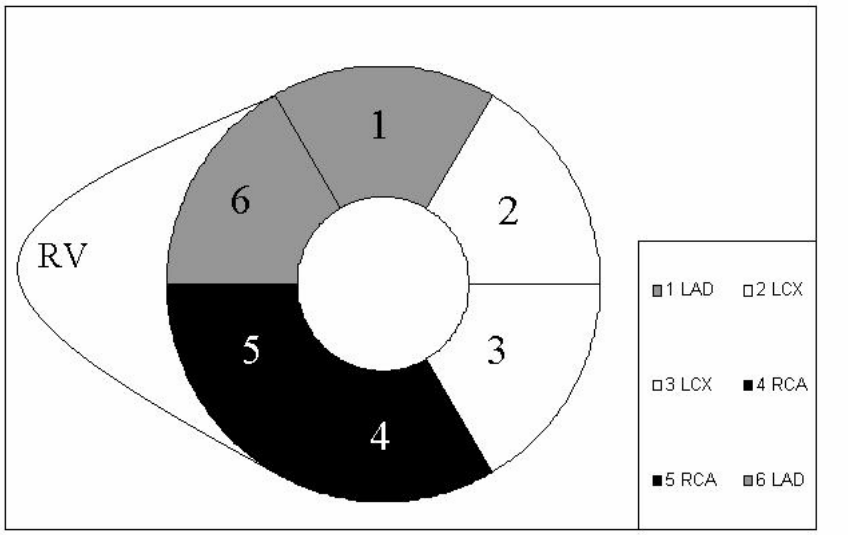

Figure 5.

Myocardial sectors

Diagram illustrating which regions of the left ventricular (LV) myocardium are assigned to the main coronary arteries. RV=right ventricle.

5.11 Reference methods

Conventional coronary angiography

Cardiac catheterization and contrast-enhanced x-ray coronary angiography were performed according to standard protocols. The images were interpreted by experienced angiographers. The level and degree of stenoses in the main branches of the coronary arteries were visually estimated, and reduction in coronary artery diameter of more than 50% was considered significant. (Study II and IV)

5.12 Statistical analysis

Comparison of LV diastolic volume, ejection fraction, cardiac output, regional diastolic wall thickness and systolic wall thickening between pre- and postoperative values was performed with paired t-tests. A significance level of $p<0.05$ was used (Study I).

Statistical data analysis was performed with SPSS version 11.5 software (SPSS, Inc., Chicago, IL, USA). All continuous data are presented as mean ± standard deviation. The significance of the difference between the groups was determined with the Mann-Whitney U-test. A two-tailed p-value ≤ 0.05 was considered statistically significant. Receiver-operating characteristic (ROC) curves were created to assess the performance of the parameters in the optimal channels. The results are given as the area under the ROC curve (AUC%) (Study II).

Variables were presented as mean ± standard deviation. The sensitivity, specificity, and diagnostic accuracy for the blinded detection of stenoses using MDCT were evaluated (Studies III and IV).

Comparison with stenoses and LV motion / myocardial perfusion in corresponding sectors were performed using Fischer´s exact test, and percentages were calculated in the cross tabulation report. All tests were two-sided, and a value of $p<0.05$ was considered indicative of statistical significance (Study III).

6. RESULTS

6.1 Effects of TMLR (Study I)

TMLR did not improve global LV function in our patients. Mean diastolic volumes before treatment were 158±37 ml and after treatment 166±61 ml (p=0.622) (Figure 6). There was no significant improvement occurred EF; mean value was 53±12% before TMLR and 50±17% after the procedure (p=0.376). Mean cardiac output, which was 4.19±0.88 l/min before and 4.33±0.37 l/min after the operation (p=0.658), did not change significantly.

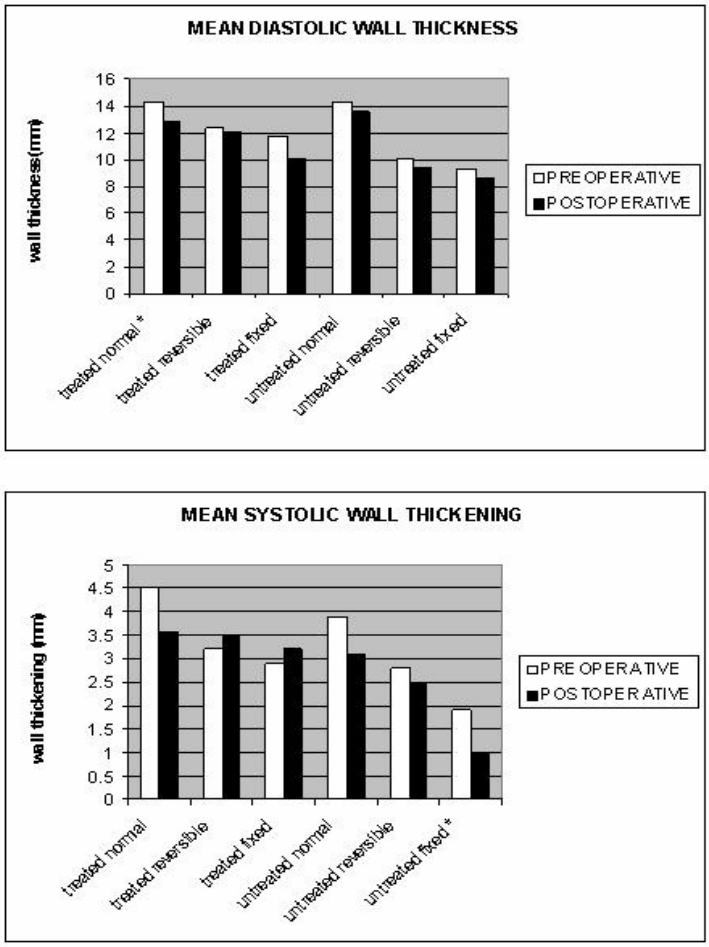

Figure 6.

Mean diastolic wall thickness and systolic wall thickening in treated (lateral and anterior) and untreated (septal and inferior) segments before and six months after transmyocardial laser revascularization (TMLR). Diastolic wall thickness in normally perfused treated segments decreased significally after treatment (p=0.01). Systolic wall thickening remained unchanged in treated segments with fixed defects after the procedure but it decreased in untreated fixed defects* (p=0.03).*

Systolic wall thickening increased in treated segments with reversible and fixed perfusion defects, although the change was not statistically significant. In untreated segments with reversible and fixed

defects, systolic wall thickening decreased. In segments with fixed defects, this decrease was statistically significant (p=0.03). We found no improvement of myocardial perfusion assessed by thallium perfusion SPECT (Figure 7).

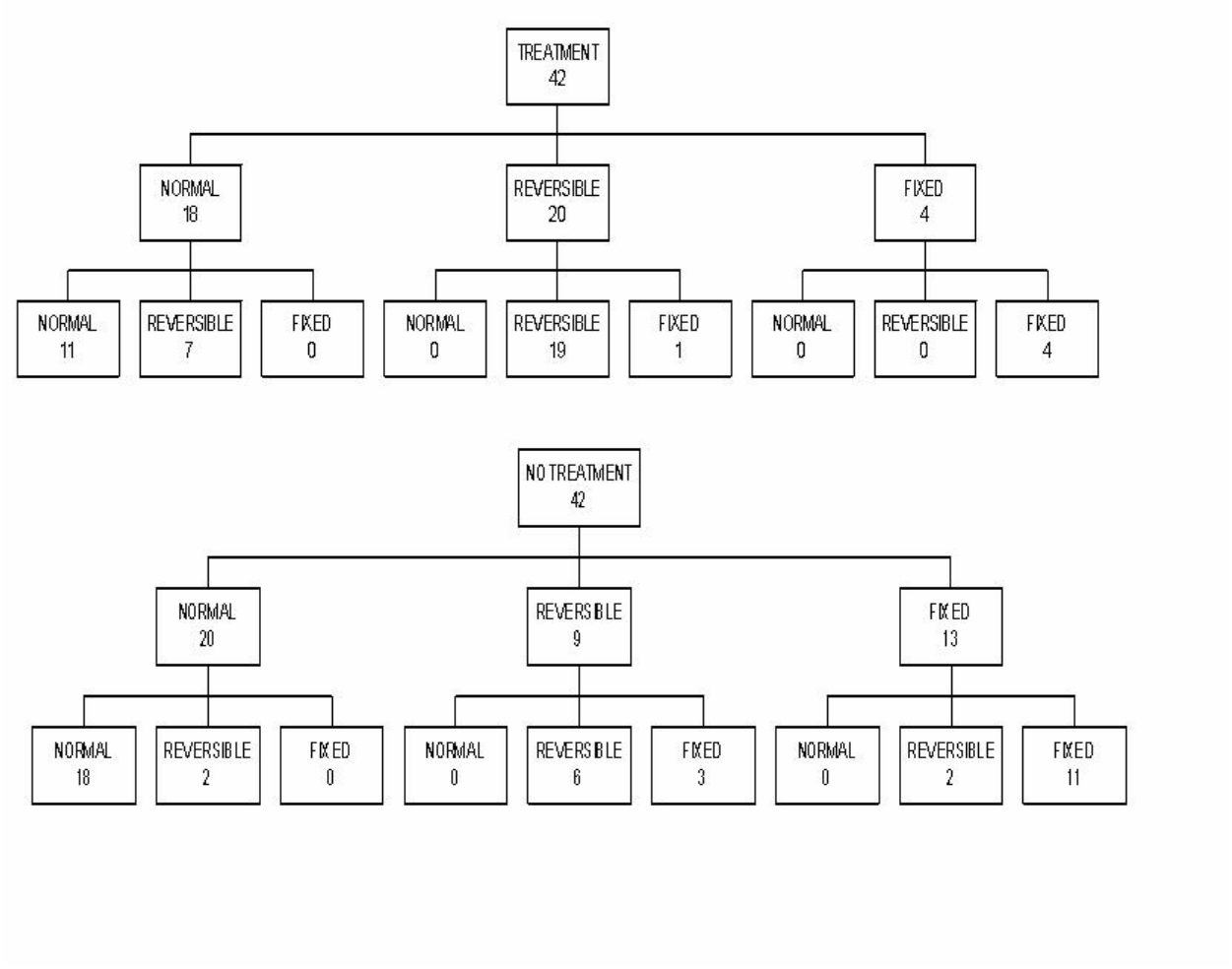

Figure 7.

Myocardial perfusion in thallium perfusion SPECT in treated (anterior and lateral) and untreated (septal and inferior) segments before and six months after transmyocardial laser revascularization (TMLR). Sections were divided into three groups (normal tissue, reversible defect, and fixed defect) on the basis of perfusion at stress and at reinjection. In the normal group, segmental intensity was >75% at stress and at reinjection, in the reversible defect group intensity was ≤75% at stress and >75% at reinjection, in the fixed defect group intensity was ≤75% at stress and at reinjection.

Without treatment 3/9 segments with reversible defects turned into segments with fixed defects with six months. On the other hand, only one of the 20 treated reversible defects turned into a fixed defect according to thallium SPECT. Laser treatment did not prevent the change from a normal to an ischemic segment.

In the thallium exercise scan 5/8 patients had a greater tolerance of workload (p=0.125) and 6/8 had longer exercise times at maximum workload (p=0.396) six months after TMLR. The test was stopped less frequently for angina symptoms after TMLR (5/8 patients) (Figure 8).

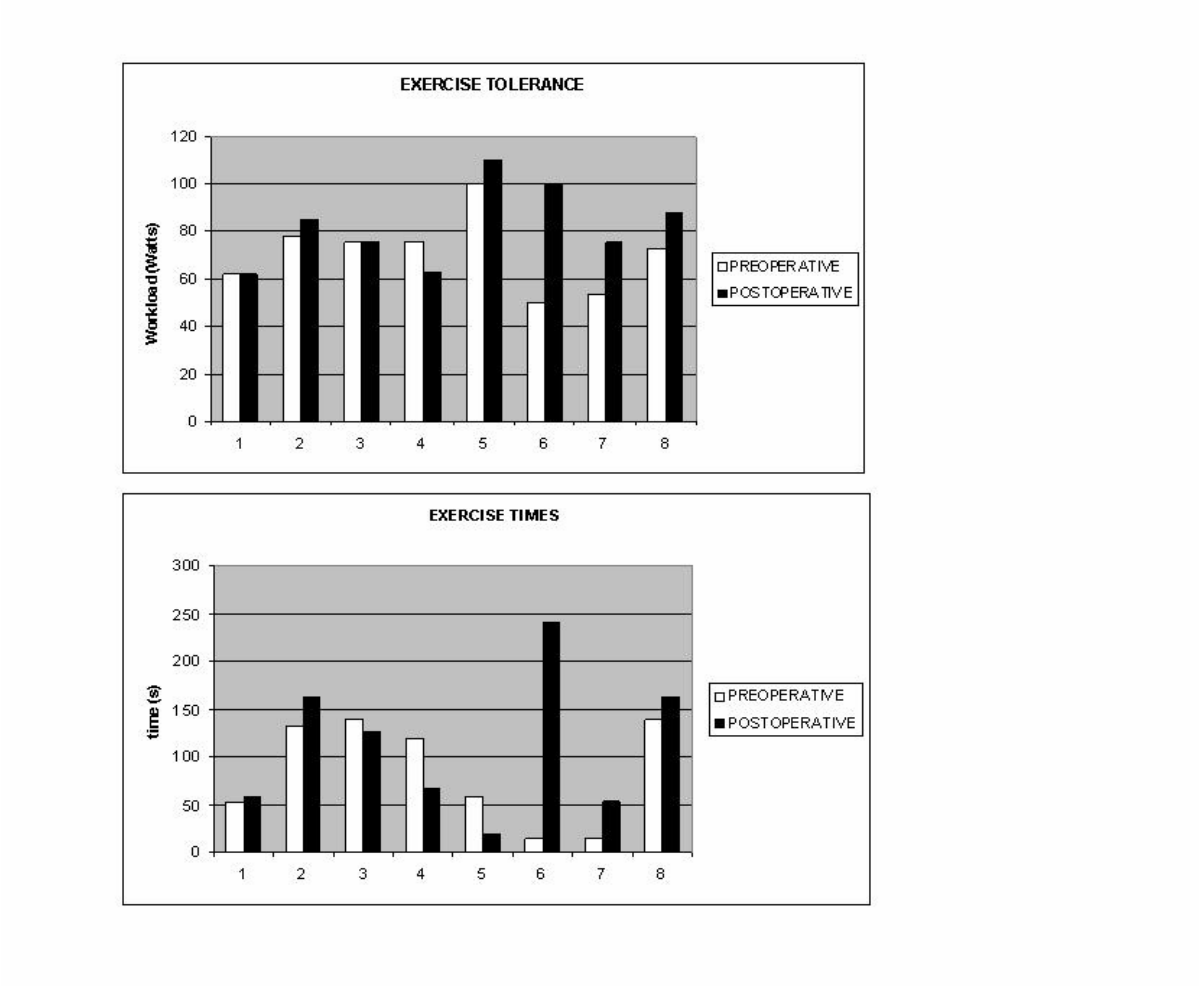

Figure 8.

Workload tolerance and exercise times in the thallium exercise scan before and six months after TMLR. Of the eight patients, five had a greater tolerance of workload and six had longer exercise times at maximum workload six months after TMLR.

Postoperatively improvement in the NYHA functional class was obvious; before the procedure, 3/8 patients belonged to group III, 4/8 to group III-IV, and 1/8 to group IV. Six months after TMRL, five patients belonged to class II, two to class II-III, and one to class III.

6.2 Myocardial infarctions in MRI and MCG (Study II)

Of the 21 MI patients, 11 had MI in only one anatomic region: 1 patient solely anterior, 1 patient solely apical, 3 patients solely lateral, and 5 patients solely inferoposterior MI. The remaining 10 MI patients had multiple MIs in more than one anatomic region. By assigning patients into more than one infarction location subgroup, altogether 9 patients had anterior MI, 10 patients apical MI, 4 patients lateral MI, and 13 patients inferoposterior MI.

Sums of MCG parameters over the mapping region

Depolarization abnormalities in remote MI

QRS area: The QRS area was larger in the MI group than in the controls (MI group 15 ± 5.7 pTs vs. controls 11 ± 3.7 pTs; $p<0.042$). The QRS area also separated the QMI subgroup but not the NQMI subgroup from the controls (QMI subgroup 16 ± 6.7 pTs; $p<0.044$ compared to the controls).

QRS integral: The QRS integral failed to separate the MI groups from the controls. The individual QRS sextiles were not more informative than the whole QRS integral.

Repolarization abnormalities in remote MI

ST-segment integral: The ST-segment integral did not separate the MI group or the NQMI subgroup from the controls. In the QMI subgroup the ST-segment integral was more negative than in the controls (QMI subgroup –1.5 ± 1.8 pTs, controls –0.3 ± 1.2 pTs; $p=0.037$). The MI group and the

NQMI subgroup, however, showed a trend similar to the QMI subgroup but the difference was not significant.

T-wave integral: The T-wave integral did not separate any of the MI groups from the controls.

STT-wave integral: The STT-wave integral did not separate the MI group or the NQMI group from the controls. The STT-wave integral was more negative in the QMI subgroup than in the controls (QMI subgroup –2.8 ± 4.4 pTs, controls 1.5 ± 4.7 pTs; p=0.034). A trend similar to QMI group was found in the MI group and in the NQMI subgroup.

Depolarization and repolarization discordances

QRS-ST discordance: The QRS-ST discordance was larger in the MI group and in the QMI subgroup than in the controls (MI group 16 ± 6.6 pTs, QMI subgroup 17 ± 7.4 pTs, controls 11 ± 3.9 pTs; p=0.020, AUC 70% and p = 0.009, AUC 74%, respectively). The NQMI subgroup showed a similar trend to the MI group and QMI subgroup but the difference was not significant.

QRS-T discordance: The QRS-T discordance was larger in the MI group and in the QMI subgroup than in the controls (MI group 13 ± 8.7 pTs, QMI subgroup 15 ± 8 pTs, controls 5.9 ± 6.2 pTs; p= 0.004, AUC 75% and p = 0.001, AUC 80%, respectively). The NQMI subgroup showed a similar trend to the MI group and QMI subgroup but the difference was not significant.

QRS-STT discordance: The QRS-STT discordance was larger in the MI group and in the QMI subgroup than in the controls (MI group 14 ± 10 pTs, QMI subgroup 17 ± 9.3 pTs, controls 5 ± 1.7 pTs; p=0.003, AUC 76% and p=0.001, AUC 80%, respectively). The NQMI subgroup showed a similar trend to the MI group and QMI subgroup but the difference was not significant.

Optimal recording locations

QRS integral: The MI groups had larger positive integral values over the inferior part of the mapping region and smaller negative integral values over the superior part of the mapping area than the

controls. The QRS integral in optimal sites separated the MI group and the QMI subgroup but not the NQMI subgroup from the controls (AUC 71% for the MI group, 77% for the QMI subgroup).

ST-segment amplitude: The MI groups had smaller negative values over the inferior part of the mapping region, and larger positive values over the superior part of the mapping area than the controls. The ST-segment amplitude in the optimal sites separated all MI groups from the controls (AUC 85% for the MI group, 85% for the NQMI subgroup, and 90% for the QMI subgroup).

T-wave amplitude: The MI groups had smaller negative values over the inferior part of the mapping region, and larger positive values over the superior part of the mapping area than the controls. The T-wave amplitude in the optimal sites separated all MI groups from the controls (AUC 91% for the MI group, 91% for the NQMI subgroup, and 92% for the QMI subgroup).

STT-wave integral: The MI groups had smaller negative values over the inferior part of the mapping region, and larger positive values over the superior part of the mapping area than the controls. The STT-wave integral in optimal sites separated all MI groups from the controls (AUC 91% for the MI group, 90% for the NQMI subgroup, and 92% for the QMI subgroup).

MFM orientation in MI

The QRS angle failed to separate any of the MI groups from the controls. The STT angle was larger in the MI group and in the QMI subgroup than in the controls (MI group 163 ± 119°, QMI subgroup 220 ± 110°, and controls 58 ± 17°; $p=0.006$ and $p<0.001$, respectively). The QRS-STT angle was not significantly different between the MI group or the NQMI subgroup and the controls. The QRS-STT angle was larger in the QMI subgroup than in the controls (QMI subgroup 94 ± 59° and controls 38 ± 46°; $p=0.011$).

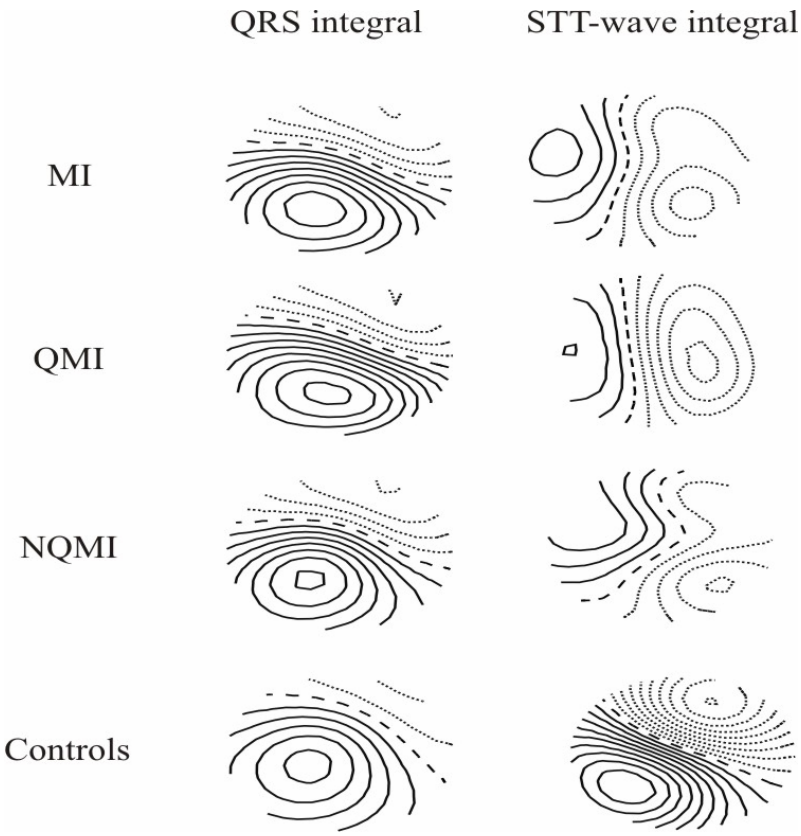

Figure 9 a.

The group mean QRS integral and STT-wave integral magnetic field maps. From top to bottom: the whole myocardial infarction patient group (MI), the Q-wave myocardial infarction subgroup (QMI), the non-Q-wave myocardial infarction subgroup (NQMI), and the healthy controls (controls). The QRS integral maps of all patient groups resemble the map of the controls. On the contrary to QRS maps, the STT-wave integral maps show much more variation in between all the MI groups and the controls. The step between two isocontour lines is 100 pTs. Positive values are denoted by solid lines, negative values by dotted lines, and zero field line by dashed line.

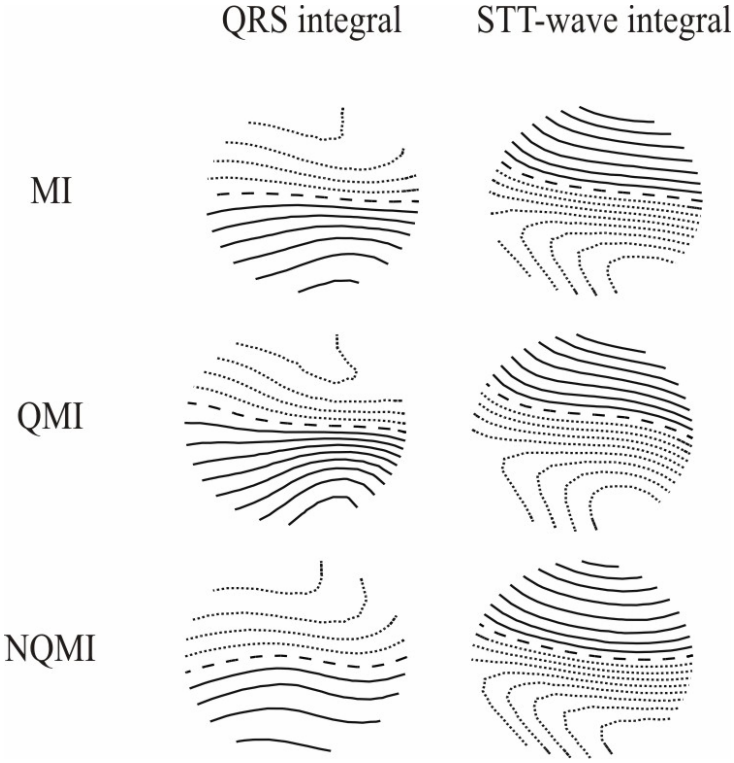

Figure 9 b.

QRS integral and STT-wave integral departure maps. From top to bottom: the whole myocardial infarction patient group (MI), the Q-wave myocardial infarction subgroup (QMI), and the non-Q-wave myocardial infarction subgroup (NQMI). In the QRS integral departure maps, the MI groups had larger positive values over the inferior part and smaller negative values over the superior part of the mapping region than the controls. In contrast, in the STT-wave integral departure maps, the MI groups had larger negative values over the inferior part and larger positive values over the superior part of the mapping region than the controls.

6.3 Assessment of coronary artery disease with MRI and MDCT (Study III)

The MDCT was performed without complications in all patients. A total of 126 (14x9) coronary artery segments were scanned. All the segments were evaluated. The mean scanning time with breath hold was 24 ± 3 (range 19-30) s and the mean heart rate was 56 ± 8 (range 43-70) beats per minute. Ten patients had β-blocker medication and therefore a low heart rate. Four patients had a heart rate of over 70 beats per minute before examination, and they received a β-blocker injection intravenously. The mean total calcium score was 555 ± 1061 (range 0-4009), and the mean calcium volumetric score was 446 ± 808 (range 0-3074) (Table 1).

PATIENT	TCC	CVS
1	65	85
2	362	294
3	852	694
4	205	174
5	4009	3074
6	35	55
7	1280	986
8	113	125
9	0	0
10	3	5
11	91	82
12	508	432
13	191	174
14	54	67
MEAN	555	446

Table 1.

Calcium score.

Calcium scores of all patients based on two different scoring systems, total calcium score (TCS) by Agatston and calcium volumetric score (CVS).

In CCA, a stenosis over 50% was found in 28 segments; 10 in RCA, 10 in LAD, and 8 in LCX segments. Sixteen segments had a stenosis of less than 50%. Six stenoses of over 50% were found in side branches.

In MDCT-CA, 8 lesions (>50%) were detected in RCA, 9 in LAD, and 6 in LCX segments. We found six soft plaques (HU< 130) in the main coronary arteries; three of those caused significant narrowing of the vessel (Figure 10). Significant calcifications in a single main coronary artery were visually detected in eight arteries.

In MDCT-CA, two stenoses in the proximal area of RCA as well as lesion in the distal part of LAD were missed because of massive calcifications. Assessment of lumen in the presence of excessive calcium impaired diagnostic quality since the lumen compromise could not be sufficiently visualized.

Two LCX stenoses were missed because of patients´ irregular heart beat and/or high heart rate (>65 beats per minute) and an artefact due to adjacent structure (overlying vessel or contrast-filled ventricle). Overestimation of stenoses and therefore false-positive lesions in RCA (2) and LAD (4) segments due to severe calcifications.

Compared with CCA, sensitivity was 82%, specificity 94%, positive predictive value 79%, and negative predictive value 95% for significant stenoses (Table 2). Sensitivity was 75%, specificity 69%, positive predictive value 77%, and negative predictive value 73% when evaluation was done by vessel.

A total of 336 (14x24) myocardial sectors were analyzed from MRI pictures. The myocardial sectors supplied by calcified or stenotic arteries observed with MDCT-CA showed regional LV wall dysfunction at rest, perfusion defects at stress, and myocardial infarction on late enhancement images (Figure 11). These changes were also detected in territories related to nonsignificantly stenosed and noncalcified arteries. Late enhancement was detected more often than LV wall dysfunction because five infarctions were only thin and subendocardial.

	RCA	LM/LAD	LCX	TOTAL
SEGMENTS	42	42	42	126
TRUE POSITIVE	8	9	6	23
FALSE POSITIVE	2	4	0	6
FALSE NEGATIVE	2	1	2	5
TRUE NEGATIVE	30	28	34	92
SENSITIVITY	0.80	0.90	0.75	0.82
SPECIFICITY	0.94	0.88	1.00	0.94
POSITIVE PREDICTIVE VALUE	0.8	0.69	1.00	0.79
NEGATIVE PREDICTIVE VALUE	0.94	0.97	0.94	0.95

Table 2.

Sensitivity and specificity of multidetector computed tomography coronary angiography (MDCT-CA) compared with conventional coronary angiography (CCA).

RCA=right coronary artery, LM=left main artery, LAD=left anterior descending artery, and LCX=left circumflex artery.

Figure 10.

Coronary artery stenosis detected with MDCT-CA

A 39-year-old man with one-vessel coronary artery disease. Multiplanar multidetector reconstruction shows that the right coronary artery has a significant (>50%) stenosis and a soft plaque also causing significant narrowing of the lumen.

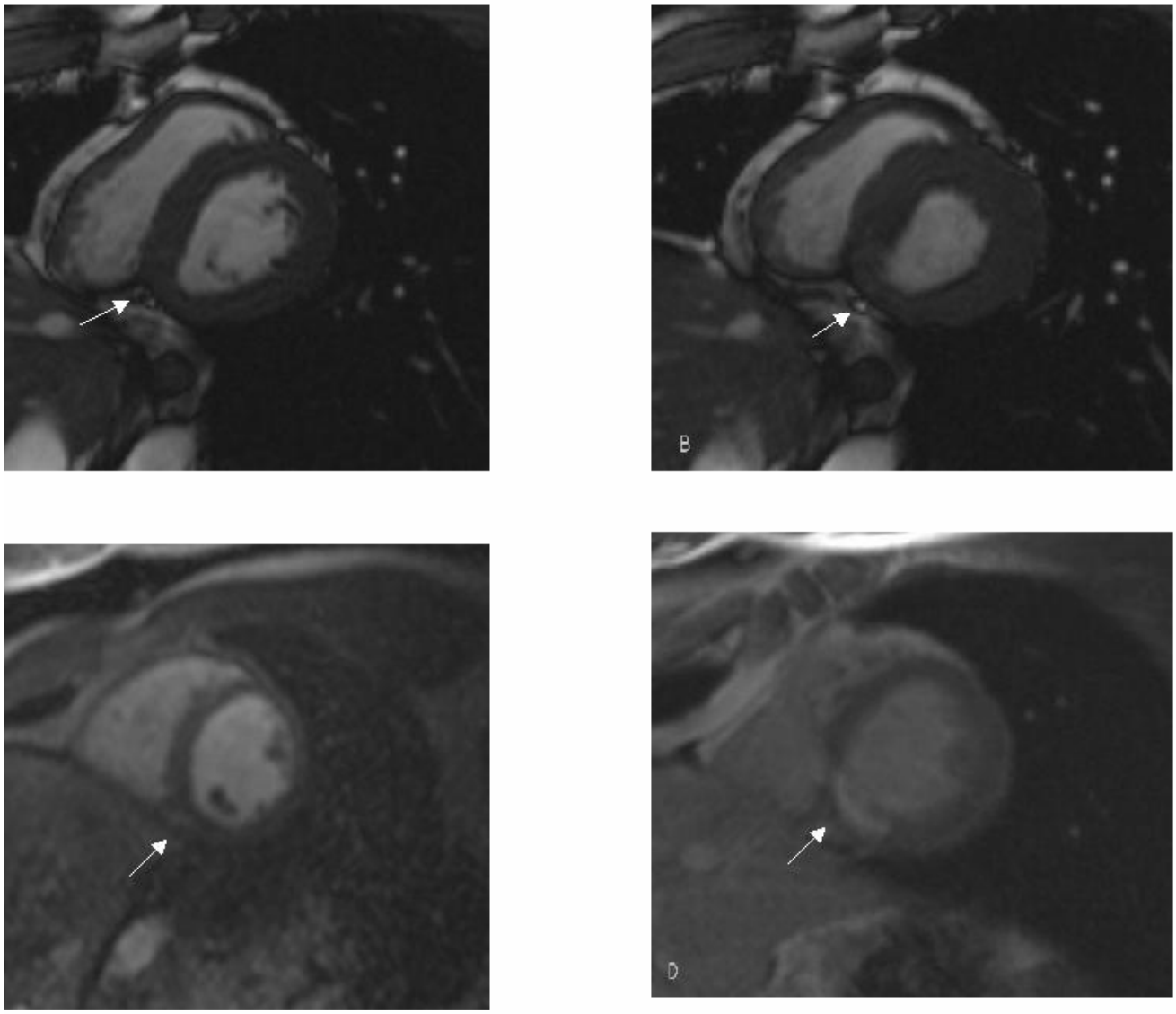

Figure 11.

Left ventricular hypokinesia, perfusion defect and infarction evaluated with MRI

MRI short-axis views of the left ventricle of a 39-year-old patient with one-vessel coronary artery disease. TrueFISP cine MRI (a.diastole; b systole) in short-axis view shows hypokinesia of sector 5.

In stress induced first-pass imaging (saturation recovery prepared turboFLASH sequence) perfusion defect is seen in the sector 5 (c). Late enhancement image (inversion recovery turboFLASH sequence) shows a transmural infarction in the same area (d).

CORONARY ARTERIES RCA/LM/LAD/ LCX	LV wall dys-function	Perfusion defect	Infarction
Only massive calcifications	50% 7/14	71% 10/14	57% 8/14
Only significant stenosis (>50%)	50% 9/18	78% 14/18	56% 10/18
Calcifications and significant stenosis	60% 6/10	80% 8/10	60% 6/10
Artery without significant (>50%) stenosis	31% 10/32	63% 20/32	50% 16/32

Table 3.

Combined results of MDCT-CA and MRI

Despite the coronary artery being classified as normal in CCA, LV wall dysfunction was observed in 5/10, perfusion defect in 3/10, and infarction in 7/10 corresponding myocardial sectors.

High and irregular heartbeat impaired image quality in MDCT-CA and caused misinterpretation of significant stenoses in two lesions. LV wall dysfunction and perfusion defect were observed in two sectors assigned to this artery. Because of massive calcifications, we missed three stenoses, which resulted in perfusion defect in 3 corresponding sectors and infarction in 2 sectors.

In five cases, the dominant main coronary artery was found to be stenosed in MDCT-CA. In these patients, LV wall dysfunction was observed in 5/7, perfusion defect in 9/11, and infarction in 4/6 sectors adjacent to the assigned sectors.

In CCA, stenoses under 50% were found in 16/32 segments, which were classified in MDCT-CA as not significantly stenosed. LV wall motion dysfunction was detected in 8/16, perfusion defect in 10/16, and infarct in 4/16 sectors assigned to these arteries with stenosis less than 50%. Stenoses in side branches evaluated with CCA (n=6) resulted in LV wall dysfunction and perfusion defect in three myocardial sectors, and infarction was detected in one sector.

In Fisher´s exact test, these combined results were not statistically significant.

6.4 Eight-row MDCT evaluation of significant coronary artery disease in patients with severe aortic valve stenosis (Study IV)

The MDCT was performed without complications in all patients. A total of 322 coronary artery segments were scanned. The mean scanning time with breath hold was 22 ± 3 (range 20-29) seconds. Fifty-six percent of patients received pre-scan intravenous B-blockers, resulting in a mean heart rate of 62 ± 8 (range 49-75) beats per minute. Two patients had a pacemaker.

The total calcium scores (TCS) were 1068 ± 1709 (range 0-7377) and calcium volumetric scores (CVS) were 866 ± 1302 (range 0-5601) (Table 4).

Overall visibility of coronary segments by MDCT-CA was 70%. Of 322 segments 224 were assessable for stenosis. A total of 98 segments of coronary arteries were nonassessable because of motion artefacts (Figure 12), disturbing adjacent structures, massive calcium depositions (Figure 13), and small vessel size (Table 5).

PATIENT	TCS	CVS
1	574	515
2	25	31
3	6	12
4	837	791
5	0	0
6	899	764
7	998	803
8	7377	5601
9	165	174
10	1497	1229
11	312	346
12	361	304
13	166	130
14	268	277
15	2029	1599
16	343	382
17	3711	3010
18	739	618
19	844	702
20	3384	2566
21	9	13
22	0	0
23	37	53
MEAN	1069	866

Table 4.

Calcium scores. *TCS=total calcium score, CVS=calcium volumetric score.*

ARTERY	MOTION ARTIFACT	ADJACENT STRUCTURE	MASSIVE CALCIUM	VESSEL SIZE
LM=2	1 (50%)	-	1 (50%)	-
LAD=12	3 (25%)	-	7 (58%)	2 (18%)
LCX=26	7 (27%)	4 (15%)	12 (46%)	3 (11%)
RCA=26	11 (42%)	4 (15%)	7 (27%)	4 (15%)
SIDE BRANCHES=32	8 (25%)	6 (19%)	10 (31%)	8 (25%)
ALL=98	30 (31%)	14 (14%)	37 (38%)	17 (17%)

Table 5.

Causes of nonassessable segments of coronary arteries.

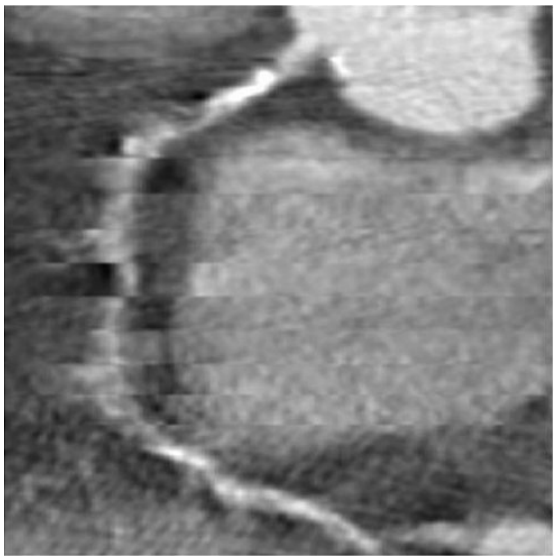

Figure 12.

Motion artifacts cause discontinuity between consecutive slices and inhibit correct analysis of significant stenoses. This was seen most often in evaluation of the right coronary artery.

Figure 13.

A 68-year-old man with a calcium score of 7377/5601. Massive calcium depositions impaired the diagnostic quality.

31 % of our patients and 50% those of with typical angina had significant CAD. In CCA, 19 stenotic lesions were found; 5 lesions were in RCA, 2 in LM, 3 in LAD, 4 in LCX segments, and 5 in side branches. In MDCT-CA 6 lesions were detected in RCA, 2 in LM, 9 in LAD, 3 in LCX, and 3 in side branches (Figure 14). In MDCT-CA, 7 lesions were missed despite sufficient image quality. These included 2 stenoses in the middle area of RCA, 3 LCX stenoses, and 2 lesions in side branches were missed. Eleven segments were incorrectly classified as significantly obstructed because of overestimation of lesion severity, mostly as a result of massive calcifications. False- positive lesions in MDCT-CA were detected in RCA (n=3), LAD (N=6), and LCX (N=2).

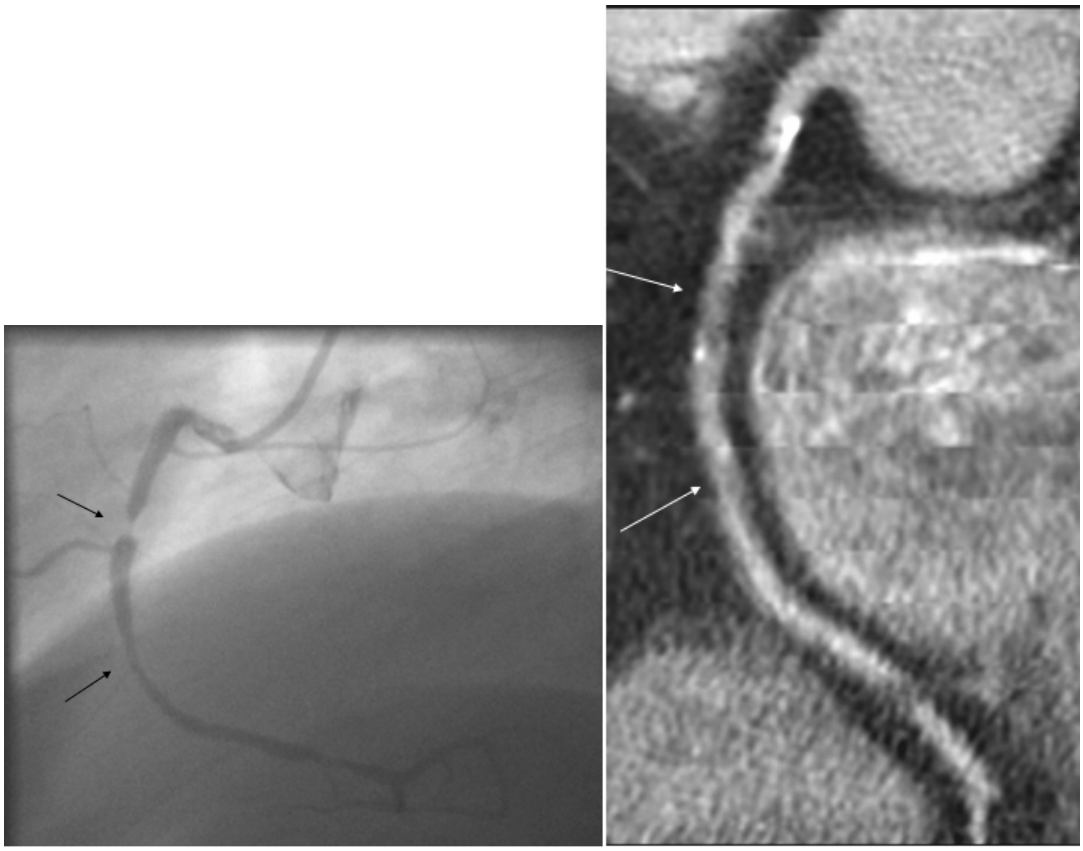

a) **b)**

Figure 14.

A 48-year-old man with one-vessel coronary artery disease. Conventional coronary angiography (CCA) (a) and multiplanar multidetector computed tomography (MDCT) reconstruction (b) shows the right coronary artery with significant stenosis in the proximal part and narrowing of the lumen (<50%) in the distal part. MDCT shows soft plaques in the stenotic areas.

Concerning angiographically diagnosed CAD**,** for all vessels including nonvisible and nonassessable ones MDCT-CA showed a sensitivity of 63%, and a specificity of 96%, a positive predictive value of 52%, and a negative predictive value of 98% (Table 6). For proximal vessel segments, sensitivity was 88%, specificity 96%, positive predictive value 70%, and negative predictive value 99%. With respect to correct diagnosis per patient 15 patients out of 23 (65%) were correctly diagnosed using MDCT. When evaluating only proximal segments, 20 (87%) patients were correctly diagnosed.

	LM	LAD	LCX	RCA	Side branches	All	All evaluable segments	All proximal segments	Proximal evaluable segments
SEGMENTS	23	69	69	69	92	322	243	92	89
TRUE POSITIVE	2	3	1	3	3	12	12	7	7
FALSE POSITIVE	0	6	2	3	0	11	11	3	3
FALSE NEGATIVE	0	0	3	2	2	7	7	1	1
TRUE NEGATIVE	21	60	63	61	87	292	213	81	78
SENSITIVITY	1.00	1.00	0.25	0.60	0.60	0.63	0.63	0.88	0.88
SPECIFICITY	1.00	0.91	0.97	0.95	1.00	0.96	0.95	0.96	0.96
POSITIVE PREDICTIVE VALUE	1.00	0.33	0.33	0.50	1.00	0.52	0.52	0.70	0.70
NEGATIVE PREDICTIVE VALUE	1.00	1.00	0.95	0.97	0.98	0.98	0.97	0.99	0.99

Table 6.

Sensitivity and specificity of multidetector computed tomography coronary angiography (MDCT-CA) compared with conventional coronary angiography (CCA).

7. DISCUSSION

Cardiac magnetic resonance imaging continues to develop and advance. SPECT perfusion imaging has been considered the reference method for evaluation of nonviable myocardium, but MRI can accurately depict structure, function, effusion, and myocardial viability, with an overall capacity unmatched by any other single imaging modality. MRI is an accepted and widely utilized tool for cardiovascular research, and its clinical use is also increasing (33). MCG reveals information complementary to body surface ECG in patients with ischemic heart disease (71). MDCT-CA is a promising noninvasive technique for detection of coronary stenoses (121). Recently, it was demonstrated that detection of calcified and noncalcified plaques in the coronary arteries of patients with suspected CAD is feasible MDCT (14).

7.1 Assessment of coronary disease with MDCT

Invasive imaging techniques, especially selective CCA, has remained vital to planning and guiding catheter-based and surgical treatment of significantly stenotic coronary lesions, but in selected patient groups CAD diagnosis should be obtained with a noninvasive method to prevent unnecessary cardiac catheterizations. Previous studies have demonstrated that both echocardiography and nuclear perfusion imaging, using pharmacological stress testing, are sensitive and safe methods, but resting or exercise-induced regional wall motion abnormalities are only nonspecific markers for CAD, and some studies have shown low specificity of thallium SPECT (11, 70, 136).

Several recent studies have demonstrated that MDCT-CA allows imaging of coronary artery stenoses, coronary calcifications (3, 49, 89, 90, 92, 93, 98, 120, 130, 131, 156, 185), and even differentiation of plaque morphology with high spatial and temporal resolution (90, 91, 132, 169).

The main objectives of Studies III and IV were to determine the accuracy of MDCT in detecting significant stenoses in the main coronary arteries and excluding of angiographically significant CAD in patients with known CAD (Study III) and in patients with AS (Study IV).

Among patients with AS, the prevalence of CAD is 40-50% in those with typical angina, 25% in those with atypical chest pain, and 20% in those without chest pain (24, 38, 52, 123). In one study, coexisting CAD was observed even in up to 60% of patients with aortic stenosis (173). These findings are in accord with ours; 31% of our AS patients and 50% of those with typical angina had significant CAD. On the other hand, in some patients no evidence of angina pectoris was found, but severe calcifications, significant stenoses, and soft plaques were present.

It is important to determine whether angina in patients with aortic stenosis is due to the valve lesion or to coexisting CAD. They can be treated simultaneously by combining aortic valve replacement with coronary artery bypass grafting (74, 140).

7.1.1 Calcium scoring

Calcium screening with CT is the most sensitive and noninvasive modality to detect coronary atherosclerosis.

Calcified deposits within the coronary arteries have been shown to be an independent predictor of CAD. Finding no coronary calcifications would exclude the severe CAD with a high probability; however, with the advent of contrast-enhanced CT of coronary arteries, noncalcified vessel lesions and other stages of the disease, reflected by e.g. lipid-rich plaques, become visible (12).

The conventional method of quantifying the extent of coronary artery calcification, introduced by Agatston and Janowitch (5), is limited by the lack of a physical gold standard by which to determine the accuracy and precision of coronary artery calcium measurements. Various approaches, including coronary artery calcium area, volume, and mass, have been explored in an effort to improve the accuracy, precision, and portability of coronary artery calcification measures. There is considerable

agreement that calcium mass is the most accurate method. We used both methods to calculate total calcium score for each patient. Most of our patients had advanced CAD or combined CAD and severe AS and therefore had fairly high calcium scores (range 0-7000) (Studies III and IV).

According to the most recent guidelines of AHA, the quantity of coronary calcium is related to the likelihood of significant CAD (192). Calcified plaques are probably the result of repetitive plaque rupture and healing, causing shrinkage of the vessel lumen with subsequent stenosis (132). Alternatively, in the presence of vessel wall calcifications, blood turbulence leads to shear stress and a higher probability of soft plaque ruptures (37).

7.1.2 Plaque imaging

CT angiography is a promising tool for a noninvasive detection and characterization of advanced types of atherosclerotic coronary lesions with or without calcifications (14). Examining coronary artery plaques by contrast-enhanced MDCT offers the possibility of noninvasively detecting complex plaque morphology and of detecting earlier stages of coronary atherosclerosis (132).

CT angiography allows to further differentiate components of coronary atherosclerosis, such as thrombus, lipids, and fibrous and calcified lesions (90, 91, 108, 185). The density of these noncalcified lesions has been reported to be between 0 and 130 HU according to the content of lipid and fibrotic tissue, as revealed by histopathology or intravascular ultrasound. Noncalcified plaques with densities below 50 HU contain higher amounts of lipids, whereas fibrotic lesions typically have densities between 50 and 130 HU (132). We differentiated calcified, fibrotic, and lipid-containing lesions causing narrowing or significant stenoses in coronary arteries. In Study IV, we found 13 soft plaques with densities varying from 0 to 124 HU. Some of these were not detected or considered as stenotic lesions in CCA.

In a meta-analysis, 68% of patients that experiencing a myocardial infarction were demonstrated not to have any significant stenoses in their coronary angiograms within the last six months. Only 18% had significant stenoses and the remaining 14 % high-grade stenoses (>70 diameter reduction) prior

to their cardiac event. This indicates that before the event vulnerable plaques need to be present (180).

The gold standard for the assessment of coronary atherosclerosis is intravascular ultrasound. However, this method is highly invasive and not suitable for the investigations of asymptomatic patients (108, 132). Evaluation of plaque morphology would be therefore one benefit offered by MDCT because earlier stages of atherosclerosis without calcifications can contain these vulnerable plaques that may rupture, thrombose, and cause sudden cardiac events, such as unheralded myocardial infarction or death (132).

7.1.3 Evaluation of stenoses

Conventional invasive coronary angiography is the clinical gold standard for detecting coronary artery stenoses. However, the small risk of serious events, discomfort for the patient, and hospitalization have prompted the search for noninvasive methods. MDCT is a promising noninvasive technique for detecting obstructive epicardial CAD.

In our study, of patients with known CAD or AS, MDCT as compared with CCA yielded a sensitivity of 82% and 63%, a specificity of 94% and 96%, a positive predictive value 83% and 52%, and a negative predictive value 89% and 98% (Studies III and IV). Respectively, in other studies, sensitivity of 68-93%, specificity of 89-99%, positive predictive value of 66-84%, and negative predictive value of 89-98 % have been reported (49, 89, 90, 92, 93, 130, 131, 156). A sensitivity of 90% and specificity of 99% was found when evaluated with eight-slice MDCT-CA (116).

The newest 64-slice CT scanners have a shorter scan times and a higher spatial resolution but also a higher temporal resolution compared with previous scanner generations. Significant coronary stenoses can be detected with the latest 64-slice CT scanner with a sensitivity of 94-99% and a specificity of 95-97%, positive predictive value of 76-97%, and negative predictive value of 92-99% compared with CCA (43, 109, 122).

Several factors are known to impair image quality and interpretation, with severe calcifications and higher heart rates at the top of the list. Patients with advanced CAD frequently have more coronary calcium than patients in whom MDCT is used as a first-line test. As in our study, this renders MDCT imaging of the coronary arteries of patients with advanced stages of CAD more difficult (98).

Massive calcium depositions

Assessment of lumen in the presence of massive calcium impaired diagnostic quality because the lumen compromise could not be sufficiently visualized. Calcifications are high-density structures causing beam-hardening artifacts and partial volume effects on computed tomography (120). We had fairly high calcium scores for most patients, making correct analysis more difficult or even inhibiting evaluation of these segments. Over 61% of our patients had score over 300. Calcium score under 300 has been assumed to be suitable for MDCT (89, 90). In our study, arteries with calcium score over 1000 were classified nonassessable. However, Kitamura and colleagues concluded that coronary artery calcification and calcium score determined by MDCT were associated with coronary arteries with severe stenosis (82).

Heart rates

Artifacts due to elevated heart rates were the main cause of degraded image quality, found to inhibit correct analysis in several other studies (49, 98, 170). A maximum of heart rate of 63-65 beats per minute has been suggested by some authors (90, 92, 98, 170). Heart rates of over 65 beats per minute yielded unsatisfactory results also in our study. Despite the finding that proximal vessel segments were visualizable in almost all patients, lowering of the patient heart rates below 65 beats per minute before undergoing MDCT-CA is advisable to achieve the best image quality (90, 170). In our study, β-blocker was used routinely when heart rate was over 65 beats per minute, but despite adequate medication, heart rates of nine patients exceeded this cut-off value (Study IV).

We also found that a large range in heart rate alteration affected image quality. This is consistent with the evaluations of Maruyama et al. with eight-slice MDCT (116).

Cardiac motion

Many coronary arteries were nonassessable because of cardiac motion artefacts. The middle part of RCA and the distal parts of LCX are the most vulnerable to motion, which results in discontinuity between consecutive slices. Optimal positioning of the image reconstruction window seems to be crucial in achieving optimal image quality. Each of the coronary arteries is known to have a different motion pattern during the cardiac cycle (49). In our studies, images of the RCA were most frequently of sufficient quality earlier in the cardiac cycle than those of LAD and LCX arteries.

Adjacent structures, small vessel size, and non-cardiac motion

Other reasons for degraded image quality include noncardiac motion artifacts (116). Two studies have reported that blending with overlying vessels led to false-positive interpretations (116, 130). In Study IV, a vessel diameter of under 1.8 mm was unassessable. Vessels smaller than 1.6 mm in diameter could not be properly judged with any visualization technique Vogl et al. (195). However, this is not of particular significance when only significant stenoses are being evaluated since smaller segments are rarely considered for revascularization (90, 131, 170).

Limitation of eight-row MDCT has earlier been documented to be low visibility of LCX, which is in accord with our findings. In our evaluation, high heart rate as well as heart rate alteration, adjacent structures, and small vessel diameter caused nonassessable segments mainly in LCX. RCA was mostly affected by cardiac motion, which is in agreement with the studies by Nieman et al. (130, 131).

7.2 Assessment of global and regional LV function

In patients with ischemic heart disease, one of the most important determinants of long term survival is the level of left ventricle (LV) dysfunction. It is important to recognize, however, that not all dysfunction of the LV is irreversible and presents with an infarction. LV function can improve following revascularization procedures, such as percutaneous coronary angioplasty (PTCA) and coronary artery bypass grafting (CABG) (79). The cine MRI is capable of visualizing abnormalities into global and regional wall motion and systolic thickening of the LV with a excellent of spatial and temporal resolution. However, except for high-grade coronary artery stenosis, abnormalities can for the most part only be identified only under stress conditions.

The purpose of Study I was to evaluate the effect of transmyocardial laser revacularization (TMLR) on global function, left ventricular (LV) wall thickness, and systolic wall thickening with cine MRI and on myocardial perfusion with thallium myocardial perfusion SPECT.

Ejection fraction (EF) is the most commonly used parameter of systolic function in clinical practice. However, it is a measure of LV performance and does not take into consideration regional contractile dysfunction, as is frequently seen with ischemic disease and primary myocardial disease (33). Myocardial wall thickening is useful measurement for regional function. In Study I, we evaluated both EF and mean diastolic thickness and wall thickening of the myocardium. No significant improvement was observed in ejection fraction after TMLR. We used a combination of segmental perfusion and wall thickening analysis to establish that laser treatment preserved systolic wall thickening in segments with reversible and fixed defects. While TMLR did not improve LV function, the procedure prevented worsening of wall motion in ischemic or scarred areas. Several observations have been made in animal models of ischemia that laser treatment improves LV systolic and diastolic function evaluated with MRI (32, 125, 126). Laham et al. have reported on the use of MRI to investigate the TMLR effect of the Holmium YAG laser. In this small (n=15), open-label

study, the authors reported significantly improved target wall thickening and wall motion at 30 days and 6 months, but no improvement was seen with SPECT imaging. The authors observed that MRI may be a promising modality for the demonstration of a true revascularization effect (102). In most patient studies, the improvement of LV function has not been as obvious, which is in agreement with our findings. Two research groups did not observe any changes in global or regional ventricular function after TMLR in regional wall motion analysis evaluated with dobutamine echocardiography (4, 27). A decrease in LV of left ventricular ejection fraction and an increase in LV end-diastolic volume were detected with radionuclide ventriculography, SPECT, and MRI (2).

In Study III, cine MRI was used to evaluate regional LV wall motion. The assessment of regional LV function with cine MRI requires a standardized section positioning. Imaging of the central three of five selective short-axis sections positioned between the mitral valve annulus and the apex in systolic long-axis views leads to accurate and reproducible basal, midcavity, and apical short-axis sections.

There was a good reproducibility of the selected intersection gap ($r=0.89$, $p<0.001$) measured mid-cavity section with end-diastolic diameters in the vertical ($r=0.83$, $p<0.001$) and horizontal ($r=0.85$, $p<0.001$) long-axis orientations (118).

First-pass and late enhancement studies were done simultaneously. Segments supplied by the different main coronary arteries were graded as normokinesia or dysfunction. We found that calcifications and significant stenoses in the main coronary arteries caused LV wall dysfunction at rest in 50% of corresponding sectors. If the main coronary artery had both calcifications and significant stenosis, LV motion dysfunction was detected in up to 60% of sectors assigned to this artery. On the other hand, LV wall dysfunction was also found in 30% of sectors supplying for not significantly stenosed coronary artery. This indicates that not all dysfunction of the LV presents significant stenosis or calcifications in the corresponding main coronary arteries. Stenoses below 50%, soft plaques, and dominance of the main coronary arteries significantly affect myocardial kinetics. By

combining contrast- enhanced MRI with cine studies, we are able to get even more information about viability and can differentiate hibernating myocardium from persistently nonviable myocardium.

7.3 MR first-pass studies

Clinical studies suggest that magnetic resonance first-pass perfusion imaging is comparable with current diagnostic tests currently used clinically for the assessment of myocardial perfusion (194). In the cascade of myocardial events during progression of ischemia, subendocardial perfusion defects are probably the earliest-documented defects, followed by transmural perfusion defects. Ideally, the perfusion study should be performed both at rest and under pharmacological stress. Wall motion abnormalities are a later feature, eventually presenting as diastolic and systolic dysfunction (147). Myocardial perfusion measurements can be combined with an evaluation of global function and regional wall thickening (194).

In Study III, we studied stress-induced myocardial contrast enhancement at first-pass. Calcifications resulted in perfusion defect in 71 % and significant stenoses in 78% of sectors assigned to these arteries. We used only stress first-pass imaging, which may show regions of artifactually low signal intensity. These could have been avoided by comparing results with rest first-pass studies. We evaluated perfusion defects by visual estimation. Qualitative image interpretation requires an experienced reader and may be subject to observer bias. Most previous studies have been done by assessing first-pass enhancement slope or myocardial perfusion reserve semiquantitatively or quantitatively. Nevertheless, we combined regional wall motion analysis and delayed enhancement with stress induced first-pass imaging, which increases specificity.

Reduction of myocardial perfusion is a sensitive indicator of myocardial ischemia because myocardial blood flow is directly correlated to myocardial oxygen supply. One group found that myocar-

dial perfusion reserve after dipyridamole infusion resulted in highly significant differences between myocardial segments supplied by stenotic coronary arteries and nonstenotic arteries. They concluded that MR perfusion imaging can be used to detect coronary artery stenosis with diagnostic accuracy (6). Based on reports by other investigators, myocardial perfusion on MR first-pass images suggests preserved or only reduced perfusion in regions supplied by competitive collateral vessels or retrograde filling of coronary vessels with subtotal occlusion. In these collateral-dependent myocardial regions and in healed infarctions, nuclear tests often suggest fixed defect, whereas MR first-pass is able to detect the preserved blood flow supplied by collateral vessels (193, 194). In addition, perfusion imaging demonstrates the effectiveness of coronary interventions (7). Lauerma et al. reported an increase of the maximal intensity slope in a group of 11 patients with proximal single-vessel stenosis of left anterior descending artery three months after PTCA or surgical revascularization (107). This result is in is agreement with that of Manning et al. Myocardial perfusion reserve (MPR) index in ischemic segments improved significantly after successful angioplasty but did not normalize when compared with nonischemic control segments of patients with single-vessel disease (115).

Delayed hyperenhancement of dysfunctional myocardium may be used to predict lack of mechanical improvement or nonviability, whereas a lack of hyperenhancement can be correlated with improvement of regional contractility or viability after revascularization. Hypoenhancement during first-pass did not serve as a reliable criterion of viability (163). One study reported, that compared with lack of early hypoenhancement, lack of delayed hyperenhancement had better diagnostic accuracy in predicting functional improvement in dysfunctional segments. Early hypoenhanced regions, which represent only the fraction of infarcted tissue with concomitant microvascular obstruction, greatly underestimate the amount of irreversibly injured myocardium (47).

In these two studies, first-pass contrast enhancement was not studied under pharmacological stress, which can more reliably identify reversible injury in the myocardium. The contrast enhancement pattern after acute MI is, however, different from that of chronic MI (47, 163)

.

7.4 Myocardial viability

7.4.1 Assessment of myocardial perfusion with SPECT and MRI

The ability to differentiate between viable and nonviable myocardium plays a critical role in the prognosis of patients with CAD. Until recently, myocardial perfusion SPECT, which we used in the first study, and PET were the primary tools for this evaluation. In the last few years, however, MRI has made a dramatic appearance in this arena with the introduction and rapid acceptance of the delayed enhancement.

Findings of several studies have confirmed a sensitivity and specificity of stress perfusion MR imaging equivalent or superior to those of SPECT. In the literature, sensitivity and specificity values of MR imaging range 64%-92% and 71%-100%, respectively (77, 161, 194).

Results of myocardial delayed enhancement correlate well with those of dobutamine stress echocardiography (197), and there is excellent agreement with PET as well. Delayed enhancement correlates with areas of decreased flow and metabolism in PET (84). MRI is, however, slightly more sensitive, and a further advantage lies in MRI is its ability to visualize small, subendocardial areas of infarction that may be missed by nuclear techniques (33).

In Study I, the thinned myocardium detected with MRI correlated well with fixed perfusion defects seen in myocardial perfusion SPECT. The hypothesis that a thinned and akinetic myocardium represents a chronic scar has earlier been tested by comparing MRI findings with those obtained by PET and SPECT in the same myocardial regions. The comparison of MR images with scintigraphic

images is easily accomplished; because both techniques are three-dimensional, identical regions can be matched (174).

We found that TMLR prevented the change from a reversible perfusion defect to a scar, but the effect of TMLR on myocardial perfusion has been inconsistent, with improved perfusion reported in some studies (2, 44, 67, 68, 119, 167) and no change in the others (1, 4, 34, 134, 166).

7.4.2 MRI and delayed enhancement studies

SPECT is the most commonly available clinical method for assessing cardiac perfusion, although MRI has nowadays become a serious competitor of current clinical methods in the evaluation of myocardial perfusion (174).

In Study III, we evaluated myocardial viability with contrast-enhanced MRI. Of myocardial sectors, 57% had an infarction scar in the area related to calcifications and 56% in that related to significant stenoses. If the main coronary artery had both calcifications and a significant stenosis, infarction(s) were detected in 60 % of corresponding sectors. This is of particular significance, since significant stenoses affect myocardial viability, but additionally, in the presence of vessel wall calcifications, blood turbulence can lead to shear stress and a higher probability of plaque ruptures (37). In our study, infarction was also seen in 50% of sectors supplying to not significantly stenosed main coronary arteries. It has been suggested that only 30% of myocardial infarctions arise from significant stenoses. Soft plaques, which are often missed in CCA, may rupture and thrombose (132). Embolism can cause perfusion and functional changes in the myocardial sectors as well. This may partly explain our findings in sectors assigned to not significantly stenosed main coronary arteries.

Delayed myocardial hyperenhancement after injection of contrast material has been shown to delineate areas of myocardial infarction in several human and animal studies (42, 80, 81, 106, 143, 149, 151, 163). However, experimental and clinical studies contradict the theory that an enhanced myocardium invariably represents a nonviable myocardium.

Within the infarct zone exhibiting delayed hyperenhancement, central areas of microvascular obstruction (the no-reflow or low-reflow region of infarct) exhibit decreased first-pass perfusion (78, 111). Thus, the infarct zone is not always histologically homogeneous and may contain dead or dying myocardium. Wu et al. reported that a group with hypoenhanced regions within infarct center, which were presumed to represent microvascular obstruction, had significantly more frequent cardiovascular complications associated with fibrous scar formation and LV remodeling (196).

One study with rats showed that delayed hyperenhanced zone includes a peripheral zone of potentially salvageable myocardium (158), which contradicts a report by Kim and co-workers, who did not detect such peripheral zone (81). On the other hand, Rogers and colleagues found that hyperenhanced regions observed one week after reperfused infarction partially recovered contractile function by seven weeks. They described a subgroup of 13 patients in whom segments with normal contrast-enhanced first-pass signal and hyperenhanced signal on delayed images had partially reversible dysfunction, and thus representing predominantly viable myocardium (155). Only one such segment was found in an other study (163). However, both studies had many segments with absence of normal first-pass enhancement and delayed hyperenhancement. The first group concluded that these latter segments show borderline improvement and likely contain an admixture of viable and necrotic myocardium. The second team concluded that most (24/25) segments with delayed hyperenhancement are nonviable (163).

Currents techniques have the spatial resolution to show transmural differentiation of late enhancement. In a direct comparison with myocardial perfusion SPECT, delayed contrast-enhanced MRI was superior to SPECT in detecting subendocardial infarctions (62). We found that late enhancement was detected more often than LV wall dysfunction in small and subendocardial infarctions. It has been shown that the lower the extent of late enhancement, the higher the probability of functional recovery (25, 80). Regional wall motion improvement has been found in the majority of

segments with up to 50% transmural late enhancement, whereas global improvement can occur if the area of late enhancement is limited to less than 25% of LV wall thickness (162).

7.4.3 Combined cardiac MRI techniques

We used a combination of rest cine MR and delayed contrast-enhanced imaging as a reference method to detect remote myocardial infarctions evaluated with MCG (Study II).

Myocardial delayed enhancement combined with cine MRI helps differentiate wall-motion abnormalities of myocardial stunning, which are reversible, from those of myocardial infarction, which are often irreversible depending on the severity of the injury. Either condition may cause a wall motion abnormality, but delayed enhancement occurs only with infarcts. Lack of delayed enhancement indicates stunning rather than infarction and a high likelihood that LV function will fully recover (190). Reversible myocardial dysfunction can be identified by contrast enhanced and cine MRI before revascularization (hibernating myocardium) (81). A few studies assessed with cine and contrast-enhanced MRI have shown that transmural late enhancement is associated with lack of functional recovery after acute myocardial infarction (25, 162).

Assessment of myocardial viability remains controversial. Results of Study III suggests combination of all three MRI methods, first-pass perfusion, regional wall motion, and delayed contrast-enhancement analysis to evaluate myocardial recovery.

The combination of first-pass enhancement analysis and wall motion assessment with stress significantly increased the specificity of MR imaging in detection of unviable sectors in study by Lauerma et al. (106).

Three MRI methods were used to study functional recovery of transmural infarction.

One study concluded that the inotropic reserve was confined to a dysfunctional myocardium with normal contrast enhancement but not with early hypoenhancement. The inotropic response in the delayed hyperenhanced myocardium was influenced by transmurality of necrosis. These observa-

tions support the use of contrast-enhanced MRI for the clinical detection of myocardial viability (48). Our result in which LV wall dysfunction was detected less often than infarction is also consistent with these observations, indicating that myocardium in thin, subendocardial infarctions may reserve contractile function.

In the clinical study by Rogers et al, patients were examined early after reperfused first acute MI. Regions with normal first-pass signal followed by hyperenhanced signal on delayed images showed systolic wall motion improvement 7 week later. Regions with hypoenhancement at first-pass did not improve, and regions with additional delayed hyperenhancement only tended to improve (97, 155).

One possible reason for these deviant results is significant differences in contrast enhancement of the infracted myocardium between animal models. Studies have shown that dogs, rats, and humans have different levels of collateral development in response to chronic ischemia. Similarly, the edematous response to ischemia/reperfusion injury may vary between species. In addition, significant differences are present in the MR pulse sequences used in various studies (137). A close correlation between late enhancement and necrosis was found in canines, whereas an overestimation of infarct size by Gd-DTPA was demonstrated in rats. In humans, the extent of enhancement possibly may depend on both the time-point after MI and the time-point after injection, since myocardial edema probably contributes to contrast enhancement in acute/subacute MI (162).

7.5 Combined information from MDCT and MRI

We combined results of two noninvasive methods MDCT and cardiac MRI, to evaluate changes caused by CAD (Study III). Stenoses in the main coronary arteries found in MDCT-CA were compared with MRI findings. LV wall motion dysfunction at rest, perfusion deficits in stress-induced first-pass studies, and late enhancement imaging corresponded variably with calcifications and significant stenoses in the different main coronary arteries. Late enhancement was detected more often

than LV wall dysfunction because some infarctions were only thin and subendocardial. LV wall motion was not disturbed in these cases. This finding is in agreement with study by Gerber et al., who suggested that nontransmural infarctions present some degree of improvement (48). However, we observed LV wall motion dysfunction, perfusion defects, and infarctions also in sectors related to not significantly stenosed coronary arteries.

Combining the results of MDCT and MRI, the following observations were made:

Firstly, false negative findings were made with MDCT-CA. Two of the proximal RCA stenoses, one LAD stenosis, and two LCX stenoses were missed. Massive calcium depositions and high heart rates resulted in misinterpretations in these cases.

Secondly, in five patients deviant dominance of the main coronary arteries was present. When a stenosed coronary artery was assessed as dominant LV wall dysfunction, perfusion defect, and infarction was observed in the adjacent myocardial sectors. This reveals that myocardial sectors should be divided according to dominance of the main coronary arteries. In our study, sectors 1 and 6 were assigned to LAD, sectors 2 and 3 to LCX and sectors 4 and 5 to RCA territories. Coronary artery territories have earlier established in nuclear and MRI studies (6, 29). DePasquale et al. assigned sectors 1, 6, and partly 2 and 5 LAD, 2 and 3 to LCX, and 4 and 5 to RCA. In an MRI study, sectors 1 and 6 were assigned to LAD, sector 3 was assigned to LCX, and sector 5 was always assigned to RCA. Segment 2 was assigned to either LAD or the LCX (depening on the angiographic appearance). Segment 4 was assigned in the same manner to either LCX or to the RCA (6).

Thirdly, stenoses of less than 50% and stenoses in side branches not evaluated with MDCT-CA but detected in CCA caused changes in myocardial perfusion and LV kinetics in our patients. This is in concordance with the finding that approximately 90% of acute myocardial infarctions arise from nonrelevant lesions (132).

Fourthly, despite some arteries being classified as normal in CCA and MDCT, we observed signs of dysfunction and ischemia in the corresponding myocardial sectors. Misinterpretations of MRI can

be one reason. Clinically established and the most commonly available techniques for the assessment of viability are dobutamine stress echocardiography, SPECT, and PET with a sensitivity range of 81-90% and a specificity range of 47-81% (162). MRI is a good technique and offers a sensitivity of 79-83% and a specificity of 88-93% (84, 106). It′s findings correlate well with above-mentioned methods, but visual interpretation is highly dependent on the reader's experience.

We used a fairly low dose of contrast media compared with the larger doses (0.1-0.3 mmol/kg) reported in several late enhancement imaging studies (47, 80, 81, 84, 149). In perfusion studies, lower amounts of contrast media (0.025-0.05 mmol/kg) have been applied (7, 106). Despite the relatively low dosage of contrast material used here, we could delineate infarctions quite well in late enhancement pictures. In addition to the amount of contrast media, delay for late enhancement and determination of correct inversion time are critical for good diagnostic images.

Our findings suggest that combining information from MDCT-CA and functional MRI is beneficial. However, further clinical investigation is needed to define the technical requirements for optimal imaging, to develop accurate quantitative image analysis techniques, to outline criteria for image interpretation, and define the clinical indications for both MR and CT imaging.

Limitation of our studies was that we had a low number of patients. We did not evaluate intraobserver or interobserver variability.

7.6 MCG

In addition to exercise ECG, several other methods, including the radionuclide techniques, MRI, and stress echocardiography, are daily practise in ischemia detection. All of these methods have, however, disadvantages, and the development of the new techniques to evaluate more accurately the extent and localization of the ischemic myocardial area is still warranted.

MCG is a noninvasive and non-contact mapping technique for studying the electromagnetic function of the heart (182). The MCG records the magnetic field induced by the same bioelectric currents that generate the ECG. In addition to the morphological features of the MCG, such as the QRS-complex and the ST-segment, the spatial distribution of the multichannel MCG signal provides information on the cardiac cavity (157).

MCG is most sensitive to currents that are tangential to the chest but it can also detect circular vortex currents that give no ECG signal (157).

Recent studies on exercise MCG have demonstrated its potential to detect transient ischemia. In CAD, ischemia induces changes in the magnetocardiographic QT dispersion (58) and orientation of magnetic field maps (71, 183). MCG has also been used to localize transient and chronic ischemia (72).

In the Study II, we evaluated the electrophysiological abnormalities produced by remote MI in MCG mapping and applied cine- and contrast-enhanced MRI as a reference method. Our results showed that several magnetocardiographic repolarization indexes could distinquish patients with remote myocardial infarction from controls. These repolarization abnormalities were more distinct in patients with Q-wave MI than in patients with non-Q-wave MI. In the former group the indices may perform as well as the conventional ECG QRS criteria in detection of healed MI. In patients with non-Q-wave MI, a trend similar to that in with Q-wave MI was found, but the abnormalities were less distinct. The relation of QRS area to ST-segment, T-wave, and STT-wave integrals improved the detection of remote MI. When comparing the MI patients with the controls, the orientation of the magnetic field differed more in the STT-wave maps than in the QRS maps. In accordance with our results, earlier MI studies have also suggested that in post-MI patients MCG may show information complementary to the ECG especially during the repolarization phase (105). Van Leeuwen et al. have shown that post-MI patients demonstrate different patterns of spatial QT-time distributions than healthy subjects (188). Kandori et al. have also found abnormalities in the MCG

signal during ST segment in patients with CAD with or without previous MI (75). In addition, current density reconstruction maps have shown ST-segment repolarization abnormalities in patients with CAD but unimpaired LV function (57)

The optimal recording sites for the QRS and STT-wave indexes did not show extensive variation in between the MI groups, in consistent with our earlier studies on exercise-induced transient ischemia (71).

QRS-ST, QRS-T, and QRS-STT discordance could separate the MI group and the QMI subgroup from the controls, with the AUCs between 70% and 80%. QRS-STT discordance has earlier been applied in detection of LV hypertrophy (76). In our study, the performance of the QRS-STT discordance was dependent on the extent of the known MI damage, with better discriminative power in the QMI subgroup, with exhibited lower LV systolic function and thus more extensive MI damage than the NQMI subgroup.

The MFM orientation is especially sensitive in reflecting the spatial changes over the MCG mapping area, even when the sums of the indexes fail to demonstrate any difference. The present study showed that, although the sums of the STT-wave indexes did not separate the MI groups from the controls, the STT angle did distinguish the MI group and the QMI subgroup from the controls. In addition, the QRS-STT angle was larger in the QMI subgroup than in the controls, whereas for the NQMI group, in spite of the similar trend, the difference was not significant.

Earlier studies have shown that the MFM orientation changes during exercise-induced myocardial ischemia both in patients with single- and multivessel disease (71, 72). Furthermore, a recent study has also shown that the QRS-STT angle is larger in patients with LV hypertrophy than in healthy controls (76).

The MCG repolarization variables are reliable in detecting remote MI and may perform as well as the conventional electrocardiographic QRS criteria in detecting healed MI. These STT-wave abnormalities are more pronounced in patients with Q-wave MI than in patients with non-Q-wave

MI. Relating the signals of depolarization and repolarization phases improves the detection of remote MI. Repolarization abnormalities are common in remote MI and thus should not always be interpreted as present ongoing ischemia.

8. CONCLUSIONS

I) In severe, progressing CAD TMLR does not improve global LV function or myocardial perfusion, but it does preserve systolic wall thickening in fixed defects (scar). It also prevents changes from ischemic myocardial regions to scar.

II) The MCG repolarization variables are informative in remote MI, and may perform as well as the conventional QRS criteria in detection of healed MI. These STT abnormalities are more pronounced in patients with Q-wave MI than in patients with non-Q-wave MIs. Combining the signals of depolarization and repolarization phases improves the detection of remote MI compared with either of these signals alone. Repolarization abnormalities are common in remote MI and thus should not always be interpreted as acute ischemia. Clinically established techniques for assessment of viability are low-dose dobutamine stress echocardiography and myocardial perfusion SPECT, but MRI can be reliably be used as a reference method.

III) Noninvasive eight-row retrospectively ECG-gated MDCT is a good tool for detecting coronary artery stenoses. CCA and MDCT-CA yielded similar results in evaluating stenotic lesions above 50% in the main subepicardial coronary branches. Combining the data from MDCT-CA and MRI revealed the variability of myocardial response to calcifications and high-grade stenoses in the main coronary arteries.

IV) Our study showed a low sensitivity (sensitivity 63%) in detecting obstructive CAD in patients with severe aortic stenosis. Compared with CCA MDCT offers superior of visualizing soft plaques and measuring calcium burden of the coronary tree. However, massive calcifications and motion artifacts, especially in the right coronary artery, can complicate correct assessment of the lumen of coronary arteries. In this patient group CCA remains as the test of choice in planning of surgical strategy.

9. ACKNOWLEDGEMENTS

This project was carried out at Helsinki Medical Imaging Center during 2000-2006.

I would like to express my gratitude to the chief Executive Officer, Docent Juhani Ahovuo at Helsinki Medical Imaging Center for placing excellent research facilities at my disposal. I also deeply appreciate the warm and motherly advice and support of Professor Leena Kivisaari.

I thank my supervisor Docent Kirsi Lauerma for encouraging and supporting me during these many years of scientific work. As an expert in cardiac imaging, she has helped me with numerous scientific problems, but has also supported me in my personal life.

I warmly thank all my coauthors. Special thanks go to Mikko Sillanpää for helping me to create excellent CT images. It has also been a privilege to cooperate with Doctor Paula Vesterinen and PhD Helena Hänninen; this theses would have been impossible without them. Technicians Helena Siljander, Aki Syrjälä, Timo päivärinta, and Ulla Nikupaavo are acknowledged for their valuable contributions.

My warmest thanks are due to my dear friend and colleague PhD Sari Kivistö, who has given me endless support and understanding throughout this effort. We have had a lot of laughs together during these years, but she has also always been there to comfort me in the bad times.

I also wish to express my gratitude to Docent Taina Autti, who has encouraged and supported me in many ways.

I owe my deepest gratitude to my official reviewers, Docents Pekka Niemi and Esko Vanninen for their constructive criticism and valuable comments in completing this manuscript.

Special thanks go to Docent Markku Kupari for sharing his enormous knowledge in cardiology and Docent Kari Virtanen for his expert advice on nuclear medicine. I wish to extend my thanks to cardiothoracic surgeons Docent Kalervo Werkkala and Doctor Jarmo Simpanen. I am sincerely grateful to Docent Pauli Hekali for his generous support and advice. I am also grateful to Docent Hannu Aronen who has encouraged me to concentrate more in scientific work than playing golf. After these six years of hard work, I will now gradually return to the golf course…

I wish to express my warmest gratitude to the coronary artery disease and aortic valve stenosis patients who participated in this study.

My dear twin-brother, Mikki, deserves my warmest gratitude for his continuous caring and support throughout my whole life. He is my closest friend and I know that I can always count on him. Special thanks goes to my oldest brother Juha and his wife Miku for their special caring and love all through my life. I am deeply indebted to my brother Sami and his wife Pike and to my sister Tiina for always being there for me. I also wish to thank my parents-in-law Kerttu and Henrik for their love and help in everyday life.

I want to thank my very close friends Marja, Anne, Anki, Sirkku and Outi for reminding me that there is life outside of work and sharing numerous moments of laughter. My warmest gratitude is due to my colleagues at the Hospital for Children and Adolescents. Doctor Sanna Toivianen-Salo is especially thanked for her supporting friendship.

Finally, my warmest thanks go to my ever-loving husband Peter, who has always believed in me. He is the optimist in our family. Without his help in family life this project would never have reached completion. I am so extremely privileged to have two amazing children, Amanda and Emil, who bring so much joy and love into my world. You, Peter, Amanda, and Emil make life worth living. I am also lucky to have a wonderful stepdaughter Emmy and stepson Axel to brighten my life.

Financial support provided by Helsinki University Central Research Funds, The Radiological Society of Finland, the P.O. Klingendahl Foundation, the Einar and Karin Stroem Foundation, The Maire Taponen Foundation, The Finnish Society of Angiology, and Instrumentarium Foundation is gratefully acknowledged.

10. REFERENCES

1. Aaberge L, Rootwelt K, Blomhoff S, Saatvedt K, Abdelnoor M, and Forfang K. Continued symptomatic improvement three to five years after transmyocardial revascularization with CO(2) laser: a late clinical follow-up of the Norwegian Randomized trial with transmyocardial revascularization. *Journal of the American College of Cardiology* 39: 1588-1593, 2002.

2. Aaberge L, Rootwelt K, Smith HJ, Nordstrand K, and Forfang K. Effects of transmyocardial revascularization on myocardial perfusion and systolic function assessed by nuclear and magnetic resonance imaging methods. *Scandinavian Cardiovascular Journal* 35: 8-13, 2001.

3. Achenbach S, Ropers D, Regenfus M, Pohle K, Giesler T, Moshage W, and Daniel WG. Noninvasive coronary angiography by magnetic resonance imaging, electron-beam computed tomography, and multislice computed tomography. *American Journal of Cardiology* 88: 70E-73E, 2001.

4. Agarwal R, Ajit M, Kurian VM, Rajan S, Arumugam SB, and Cherian KM. Transmyocardial laser revascularization: early results and 1-year follow-up.[see comment]. *Annals of Thoracic Surgery* 67: 432-436, 1999.

5. Agatston AS, Janowitz WR, Hildner FJ, Zusmer NR, Viamonte M, Jr., and Detrano R. Quantification of coronary artery calcium using ultrafast computed tomography. *Journal of the American College of Cardiology* 15: 827-832, 1990.

6. Al-Saadi N, Nagel E, Gross M, Bornstedt A, Schnackenburg B, Klein C, Klimek W, Oswald H, and Fleck E. Noninvasive detection of myocardial ischemia from perfusion reserve based on cardiovascular magnetic resonance. *Circulation* 101: 1379-1383, 1999.

7. Al-Saadi N, Nagel E, Gross M, Schnackenburg B, Paetsch I, Klein C, and Fleck E. Improvement of myocardial perfusion reserve early after coronary intervention: assessment with

cardiac magnetic resonance imaging. *Journal of the American College of Cardiology* 36: 1557-1564, 2000.

8. Alfakih K, Reid S, Jones T, and Sivananthan M. Assessment of ventricular function and mass by cardiac magnetic resonance imaging. [Review] [36 refs]. *European Radiology* 14: 1813-1822, 1813.

9. Baer FM, Theissen P, Schneider CA, Eberhard V, Sechtem U, Schicha H, and Erdmann E. Dobutamine magnetic resonance imaging predicts contractile recovery of chronically dysfunctional myocardium after succesful revascularization. *Journal of the American College of Cardiology* 31: 1040-1048, 1997.

10. Baer FM, Voth E, LaRosee K, Schneider CA, Theissen P, Deutsch HJ, Schicha H, Erdmann E, and Sechtem U. Comparison of dobutamine transesophageal echocardiography and dobutamine magnetic resonance imaging for detection of residual myocardial viability. *American Journal of Cardiology* 78: 415-419, 1996.

11. Baroni M, Maffei S, Terrazzi M, Palmieri C, Paoli F, and Biagini A. Mechanisms of regional ischaemic changes during dipyridamole echocardiography in patients with severe aortic valve stenosis and normal coronary arteries. *Heart* 75: 492-497, 1996.

12. Becker C. Estimation of cardiac event risk by MDCT. *European Radiology* 15: B17-B22, 2005.

13. Becker CR, Kleffel T, Crispin A, Knez A, Young J, Schoepf UJ, Haberl R, and Reiser MF. Coronary artery calcium measurement: agreement of multirow detector and electron beam CT. *AJR American Journal of Roentgenology* 176: 1295-1298, 2001.

14. Becker CR, Nikolaou K, Muders M, Babaryka G, Crispin A, Schoepf UJ, Loehrs U, and Reiser MF. Ex vivo coronary atherosclerotic plaque characterization with multi-detector-row CT. *European Radiology* 13: 2094-2098, 2003.

15. Berges A, Van Nassauw L, Timmermans JP, and Vrints C. Role of nitric oxide during coronary endothelial dysfunction after myocardial infarction. *European Journal of Pharmacology* 516: 60-70, 2005.

16. Berman DS, Hachamovitch R, Kiat H, Cohen I, Cabico JA, Wang FP, Friedman JD, Germano G, Van Train K, and Diamond GA. Incremental value of prognostic testing in patients with known or suspected ischemic heart disease: a basis for optimal utilization of exercise technetium-99m sestamibi myocardial perfusion single-photon emission computed tomography.[erratum appears in J Am Coll Cardiol 1996 Mar 1;27(3):756]. *Journal of the American College of Cardiology* 26: 639-647, 1995.

17. Bolli R, Zhu WX, Thornby JI, O'Neill PG, and Roberts R. Time course and determinants of recovery of function after reversible ischemia in conscious dogs. *American Journal of Physiology* 254: H102-H114, 1988.

18. Brasch RC. New directions in the development of MR imaging contrast media. [Review] [77 refs]. *Radiology* 183: 1-11, 1992.

19. Braunwald E and Kloner RA. The stunned myocardium: prolonged, postischemic ventricular dysfunction. [Review] [35 refs]. *Circulation* 66: 1146-1149, 1982.

20. Braunwald E and Rutherford JD. Reversible ischemic left ventricular dysfunction: evidence for the "hibernating myocardium". *Journal of the American College of Cardiology* 8: 1467-1470, 1986.

21. Callister TQ, Cooil B, Raya SP, Lippolis NJ, Russo DJ, and Raggi P. Coronary artery disease: improved reproducibility of calcium scoring with an electron-beam CT volumetric method.[see comment]. *Radiology* 208: 807-814, 1998.

22. Carr JC, Simonetti O, Bundy J, LI D, Pereles S, and Finn PJ. Cine MR angiography of the heart with segmented true fast imaging with steady-state precession. *Radiology* 219: 828-834, 2001.

23. Cerqueira MD, Weissman NJ, Dilsizian V, Jacobs AK, Kaul S, Laskey WK, Pennell DJ, Rumberger JA, Ryan T, Verani MS, American Heart Association Writing Group on Myocardial S, and Registration for Cardiac I. Standardized myocardial segmentation and nomenclature for tomographic imaging of the heart. A statement for healthcare professionals from the Cardiac Imaging Committee of the Council on Cliniical Cardiology of the American Heart Association. *The International Journal of Cardiovascular Imaging* 18: 539-542, 2002.

24. Chobadi R, Wurzel M, Teplitsky I, Menkes H, and Tamari I. Coronary artery disease in patients 35 years of age or older with valvular aortic stenosis. *American Journal of Cardiology* 64: 811-812, 1989.

25. Choi KM, Kim RJ, Gubernikoff G, Vargas JD, Parker M, and Judd RM. Transmural extent of acute myocardial infarction predicts long-term improvement in contractile function. *Circulation* 104: 1101-1107, 2001.

26. Cohen D, Savard P, Rifkin RD, Lepeschkin E, and Strauss WE. Magnetic measurement of S-T and T-Q segment shifts in humans. Part II: Exercise-induced S-T segment depression. *Circulation Research* 53: 274-279, 1983.

27. Cooley DA, Frazier OH, Kadipasaoglu KA, Lindenmeir MH, Pehlivanoglu S, Kolff JW, Wilansky S, and Moore WH. Transmyocardial laser revascularization: clinical experience with twelve-month follow-up. *Journal of Thoracic & Cardiovascular Surgery* 111: 791-797, 1996.

28. Cullen JH, Horsfield MA, Reek CR, Cherryman GR, Barnett DB, and Samani NJ. A myocardial perfusion reserve index in humans using first-pass contrast-enhanced magnetic resonance imaging.[see comment]. *Journal of the American College of Cardiology* 33: 1386-1394, 1999.

29. DePasquale EE, Nody AC, DePuey EG, Garcia EV, Pilcher G, Bredlau C, Roubin G, Gober A, Gruentzig A, D'Amato P, and et al. Quantitative rotational thallium-201 tomography for identifying and localizing coronary artery disease. *Circulation* 77: 316-327, 1988.

30. Devries S, Wolfkiel C, Shah V, Chomka E, and Rich S. Reproducibility of the measurement of coronary calcium with ultrafast computed tomography. *American Journal of Cardiology* 75: 973-975, 1995.

31. Duerinckx AJ. Myocardial viability using MR imaging: is it ready for clinical use?[comment]. *AJR American Journal of Roentgenology* 174: 1741-1743, 2000.

32. Dutcher J, Huang Y, and Wang Y. Transmyocardial laser revascularization (TMLR) preserves left ventricular function in acute ischemia (Abstract). *Journal of Cardiovascular Magnetic Resonance* 1: 273, 1999.

33. Earls JP, Ho VB, Foo TK, Castillo E, and Flamm SD. Cardiac MRI: recent progress and continued challenges.[erratum appears in J Magn Reson Imaging. 2002 Nov;16(5):620.]. [Review] [169 refs]. *Journal of Magnetic Resonance Imaging* 16: 111-127, 2002.

34. Eckstein FS, Scheule AM, Vogel U, Schmid ST, Miller S, Jurmann MJ, and Ziemer G. Transmyocardial laser revascularization in the acute ischaemic heart: no improvement of acute myocardial perfusion or prevention of myocardial infarction. *European Journal of Cardio Thoracic Surgery* 15: 702-708, 1999.

35. Edelman RR. Contrast-enhanced MR imaging of the heart: overview of the literature. [Review] [215 refs]. *Radiology* 232: 653-668, 2004.

36. Emmett L, Iwanochko RM, Freeman MR, Barolet A, Lee DS, and Husain M. Reversible regional wall motion abnormalities on exercise technetium-99m-gated cardiac single photon emission computed tomography predict high-grade angiographic stenoses. *Journal of the American College of Cardiology* 39: 991-998, 2002.

37. Erbel R, Schmermund A, Mohlenkamp S, Sack S, and Baumgart D. Electron-beam computed tomography for detection of early signs of coronary arteriosclerosis. [Review] [75 refs]. *European Heart Journal* 21: 720-732, 2000.

38. Exadactylos N, Surgue DD, and Oakley CM. Prevalence of coronary artery disease in patients with isolated aortic valve stenosis. *British Heart Journal* 51: 121-124, 1984.

39. Falk E and Fuster V. Angina pectoris and disease progression.[comment]. *Circulation* 92: 2033-2035, 1995.

40. Feinstein JA, Epstein FH, Arai AE, Foo TK, Hartley MR, Balaban RS, and Wolff SD. Using cardiac phase to order reconstruction (CAPTOR): a method to improve diastolic images. *Journal of Magnetic Resonance Imaging* 7: 794-798, 1997.

41. Ficaro EP, Fessler JA, Shreve PD, Kritzman JN, Rose PA, and Corbett JR. Simultaneous transmission/emission myocardial perfusion tomography. Diagnostic accuracy of attenuation-corrected 99mTc-sestamibi single-photon emission computed tomography. *Circulation* 93: 463-473, 1996.

42. Fieno DS, Kim RJ, Chen EL, Lomasney JW, Klocke FJ, and Judd RM. Contrast-enhanced magnetic resonance imaging of myocardium at risk: distinction between reversible and irreversible injury throughout infarct healing. *Journal of the American College of Cardiology* 36: 1985-1991, 2000.

43. Fine JJ, Hopkins CB, Ruff N, and Newton CF. Comparison of accuracy of 64-slice cardiovascular computed tomography with coronary angiography in patients with suspected coronary artery disease. *American Journal of Cardiology* 97: 173-174, 2005.

44. Frazier OH, March RJ, and Horvath KA. Transmyocardial revascularization with a carbon dioxide laser in patients with end-stage coronary artery disease.[see comment]. *New England Journal of Medicine* 341: 1021-1028, 1999.

45. Fujino K, Sumi M, Saito K, Murakami M, Higuchi T, Nakaya Y, and Mori H. Magnetocardiograms of patients with left ventricular overloading recorded with a second-derivative SQUID gradiometer. *Journal of Electrocardiology* 17: 219-228, 1984.

46. Garcia-Dorado D, Theroux P, Solares J, Alonso J, Fernandez-Aviles F, Elizaga J, Soriano J, Botas J, and Munoz R. Determinants of hemorrhagic infarcts. Histologic observations from experiments involving coronary occlusion, coronary reperfusion, and reocclusion. *American Journal of Pathology* 137: 301-311, 1990.

47. Gerber BL, Garot J, Bluemke DA, Wu KC, and Lima JA. Accuracy of contrast-enhanced magnetic resonance imaging in predicting improvement of regional myocardial function in patients after acute myocardial infarction. *Circulation* 106: 1083-1089, 2002.

48. Gerber BL, Rochitte CE, Bluemke DA, Melin JA, Crosille P, Becker LC, and Lima JA. Relation between Gd-DTPA contrast enhancement and regional inotropic response in the periphery and center of myocardial infarction. *Circulation* 104: 998-1004, 1004.

49. Giesler T, Baum U, Ropers D, Ulzheimer S, Wenkel E, Mennicke M, Bautz W, Kalender WA, Daniel WG, and Achenbach S. Noninvasive visualization of coronary arteries using contrast-enhanced multidetector CT: influence of heart rate on image quality and stenosis detection. *AJR American Journal of Roentgenology* 179: 911-916, 2002.

50. Giorgetti A, Pingitore A, Favilli B, Kusch A, Lombardi M, and Marzullo P. Baseline/postnitrate tetrofosmin SPECT for myocardial viability assessment in patients with postischemic severe left ventricular dysfunction: new evidence from MRI. *Journal of Nuclear Medicine* 46: 1285-1293, 1285.

51. Goldin JG, Yoon HC, Greaser LE, 3rd, Heinze SB, McNitt-Gray MM, Brown MS, Sayre JW, Emerick AM, and Aberle DR. Spiral versus electron-beam CT for coronary artery calcium scoring. *Radiology* 221: 213-221, 2001.

52. Green SJ, Pizzarello RA, Padmanabhan VT, Ong LY, Hall MH, and Tortolani AJ. Relation of angina pectoris to coronary artery disease in aortic valve stenosis. *American Journal of Cardiology* 55: 1063-1065, 1985.

53. Greenberg SB and Sandhu SK. Ventricular function. [Review] [93 refs]. *Radiologic Clinics of North America* 37: 341-359, 1999.

54. Guillem P. Assessment of cardiac function by CMR. *European Radiology* 15: B21-31, 2005.

55. Gutberlet M, Frohlich M, Mehl S, Amthauer H, Hausmann H, Meyer R, Siniawski H, Ruf J, Plotkin M, Denecke T, Schnackenburg B, Hetzer R, and Felix R. Myocardial viability assessment in patients with highly impaired left ventricular function: comparison of delayed enhancement, dobutamine stress MRI, end-diastolic wall thickness, and TI201-SPECT with functional recovery after revascularization. *European Radiology* 15: 872-880, 2005.

56. Haase A. Snapshot FLASH MRI. Applications to T1, T2, and chemical-shift imaging. *Magnetic Resonance in Medicine* 13: 77-89, 1990.

57. Hailer B, Chaikovsky I, Auth-Eisernitz S, Schafer H, Steinberg F, and Gronemeyer DH. Magnetocardiography in coronary artery disease with a new system in an unshielded setting. *Clinical Cardiology* 26: 465-471, 2003.

58. Hailer B, Van Leeuwen P, Lange S, and Wehr M. Spatial distribution of QT dispersion measured by magnetocardiography under stress in coronary artery disease. *Journal of Electrocardiology* 32: 207-216, 1999.

59. Hanninen H, Takala P, Makijarvi M, Montonen J, Korhonen P, Oikarinen L, Simelius K, Nenonen J, Katila T, and Toivonen L. Recording locations in multichannel magnetocardiography and body surface potential mapping sensitive for regional exercise-induced myocardial ischemia. *Basic Research in Cardiology* 96: 405-414, 2001.

60. Hartiala J and Knuuti J. Imaging of the heart by MRI and PET. [Review] [66 refs]. *Annals of Medicine* 27: 35-45, 1995.

61. Heo J, Powers J, and Iskandrian AE. Exercise-rest same-day SPECT sestamibi imaging to detect coronary artery disease. *Journal of Nuclear Medicine* 38: 200-203, 1997.

62. Hillenbrand HB, Kim RJ, Parker MA, Fieno DS, and Judd RM. Early assessment of myocardial salvage by contrast-enhanced magnetic resonance imaging. *Circulation* 102: 1678-1683, 2000.

63. Hoffmann R, Lethen H, Marwick T, Arnese M, Fioretti P, Pingitore A, Picano E, Buck T, Erbel R, Flachskampf FA, and Hanrath P. Analysis of interinstitutional observer agreement in interpretation of dobutamine stress echocardiograms. *Journal of the American College of Cardiology* 27: 330-336, 1996.

64. Hoffmann R, von Bardeleben S, ten Cate F, Borges AC, Kasprzak J, Firschke C, Lafitte S, Al-Saadi N, Kuntz-Hehner S, Engelhardt M, Becher H, and Vanoverschelde JL. Assessment of systolic left ventricular function: a multi-centre comparison of cineventriculography, cardiac magnetic resonance imaging, unenhanced and contrast-enhanced echocardiography.[see comment]. *European Heart Journal* 26: 607-616, 2005.

65. Hombach V, Kochs M, Weismuller P, Clausen M, Henze E, Richter P, Hoher M, Peper A, Eggeling T, Adam WE, and et al. Localization of ectopic ventricular depolarization by ISPECT-radionuclide ventriculography and by magnetocardiography. ISPECT and MCG for ectopic mapping. *International Journal of Cardiac Imaging* 7: 225-235, 1991.

66. Hong C, Becker CR, Schoepf UJ, Ohnesorge B, Bruening R, and Reiser MF. Coronary artery calcium: absolute quantification in nonenhanced and contrast-enhanced multi-detector row CT studies. *Radiology* 223: 474-480, 2002.

67. Horvath KA, Cohn LH, Cooley DA, Crew JR, Frazier OH, Griffith BP, Kadipasaoglu K, Lansing A, Mannting F, March R, Mirhoseini MR, and Smith C. Transmyocardial laser revascularization: results of a multicenter trial with transmyocardial laser revascularization used as sole therapy for end-stage coronary artery disease. *Journal of Thoracic & Cardiovascular Surgery* 113: 645-653, 1997.

68. Horvath KA, Mannting F, Cummings N, Shernan SK, and Cohn LH. Transmyocardial laser revascularization: operative techniques and clinical results at two years. *Journal of Thoracic & Cardiovascular Surgery* 111: 1047-1053, 1996.

69. Huang H, Virmani R, Younis H, Burke AP, Kamm RD, and Lee RT. The impact of calcification on the biomechanical stability of atherosclerotic plaques. *Circulation* 103: 1051-1056, 1051.

70. Huikuri HV, Korhonen UR, Ikaheimo MJ, Heikkila J, and Takkunen JT. Detection of coronary artery disease by thallium imaging using a combined intravenous dipyridamole and isometric handgrip test in patients with aortic valve stenosis. *American Journal of Cardiology* 59: 336-340, 1987.

71. Hänninen H, Takala P, Korhonen P, Oikarinen L, Makijarvi M, Nenonen J, Katila T, and Toivonen L. Features of ST segment and T-wave in exercise-induced myocardial ischemia evaluated with multichannel magnetocardiography. *Annals of Medicine* 34: 120-129, 2002.

72. Hänninen H, Takala P, Mäkijärvi M, Montonen J, Korhonen P, Oikarinen L, Nenonen J, Katila T, and Toivonen L. Detection of exercise induced myocardial ischemia by multichannel magnetocardiograhpy in single vessel coronary artery disease. *Annals of Noninvasive Electrocardiology* 5: 147-157, 2000.

73. Ishida N, Sakuma H, Motoyasu M, Okinaka T, Isaka N, Nakano T, and Takeda K. Noninfarcted myocardium: correlation between dynamic first-pass contrast-enhanced myocardial MR imaging and quantitative coronary angiography. *Radiology* 229: 209-216, 2003.

74. Iung B, Drissi MF, Michel PL, De Pamphilis O, Tsezana R, Cormier B, Vahanian A, and Acar J. Prognosis of valve replacement for aortic stenosis with or without coexisting coronary heart disease: a comparative study. *Journal of Heart Valve Disease* 2: 430-439, 1993.

75. Kandori A, Kanzaki H, Miyatake K, Hashimoto S, Itoh S, Tanaka N, Miyashita T, and Tsukada K. A method for detecting myocardial abnormality by using a current-ratio map calculated

from an exercise-induced magnetocardiogram. *Medical & Biological Engineering & Computing* 39: 29-34, 2001.

76. Karvonen M, Oikarinen L, Takala P, Kaartinen M, Rossinen J, Hanninen H, Montonen J, Nenonen J, Makijarvi M, Keto P, Toivonen L, Nieminen MS, and Katila T. Magnetocardiographic indices of left ventricular hypertrophy.[see comment]. *Journal of Hypertension* 20: 2285-2292, 2002.

77. Keijer JT, van Rossum AC, van Eenige MJ, Bax JJ, Visser FC, Teule JJ, and Visser CA. Magnetic resonance imaging of regional myocardial perfusion in patients with single-vessel coronary artery disease: quantitative comparison with (201)Thallium-SPECT and coronary angiography. *Journal of Magnetic Resonance Imaging* 11: 607-615, 2000.

78. Kim RJ, Chen EL, Lima JA, and Judd RM. Myocardial Gd-DTPA kinetics determine MRI contrast enhancement and reflect the extent and severity of myocardial injury after acute reperfused infarction. *Circulation* 94: 3318-3326, 1996.

79. Kim RJ, Choi KM, and Judd RM. Assessment of myocardial viability by contrast enhancement. In: *Cardiovascular MRI and MRA*, edited by Higgins CB and De Roos A, 2003, p. 209-238.

80. Kim RJ, Fieno DS, Parrish TB, Harris K, Chen EL, Simonetti O, Bundy J, Finn JP, Klocke FJ, and Judd RM. Relationship of MRI delayed contrast enhancement to irreversible injury, infarct age, and contractile function. *Circulation* 100: 1992-2002, 1999.

81. Kim RJ, Wu E, Rafael A, Chen EL, Parker MA, Simonetti O, Klocke FJ, Bonow RO, and Judd RM. The use of contrast-enhanced magnetic resonance imaging to identify reversible myocardial dysfunction.[see comment]. *New England Journal of Medicine* 343: 1445-1453, 2000.

82. Kitamura A, Kobayashi T, Ueda K, Okada T, Awata N, Sato S, and Shimamoto T. Evaluation of coronary artery calcification by multi-detector row computed tomography for the detection of coronary artery stenosis in Japanese patients. *Journal of Epidemiology* 15: 187-193, 2005.

83. Klein AL, Marquis JF, Higginson LA, Morton BC, Williams WL, Davies RA, and Beanlands DS. Intravenous dipyridamole-induced myocardial ischemia during percutaneous transluminal coronary angioplasty in humans. *American Journal of Cardiology* 63: 419-422, 1989.

84. Klein C, Nekolla SG, Bengel FM, Momose M, Sammer A, Haas F, Schnackenburg B, Delius W, Mudra H, Wolfram D, and Schwaiger M. Assessment of myocardial viability with contrast-enhanced magnetic resonance imaging: comparison with positron emission tomography. *Circulation* 105: 162-167, 2002.

85. Klingenbeck-Regn K, Schaller S, Flohr T, Ohnesorge B, Kopp AF, and Baum U. Subsecond multi-slice computed tomography: basics and applications. *European Journal of Radiology* 31: 110-124, 1999.

86. Kloner RA and Jennings RB. Consequences of brief ischemia: stunning, preconditioning, and their clinical implications: part 1. [Review] [85 refs]. *Circulation* 104: 2981-2989, 2001.

87. Kloner RA and Jennings RB. Consequences of brief ischemia: stunning, preconditioning, and their clinical implications: part 2. [Review] [115 refs]. *Circulation* 104: 3158-3167, 2001.

88. Knez A, Becker C, Ohnesorge B, Haberl R, Reiser M, and Steinbeck G. Noninvasive detection of coronary artery stenosis by multislice helical computed tomography. *Circulation* 101: E221-222, 2000.

89. Kopp AF. Angio-CT: heart and coronary arteries. [Review] [21 refs]. *European Journal of Radiology* 45 Suppl 1: S32-36, 2003.

90. Kopp AF, Kuttner A, Heuschmid M, Schroder S, Ohnesorge B, and Claussen CD. Multidetector-row CT cardiac imaging with 4 and 16 slices for coronary CTA and imaging of atherosclerotic plaques. [Review] [51 refs]. *European Radiology* 12 Suppl 2: S17-24, 2002.

91. Kopp AF, Schroeder S, Baumbach A, Kuettner A, Georg C, Ohnesorge B, Heuschmid M, Kuzo R, and Claussen CD. Non-invasive characterisation of coronary lesion morphology and

composition by multislice CT: first results in comparison with intracoronary ultrasound. *European Radiology* 11: 1607-1611, 2001.

92. Kopp AF, Schroeder S, Kuettner A, Baumbach A, Georg C, Kuzo R, Heuschmid M, Ohnesorge B, Karsch KR, and Claussen CD. Non-invasive coronary angiography with high resolution multidetector-row computed tomography. Results in 102 patients. *European Heart Journal* 23: 1714-1725, 2002.

93. Kopp AF, Schroeder S, Kuettner A, Heuschmid M, Georg C, Ohnesorge B, Kuzo R, and Claussen CD. Coronary arteries: retrospectively ECG-gated multi-detector row CT angiography with selective optimization of the image reconstruction window. *Radiology* 221: 683-688, 2001.

94. Korhonen P, Montonen J, Endt P, Makijarvi M, Trahms L, Katila T, and Toivonen L. Magnetocardiographic intra-QRS fragmentation analysis in the identification of patients with sustained ventricular tachycardia after myocardial infarction. *Pacing & Clinical Electrophysiology* 24: 1179-1186, 2001.

95. Kostler H, Ritter C, Lipp M, Beer M, Hahn D, and Sandstede J. Prebolus quantitative MR heart perfusion imaging. *Magnetic Resonance in Medicine* 52: 296-299, 2004.

96. Kostler H, Ritter C, Reiss-Zimmermann M, Beer M, Hahn D, and Sandstede J. Correction for partial volume errors in MR heart perfusion imaging. *Magnetic Resonance in Medicine* 51: 848-852, 2004.

97. Kramer CM, Rogers WJ, Jr., Mankad S, Theobald TM, Pakstis DL, and Hu YL. Contractile reserve and contrast uptake pattern by magnetic resonance imaging and functional recovery after reperfused myocardial infarction. *Journal of the American College of Cardiology* 36: 1835-1840, 2000.

98. Kuettner A, Kopp AF, Schroeder S, Rieger T, Brunn J, Meisner C, Heuschmid M, Trabold T, Burgstahler C, Martensen J, Schoebel W, Selbmann HK, and Claussen CD. Diagnostic accuracy of multidetector computed tomography coronary angiography in patients with an-

giographically proven coronary artery disease.[see comment]. *Journal of the American College of Cardiology* 43: 831-839, 2004.

99. Kuhle WG, Porenta G, Huang SC, Buxton D, Gambhir SS, Hansen H, Phelps ME, and Schelbert HR. Quantification of regional myocardial blood flow using 13N-ammonia and reoriented dynamic positron emission tomographic imaging. *Circulation* 86: 1004-1017, 1992.

100. Kuijpers D, Janssen CH, van Dijkman PR, and Oudkerk M. Dobutamine stress MRI. Part I. Safety and feasibility of dobutamine cardiovascular magnetic resonance in patients suspected of myocardial ischemia. *European Radiology* 14: 1823-1828, 2004.

101. Kuijpers D, van Dijkman PR, Janssen CH, Vliegenthart R, Zijlstra F, and Oudkerk M. Dobutamine stress MRI. Part II. Risk stratification with dobutamine cardiovascular magnetic resonance in patients suspected of myocardial ischemia. *European Radiology* 14: 2046-2052, 2004.

102. Laham RJ, Simons M, Pearlman JD, Ho KK, and Baim DS. Magnetic resonance imaging demonstrates improved regional systolic wall motion and thickening and myocardial perfusion of myocardial territories treated by laser myocardial revascularization. *Journal of the American College of Cardiology* 39: 1-8, 2002.

103. Lamb H. Clinical approach to cardiovascular MRI, techniques. In: *Cardiovascular MRI and MRA*, edited by Higgins CB and De Roos A, 2003, p. 3-18.

104. Lange RA and Hillis LD. Transmyocardial laser revascularization.[see comment][comment]. *New England Journal of Medicine* 341: 1075-1076, 1999.

105. Lant J, Stroink G, ten Voorde B, Horacek BM, and Montague TJ. Complementary nature of electrocardiographic and magnetocardiographic data in patients with ischemic heart disease. *Journal of Electrocardiology* 23: 315-322, 1990.

106. Lauerma K, Niemi P, Hanninen H, Janatuinen T, Voipio-Pulkki LM, Knuuti J, Toivonen L, Makela T, Makijarvi MA, and Aronen HJ. Multimodality MR imaging assessment of

myocardial viability: combination of first-pass and late contrast enhancement to wall motion dynamics and comparison with FDG PET-initial experience. *Radiology* 217: 729-736, 2000.

107. Lauerma K, Virtanen KS, Sipila LM, Hekali P, and Aronen HJ. Multislice MRI in assessment of myocardial perfusion in patients with single-vessel proximal left anterior descending coronary artery disease before and after revascularization. *Circulation* 96: 2859-2867, 1997.

108. Leber AW, Knez A, Becker A, Becker C, von Ziegler F, Nikolaou K, Rist C, Reiser M, White C, Steinbeck G, and Boekstegers P. Accuracy of multidetector spiral computed tomography in identifying and differentiating the composition of coronary atherosclerotic plaques: a comparative study with intracoronary ultrasound. *Journal of the American College of Cardiology* 43: 1241-1247, 2003.

109. Leschka S, Alkadhi H, Plass A, Desbiolles L, Grunenfelder J, Marincek B, and Wildermuth S. Accuracy of MSCT coronary angiography with 64-slice technology: first experience.[see comment]. *European Heart Journal* 26: 1482-1487, 2005.

110. Lim TH and Choi SI. MRI of myocardial infarction. [Review] [48 refs]. *Journal of Magnetic Resonance Imaging* 10: 686-693, 1999.

111. Lima JA, Judd RM, Bazille A, Schulman SP, Atalar E, and Zerhouni EA. Regional heterogeneity of human myocardial infarcts demonstrated by contrast-enhanced MRI. Potential mechanisms. *Circulation* 92: 1117-1125, 1993.

112. Makijarvi M. Recording of abnormal late ventricular activity by high-resolution magnetocardiography. *International Journal of Cardiac Imaging* 7: 237-241, 1991.

113. Makijarvi M, Nenonen J, Leinio M, Montonen J, Toivonen L, Nieminen MS, Katila T, and Siltanen P. Localization of accessory pathways in Wolff-Parkinson-White syndrome by high-resolution magnetocardiographic mapping. *Journal of Electrocardiology* 25: 143-155, 1992.

114. Makijarvi M, Nenonen J, Toivonen L, Montonen J, Katila T, and Siltanen P. Magnetocardiography: supraventricular arrhythmias and preexcitation syndromes. *European Heart Journal* 14: 46-52, 1993.

115. Manning WJ, Atkinson DJ, Grossman W, Paulin S, and Edelman RR. First-pass nuclear magnetic resonance imaging studies using gadolinium-DTPA in patients with coronary artery disease. *Journal of the American College of Cardiology* 18: 959-965, 1991.

116. Maruyama T, Yoshizumi T, Tamura R, Takashima S, Toyoshima H, Konishi I, Yamashita S, and Yamasaki K. Comparison of visibility and diagnostic capability of noninvasive coronary angiography by eight-slice multidetector-row computed tomography versus conventional coronary angiography. *American Journal of Cardiology* 93: 537-542, 2004.

117. Maunoury C, Chen CC, Chua KB, and Thompson CJ. Quantification of left ventricular function with thallium-201 and technetium-99m-sestamibi myocardial gated SPECT.[erratum appears in J Nucl Med 1997 Nov;38(11):1834]. *Journal of Nuclear Medicine* 38: 958-961, 1997.

118. Messroghli DR, Bainbridge GJ, Alfakih K, Jones TR, Plein S, Ridgway JP, and Sivananthan MU. Assessment of regional left ventricular function: accuracy and reproducibility of positioning standard short-axis sections in cardiac MR imaging. *Radiology* 235: 229-236, 2005.

119. Mirhoseini M, Shelgikar S, and Cayton MM. New concepts in revascularization of the myocardium. *Annals of Thoracic Surgery* 45: 415-420, 1988.

120. Mollet NR, Cademartiri F, Nieman K, Saia F, Lemos PA, McFadden EP, Pattynama PM, Serruys PW, Krestin GP, and de Feyter PJ. Multislice spiral computed tomography coronary angiography in patients with stable angina pectoris. *Journal of the American College of Cardiology* 43: 2265-2270, 2004.

121. Mollet NR, Cademartiri F, Nieman K, Saia F, Lemos PA, McFadden EP, Serruys PW, Krestin GP, and de Feyter PJ. Noninvasive assessment of coronary plaque burden using multislice computed tomography. *American Journal of Cardiology* 95: 1165-1169, 2005.

122. Mollet NR, Cademartiri F, van Mieghem CAG, Runza G, McFadden EP, Baks T, Serruys PW, Krestin GP, and De Feyter PJ. High-resolution spiral computed tomography coronary angiography in patients referred for diagnopstic conventional coronary angiography. *Circulation* 112: 2318-2323, 2005.

123. Morrison GW, Thomas RD, Grimmer SF, Silverton PN, and Smith DR. Incidence of coronary artery disease in patients with valvular heart disease. *British Heart Journal* 44: 630-637, 1980.

124. Moshage W, Achenbach S, Gohl K, and Bachmann K. Evaluation of the non-invasive localization accuracy of cardiac arrhythmias attainable by multichannel magnetocardiography (MCG). *International Journal of Cardiac Imaging* 12: 47-59, 1996.

125. Muehling OM, Wilke NM, and Huang Y. Cine magnetic resonance imaging shows improved regional thickening in remote and chronic ischemic myocardium after transmyocardial laser revascularization (Abstract). *Journal of Cardiovascular Magnetic Resonance* 1: 345, 1999.

126. Muehling OM, Wilke NM, and Huang Yea. Cine magnetic resonance imaging shows preserved global and diastolic function after transmyocardial laser revascularization (TMLR) (Abstract). *Journal of Cardiovascular Magnetic Resonance* 1: 345, 1999.

127. Nagel E. Left ventricular function in ischemic heart disease. In: *Cardiovascular MRI and MRA*, edited by Higgins CB and De Roos A, 2003, p. 191-199.

128. Nagel E, Lehmkuhl HB, Bocksch W, Klein C, Vogel U, Frantz E, Ellmer A, Dreysse S, and Fleck E. Noninvasive diagnosis of ischemia-induced wall motion abnormalities with the use of high-dose dobutamine stress MRI: comparison with dobutamine stress echocardiography.[see comment]. *Circulation* 99: 763-770, 1999.

129. Nenonen J, Montonen J, and Mäkijärvi M. Principles of magnetocardiographic mapping. *Shenasa M, Borgreffe M, Breithardt G, eds Futura Publishing Co, Mount Kisco, NY*, 2002.

130. Nieman K, Oudkerk M, Rensing BJ, van Ooijen P, Munne A, van Geuns RJ, and de Feyter PJ. Coronary angiography with multi-slice computed tomography. *Lancet* 357: 599-603, 2001.

131. Nieman K, Rensing BJ, van Geuns RJ, Munne A, Ligthart JM, Pattynama PM, Krestin GP, Serruys PW, and de Feyter PJ. Usefulness of multislice computed tomography for detecting obstructive coronary artery disease. *American Journal of Cardiology* 89: 913-918, 2002.

132. Nikolaou K, Sagmeister S, Knez A, Klotz E, Wintersperger BJ, Becker CR, and Reiser MF. Multidetector-row computed tomography of the coronary arteries: predictive value and quantitative assessment of non-calcified vessel-wall changes. *European Radiology* 13: 2505-2512, 2003.

133. Nishimura S, Mahmarian JJ, Boyce TM, and Verani MS. Quantitative thallium-201 single-photon emission computed tomography during maximal pharmacologic coronary vasodilation with adenosine for assessing coronary artery disease. *Journal of the American College of Cardiology* 18: 736-745, 1991.

134. Nägele H, Stubbe HM, Nienaber C, and Rodiger W. Results of transmyocardial laser revascularization in non-revascularizable coronary artery disease after 3 years follow-up [ssee comments][see comment]. *European Heart Journal* 19: 1525-1530, 1998.

135. Ohnesorge B, Flohr T, Becker C, Kopp AF, Schoepf UJ, Baum U, Knez A, Klingenbeck-Regn K, and Reiser MF. Cardiac imaging by means of electrocardiographically gated multisection spiral CT: initial experience. *Radiology* 217: 564-571, 2000.

136. Osbakken MD, Bove AA, and Spann JF. Left ventricular regional wall motion and velocity of shortening in chronic mitral and aortic regurgitation. *American Journal of Cardiology* 47: 1005-1009, 1981.

137. Oshinski JN, Yang Z, Jones JR, Mata JF, and French BA. Imaging time after Gd-DTPA injection is critical in using delayed enhancement to determine infarct size accurately with magnetic resonance imaging.[see comment]. *Circulation* 104: 2838-2842, 2001.

138. Paelinck BP, Lamb HJ, Bax JJ, Van der Wall EE, and de Roos A. Assessment of diastolic function by cardiovascular magnetic resonance. [Review] [46 refs]. *American Heart Journal* 144: 198-205, 2002.

139. Pasterkamp G, Schoneveld AH, Hijnen DJ, de Kleijn DP, Teepen H, van der Wal AC, and Borst C. Atherosclerotic arterial remodeling and the localization of macrophages and matrix metalloproteases 1, 2 and 9 in the human coronary artery. *Atherosclerosis* 150: 245-253, 2000.

140. Patsilinakos SP, Kranidis AI, Antonelis IP, Filippatos G, Houssianakou IK, Zamanis NI, Sioras E, Tsiotika T, Kardaras F, and Anthopoulos LP. Detection of coronary artery disease in patients with severe aortic stenosis with noninvasive methods. *Angiology* 50: 309-317, 1999.

141. Paul AK, Hasegawa S, Yoshioka J, Mu X, Maruyama K, Kusuoka H, and Nishimura T. Characteristics of regional myocardial stunning after exercise in gated myocardial SPECT. *Journal of Nuclear Cardiology* 9: 388-394, 2002.

142. Paul AK and Nabi HA. Gated myocardial perfusion SPECT: basic principles, technical aspects, and clinical applications. [Review] [72 refs]. *Journal of Nuclear Medicine Technology* 32: 179-187, 2004.

143. Pereira RS, Prato FS, Lekx KS, Sykes J, and Wisenberg G. Contrast-enhanced MRI for the assessment of myocardial viability after permanent coronary artery occlusion. *Magnetic Resonance in Medicine* 44: 309-316, 2000.

144. Pereles FS, Kapoor V, Carr JC, Simonetti OP, Krupinski EA, Baskaran V, and Finn JP. Usefulness of segmented trueFISP cardiac pulse sequence in evaluation of congenital and acquired adult cardiac abnormalities. *AJR American Journal of Roentgenology* 177: 1155-1160, 2001.

145. Pesola K, Nenonen J, Fenici R, Lotjonen J, Makijarvi M, Fenici P, Korhonen P, Lauerma K, Valkonen M, Toivonen L, and Katila T. Bioelectromagnetic localization of a pacing catheter in the heart. *Physics in Medicine & Biology* 44: 2565-2578, 1999.

146. Pettigrew RI, Oshinski JN, Chatzimavroudis G, and Dixon WT. MRI techniques for cardiovascular imaging. [Review] [39 refs]. *Journal of Magnetic Resonance Imaging* 10: 590-601, 1999.

147. Prasad S, Lydne J, Chai P, and Gatehouse P. Role of CMR in assessment of myocardial perfusion. *European Radiology* 15: B42-47, 2005.

148. Prokop M. General principles of MDCT. *European Journal of Radiology* 45: S4-S10, 2002.

149. Ramani K, Judd RM, Holly TA, Parrish TB, Rigolin VH, Parker MA, Callahan C, Fitzgerald SW, Bonow RO, and Klocke FJ. Contrast magnetic resonance imaging in the assessment of myocardial viability in patients with stable coronary artery disease and left ventricular dysfunction. *Circulation* 98: 2687-2694, 1998.

150. Reffelmann T and Kloner RA. The "no-reflow" phenomenon: basic science and clinical correlates. [Review] [20 refs]. *Heart* 87: 162-168, 2002.

151. Rehwald WG. Myocardial magnetic resonance imaging contrast agent concentrations after reversible and irreversible ischemic injury. *Circulation* 105: 224-229, 2001.

152. Reid BA. Nuclear Cardiology. In: *Caffey`s Pediatric Diagnostic Imaging*, edited by Kunh P, Slovis TL and Haller JO, 2004, p. 1252-1254.

153. Reimer KA, Lowe JE, Rasmussen MM, and Jennings RB. The wavefront phenomenon of ischemic cell death. 1. Myocardial infarct size vs duration of coronary occlusion in dogs. *Circulation* 56: 786-794, 1977.

154. Reimer P, Parizel PM, and Stichnoth FA. *A practical approach clinical MR Imaging*. Germany: Springer-Verlag Berlin Heidelberg New York, 1999.

155. Rogers WJ, Jr., Kramer CM, Geskin G, Hu YL, Theobald TM, Vido DA, Petruolo S, and Reichek N. Early contrast-enhanced MRI predicts late functional recovery after reperfused myocardial infarction.[see comment]. *Circulation* 99: 744-750, 1999.

156. Ropers D, Baum U, Pohle K, Anders K, Ulzheimer S, Ohnesorge B, Schlundt C, Bautz W, Daniel WG, and Achenbach S. Detection of coronary artery stenoses with thin-slice multi-detector row spiral computed tomography and multiplanar reconstruction. *Circulation* 107: 664-666, 2003.

157. Saarinen M, Karp PJ, Katila TE, and Siltanen P. The magnetocardiogram in cardiac disorders. *Cardiovascular Research* 8: 820-834, 1974.

158. Saeed M, Bremerich J, Wendland MF, Wyttenbach R, Weinmann HJ, and Higgins CB. Reperfused myocardial infarction as seen with use of necrosis-specific versus standard extracellular MR contrast media in rats. *Radiology* 213: 247-257, 1999.

159. Saeed M, Watzinger N, Krombach GA, and Higgins CB. Contrast Media. In: *Cardiovascular MRI and MRA*, edited by Higgins CB and De Roos A, 2003, p. 82-100.

160. Sakuma H, Fujita N, Foo TK, Caputo GR, Nelson SJ, Hartiala J, Shimakawa A, and Higgins CB. Evaluation of left ventricular volume and mass with breath-hold cine MR imaging. *Radiology* 188: 377-380, 1993.

161. Sakuma H, Suzawa N, Ichikawa Y, Makino K, Hirano T, Kitagawa K, and Takeda K. Diagnostic accuracy of stress first-pass contrast-enhanced myocardial perfusion MRI compared with stress myocardial perfusion scintigraphy. *AJR American Journal of Roentgenology* 185: 95-102, 2005.

162. Sandstede JJ. Assessment of myocardial viability by MR imaging. *European Radiology* 13: 52-61, 2003.

163. Sandstede JJ, Lipke C, Beer M, Harre K, Pabst T, Kenn W, Neubauer S, and Hahn D. Analysis of first-pass and delayed contrast-enhancement patterns of dysfunctional myocardium on

MR imaging: use in the prediction of myocardial viability.[see comment]. *AJR American Journal of Roentgenology* 174: 1737-1740, 1999.

164. Schmermund A, Denktas AE, Rumberger JA, Christian TF, Sheedy PF, 2nd, Bailey KR, and Schwartz RS. Independent and incremental value of coronary artery calcium for predicting the extent of angiographic coronary artery disease: comparison with cardiac risk factors and radionuclide perfusion imaging. *Journal of the American College of Cardiology* 34: 777-786, 1999.

165. Schmitz L, Czerski K, Brockmeier K, Agrawal R, Steinhoff U, Trahms L, and Oeff M. Magnetocardiographic turbulence analysis in patients with the long QT syndrome. *Journal of Electrocardiology* 30: 105-113, 1998.

166. Schneider J, Diegeler A, Krakor R, Walther T, Kluge R, and Mohr FW. Transmyocardial laser revascularization with the holmium:YAG laser: loss of symptomatic improvement after 2 years. *European Journal of Cardio Thoracic Surgery* 19: 164-169, 2001.

167. Schofield PM, Sharples LD, Caine N, Burns S, Tait S, Wistow T, Buxton M, and Wallwork J. Transmyocardial laser revascularisation in patients with refractory angina: a randomised controlled trial.[see comment][erratum appears in Lancet 1999 May 15;353(9165):1714]. *Lancet* 353: 519-524, 1999.

168. Schreiber WG, Schmitt M, Kalden P, Mohrs OK, Kreitner KF, and Thelen M. Dynamic contrast-enhanced myocardial perfusion imaging using saturation-prepared TrueFISP. *Journal of Magnetic Resonance Imaging* 16: 641-652, 2002.

169. Schroeder S, Kopp AF, Baumbach A, Kuettner A, Georg C, Ohnesorge B, Herdeg C, Claussen CD, and Karsch KR. Non-invasive characterisation of coronary lesion morphology by multi-slice computed tomography: a promising new technology for risk stratification of patients with coronary artery disease. *Heart (British Cardiac Society)* 85: 576-578, 2001.

170. Schroeder S, Kopp AF, Kuettner A, Burgstahler C, Herdeg C, Heuschmid M, Baumbach A, Claussen CD, Karsch KR, and Seipel L. Influence of heart rate on vessel visibility in non-

invasive coronary angiography using new multislice computed tomography: experience in 94 patients. *Clinical Imaging* 26: 106-111, 2002.

171. Schwitter J, Nanz D, Kneifel S, Bertschinger K, Buchi M, Knusel PR, Marincek B, Luscher TF, and von Schulthess GK. Assessment of myocardial perfusion in coronary artery disease by magnetic resonance: a comparison with positron emission tomography and coronary angiography. *Circulation* 103: 2230-2235, 2001.

172. Sechtem U, Baer FM, Voth E, Theissen P, and Schneider CA. Stress functional MRI: detection of ischemic heart disease and myocardial viability. [Review] [45 refs]. *Journal of Magnetic Resonance Imaging* 10: 667-675, 1999.

173. Selzer A. Changing Aspects of the Natural History of Valvular Aortic Stenosis. *The New England Journal of Medicine* 317: 91-98, 1987.

174. Sensky PR and Cherryman GR. Myocardial perfusion in ischemic heart disease. In: *Cardiovascular MRI and MRA*, edited by Higgins CB and De Roos A, 2003, p. 173-189.

175. Sharir T, Germano G, Kavanagh PB, Lai S, Cohen I, Lewin HC, Friedman JD, Zellweger MJ, and Berman DS. Incremental prognostic value of post-stress left ventricular ejection fraction and volume by gated myocardial perfusion single photon emission computed tomography. *Circulation* 100: 1035-1042, 1035.

176. Siltanen P. Magnetocardiography. *MacFarlane P (Eds) Comprehensive Electrocardiology Volume II Pergamon Press New York Oxford Beijing Frankfurt Sao Paolo Sydney Tokyo Toronto*: 1408-1438, 1989.

177. Simonetti OP, Kim RJ, Fieno DS, Hillenbrand HB, Wu E, Bundy JM, Finn JP, and Judd RM. An improved MR imaging technique for the visualization of myocardial infarction. *Radiology* 218: 215-223, 2001.

178. Smith HJ. Modalities and methods. In: *A Global TextBook of Radiology*, edited by Pettersson H. Lund: The Nicer Institute, 1995, p. 47-114.

179. Sprung K. Basic techniques of cardiac MR. *European Radiology* 15: B10-16, 2005.

180. Stary HC, Chandler AB, Dinsmore RE, Fuster V, Glagov S, Insull W, Jr., Rosenfeld ME, Schwartz CJ, Wagner WD, and Wissler RW. A definition of advanced types of atherosclerotic lesions and a histological classification of atherosclerosis. A report from the Committee on Vascular Lesions of the Council on Arteriosclerosis, American Heart Association. [Review] [174 refs]. *Circulation* 92: 1355-1374, 1995.

181. Sutton D and Gregsson RHS. Arteriography and Interventional angiography. In: *Text Book of Radiology and Imaging*, edited by Sutton D, 2004, p. 673-742.

182. Takala P, Hanninen H, Montonen J, Korhonen P, Makijarvi M, Nenonen J, Oikarinen L, Toivonen L, and Katila T. Heart rate adjustment of magnetic field map rotation in detection of myocardial ischemia in exercise magnetocardiography. *Basic Research in Cardiology* 97: 88-96, 2002.

183. Takala P, Hanninen H, Montonen J, Makijarvi M, Nenonen J, Toivonen L, and Katila T. Beat-to-beat analysis method for magnetocardiographic recordings during interventions. *Physics in Medicine & Biology* 46: 975-982, 2001.

184. Topol EJ and Nissen SE. Our preoccupation with coronary luminology. The dissociation between clinical and angiographic findings in ischemic heart disease.[see comment]. [Review] [85 refs]. *Circulation* 92: 2333-2342, 1995.

185. Treede H, Becker C, Reichenspurner H, Knez A, Detter C, Reiser M, and Reichart B. Multidetector computed tomography (MDCT) in coronary surgery: first experiences with a new tool for diagnosis of coronary artery disease. *Annals of Thoracic Surgery* 74: S1398-1402, 2002.

186. van Leeuwen P, Hailer B, Bader W, Geissler J, Trowitzsch E, and Gronemeyer DH. Magnetocardiography in the diagnosis of fetal arrhythmia. *British Journal of Obstetrics & Gynaecology* 106: 1200-1208, 1999.

187. Van Leeuwen P, Hailer B, Lange S, and Gronemeyer D. Spatial distribution of repolarization times in patients with coronary artery disease. *Pacing & Clinical Electrophysiology* 26: 1706-1714, 2003.

188. Van Leeuwen P, Hailer B, and Wehr M. Spatial distribution of QT intervals: an alternative approach to QT dispersion. *Pacing & Clinical Electrophysiology* 19: 1894-1899, 1996.

189. Wang S, Detrano RC, Secci A, Tang W, Doherty TM, Puentes G, Wong N, and Brundage BH. Detection of coronary calcification with electron-beam computed tomography: evaluation of interexamination reproducibility and comparison of three image-acquisition protocols. *American Heart Journal* 132: 550-558, 1996.

190. Weiss RC, Aletras AH, London JL, Taylor Jl, Epstein FH, Wassmuth R, Balaban RS, and Arai AE. Stunned, infarcted, and normal myocardium in dogs: simultaneous differentiation by using gadolinium-enhanced cine MR imaging with magnetization transfer contrast. *Radiology* 226: 723-730, 2002.

191. Wendland MF, Saeed M, Lund G, and Higgins CB. Contrast-enhanced MRI for quantification of myocardial viability. [Review] [55 refs]. *Journal of Magnetic Resonance Imaging* 10: 694-702, 1999.

192. Wexler L, Brundage B, Crouse J, Detrano R, Fuster V, Maddahi J, Rumberger J, Stanford W, White R, and Taubert K. Coronary artery calcification: pathophysiology, epidemiology, imaging methods, and clinical implications. A statement for health professionals from the American Heart Association. Writing Group. *Circulation* 94: 1175-1192, 1996.

193. Wilke N, Jerosch-Herold M, Wang Y, Huang Y, Christensen BV, Stillman AE, Ugurbil K, McDonald K, and Wilson RF. Myocardial perfusion reserve: assessment with multisection, quantitative, first-pass MR imaging. *Radiology* 204: 373-384, 1997.

194. Wilke NM, Jerosch-Herold M, Zenovich A, and Stillman AE. Magnetic resonance first-pass myocardial perfusion imaging: clinical validation and future applications. [Review] [47 refs]. *Journal of Magnetic Resonance Imaging* 10: 676-685, 1999.

195. Vogl TJ, Abolmaali ND, Diebold T, Engelmann K, Ay M, Dogan S, Wimmer-Greinecker G, Moritz A, and Herzog C. Techniques for the detection of coronary atherosclerosis: multi-detector row CT coronary angiography. *Radiology* 223: 212-220, 2002.

196. Wu KC, Zerhouni EA, Judd RM, Lugo-Olivieri CH, Barouch LA, Schulman SP, Blumenthal RS, and Lima JA. Prognostic significance of microvascular obstruction by magnetic resonance imaging in patients with acute myocardial infarction. *Circulation* 97: 765-772, 1998.

197. Zamorano J, Delgado J, Almeria C, Moreno R, Gomez Sanchez M, Rodrigo J, Fernandez C, Ferreiros J, Rufilanchas J, and Sanchez-Harguindey L. Reason for discrepancies in identifying myocardial viability by thallium-201 redistribution, magnetic resonance imaging, and dobutamine echocardiography. *American Journal of Cardiology* 90: 455-459, 2002.

198. Zollikofer C. Interventional radiolgy. In: *A Global TextBook of Radiology*, edited by Pettersson H. Lund: The NICER Institute, 1995, p. 143-165.

199. Zur Y, Wood ML, and Neuringer LJ. Motion-insensitive, steady-state free precession imaging. *Magnetic Resonance in Medicine* 16: 444-459, 1990.